

World Journal of *Radiology*

World J Radiol 2017 October 28; 9(10): 371-404



Editorial Board

2014-2017

The *World Journal of Radiology* Editorial Board consists of 365 members, representing a team of worldwide experts in radiology. They are from 36 countries, including Afghanistan (1), Argentina (2), Australia (5), Austria (7), Belgium (2), Brazil (8), Canada (6), Chile (1), China (43), Croatia (1), Denmark (4), Egypt (6), France (5), Germany (22), Greece (10), India (12), Iran (6), Ireland (2), Israel (3), Italy (47), Japan (13), Netherlands (1), New Zealand (1), Pakistan (1), Poland (2), Portugal (1), Serbia (1), Singapore (3), Slovakia (1), South Korea (18), Spain (4), Sweden (2), Switzerland (4), Thailand (1), Turkey (26), United Kingdom (11), and United States (82).

EDITORS-IN-CHIEF

Kai U Juergens, *Bremen*
Edwin JR van Beek, *Edinburgh*
Thomas J Vogl, *Frankfurt*

GUEST EDITORIAL BOARD MEMBERS

Wing P Chan, *Taipei*
Chung-Huei Hsu, *Taipei*
Chin-Chang Huang, *Taipei*
Tsong-Long Hwang, *Taoyuan*
Jung-Lung Hsu, *Taipei*
Chia-Hung Kao, *Taichung*
Yu-Ting Kuo, *Tainan*
Hon-Man Liu, *Taipei*
Hui-Lung Liang, *Kaohsiung*
Chun Chung Lui, *Kaohsiung*
Sen-Wen Teng, *Taipei*
Yung-Liang (William) Wan, *Taoyuan*

MEMBERS OF THE EDITORIAL BOARD



Afghanistan

Takao Hiraki, *Okayama*



Argentina

Patricia Carrascosa, *Vicente Lopez*
Maria C Ziadi, *Rosario*



Australia

Lourens Bester, *Sydney*
Gemma A Figtree, *Sydney*



Austria

Herwig R Cerwenka, *Graz*
Gudrun M Feuchtnner, *Innsbruck*
Benjamin Henninger, *Innsbruck*
Rupert Lanzenberger, *Vienna*
Shu-Ren Li, *Vienna*
Veronika Schopf, *Vienna*
Tobias De Zordo, *Innsbruck*



Belgium

Steve Majerus, *Liege*
Kathelijne Peremans, *Merelbeke*



Brazil

Clerio F Azevedo, *Rio de Janeiro*
Patrícia P Alfredo, *São Paulo*
Eduardo FC Fleury, *São Paulo*
Edward Araujo Júnior, *São Paulo*
Wellington P Martins, *Ribeirao Preto*
Ricardo A Mesquita, *Belo Horizonte*
Vera MC Salemi, *São Paulo*
Claudia Szobot, *Porto Alegre*
Lilian YI Yamaga, *São Paulo*



Canada

Marie Arsalidou, *Toronto*
Otman A Basir, *Waterloo*

Tarik Zine Belhocine, *Toronto*
James Chow, *Toronto*
Tae K Kim, *Toronto*
Anastasia Oikonomou, *Toronto*



China

Hong-Wei Chen, *Wuxi*
Feng Chen, *Hangzhou*
Jian-Ping Chu, *Guangzhou*
Guo-Guang Fan, *Shenyang*
Bu-Lang Gao, *Shijiazhuang*
Qi-Yong Gong, *Chengdu*
Ying Han, *Beijing*
Xian-Li Lv, *Beijing*
Yi-Zhuo Li, *Guangzhou*
Xiang-Xi Meng, *Harbin*
Yun Peng, *Beijing*
Jun Shen, *Guangzhou*
Ze-Zhou Song, *Hangzhou*
Wai Kwong Tang, *Hong Kong*
Gang-Hua Tang, *Guangzhou*
Jie Tian, *Beijing*
Lu-Hua Wang, *Beijing*
Xiao-bing Wang, *Xi'an*
Yi-Gen Wu, *Nanjing*
Kai Wu, *Guangzhou*
Hui-Xiong Xu, *Shanghai*
Zuo-Zhang Yang, *Kunming*
Xiao-Dan Ye, *Shanghai*
David T Yew, *Hong Kong*
Ting-He Yu, *Chongqing*
Zheng Yuan, *Shanghai*
Min-Ming Zhang, *Hangzhou*
Yudong Zhang, *Nanjing*
Dong Zhang, *Chongqing*
Wen-Bin Zeng, *Changsha*

Yue-Qi Zhu, *Shanghai*



Croatia

Goran Kusec, *Osijek*



Denmark

Poul E Andersen, *Odense*
Lars J Petersen, *Aalborg*
Thomas Z Ramsøy, *Frederiksberg*
Morten Ziebell, *Copenhagen*



Egypt

Mohamed F Bazeed, *Mansoura*
Mohamed Abou El-Ghar, *Mansoura*
Reem HA Mohamed, *Cairo*
Mohamed R Nouh, *Alexandria*
Ahmed AKA Razek, *Mansoura*
Ashraf A Zytoon, *Shebin El-Koom*



France

Sabine F Bensamoun, *Compiègne*
Romaric Loffroy, *Dijon*
Stephanie Nougaret, *Montpellier*
Hassane Oudadesse, *Rennes*
Vincent Vinh-Hung, *Fort-de-France*



Germany

Henryk Barthel, *Leipzig*
Peter Bannas, *Hamburg*
Martin Beeres, *Frankfurt*
Ilja F Ciernik, *Dessau*
A Dimitrakopoulou-Strauss, *Heidelberg*
Peter A Fasching, *Erlangen*
Andreas G Schreyer, *Regensburg*
Philipp Heusch, *Duesseldorf*
Sonja M Kirchhoff, *Munich*
Sebastian Ley, *Munich*
Adel Maataoui, *Frankfurt am Main*
Stephan M Meckel, *Freiburg*
Hans W Muller, *Duesseldorf*
Kay Raum, *Berlin*
Dirk Rades, *Luebeck*
Marc-Ulrich Regier, *Hamburg*
Alexey Surov, *Halle*
Martin Walter, *Magdeburg*
Axel Wetter, *Essen*
Christoph Zilkens, *Düsseldorf*



Greece

Panagiotis Antoniou, *Thessaloniki*
Nikos Efthimiou, *Athens*
Dimitris Karnabatidis, *Patras*
George Latsios, *Athens*
Stylianios Megremis, *Iraklion*

Alexander D Rapidis, *Athens*
Kiki Theodorou, *Larissa*
Ioannis A Tsalafoutas, *Athens*
Evanthia E Tripoliti, *Ioannina*
Athina C Tsili, *Ioannina*



India

Ritesh Agarwal, *Chandigarh*
Chandan J Das, *New Delhi*
Prathamesh V Joshi, *Mumbai*
Naveen Kalra, *Chandigarh*
Chandrasekharan Kesavadas, *Trivandrum*
Jyoti Kumar, *New Delhi*
Atin Kumar, *New Delhi*
Kaushala P Mishra, *Allahabad*
Daya N Sharma, *New Delhi*
Binit Sureka, *New Delhi*
Sanjay Sharma, *New Delhi*
Raja R Yadav, *Allahabad*



Iran

Majid Assadi, *Bushehr*
SeyedReza Najafizadeh, *Tehran*
Mohammad Ali Oghabian, *Tehran*
Amir Reza Radmard, *Tehran*
Ramin Sadeghi, *Mashhad*
Hadi Rokni Yazdi, *Tehran*



Ireland

Tadhg Gleeson, *Wexford*
Frederik JAI Vernimmen, *Cork*



Israel

Dafna Ben Bashat, *Tel Aviv*
Amit Gefen, *Tel Aviv*
Tamar Sella, *Jerusalem*



Italy

Adriano Alippi, *Rome*
Dante Amelio, *Trento*
Michele Anzidei, *Rome*
Filippo F Angileri, *Messinas*
Stefano Arcangeli, *Rome*
Roberto Azzoni, *San Donato milanese*
Tommaso V Bartolotta, *Palermo*
Tommaso Bartalena, *Imola*
Livia Bernardin, *San Bonifacio*
Federico Boschi, *Verona*
Sergio Casciaro, *Lecce*
Emanuele Casciani, *Rome*
Musa M Can, *Napoli*
Alberto Cuocolo, *Napoli*
Michele Ferrara, *Coppito*
Mauro Feola, *Fossano*
Giampiero Francica, *Castel Volturno*
Luigi De Gennaro, *Rome*
Giulio Giovannetti, *Pisa*

Francesca Iacobellis, *Napoli*
Formato Invernizzi, *Monza Brianza*
Francesco Lassandro, *Naples*
Lorenzo Livi, *Florence*
Pier P Mainenti, *Napoli*
Laura Marzetti, *Chieti*
Giuseppe Malinverni, *Crescentino*
Enrica Milanese, *Turin*
Giovanni Morana, *Treviso*
Lorenzo Monti, *Milan*
Silvia D Morbelli, *Genoa*
Barbara Palumbo, *Perugia*
Cecilia Parazzini, *Milan*
Stefano Pergolizzi, *Messina*
Antonio Pinto, *Naples*
Camillo Porcaro, *Rome*
Carlo C Quattrocchi, *Rome*
Alberto Rebonato, *Perugia*
Giuseppe Rizzo, *Rome*
Roberto De Rosa, *Naples*
Domenico Rubello, *Rovigo*
Andrea Salvati, *Bari*
Sergio Sartori, *Ferrara*
Luca M Sconfienza, *Milano*
Giovanni Storto, *Rionero*
Nicola Sverzellati, *Parma*
Alberto S Tagliafico, *Genova*
Nicola Troisi, *Florence*



Japan

Yasuhiko Hori, *Chiba*
Hidetoshi Ikeda, *Koriyama*
Masahito Kawabori, *Sapporo*
Tamotsu Kamishima, *Sapporo*
Hiro Kiyosue, *Yufu*
Yasunori Minami, *Osaka-sayama*
Yasuhiro Morimoto, *Kitakyushu*
Satoru Murata, *Tokyo*
Shigeki Nagamachi, *Miyazaki*
Hiroshi Onishi, *Yamanashi*
Morio Sato, *Wakayama Shi*
Yoshito Tsushima, *Maebashi*
Masahiro Yanagawa, *Suita*



Netherlands

Willem Jan van Rooij, *Tilburg*



New Zealand

W Howell Round, *Hamilton*



Pakistan

Wazir Muhammad, *Abbottabad*



Poland

Maciej S Baglaj, *Wroclaw*

Piotr Czauderna, *Gdansk*



Portugal

Joao Manuel RS Tavares, *Porto*



Serbia

Olivera Ciraj-Bjelac, *Belgrade*



Singapore

Gopinathan Anil, *Singapore*
Terence KB Teo, *Singapore*
Cher Heng Tan, *Singapore*



Slovakia

Stefan Sivak, *Martin*



South Korea

Ki Seok Choo, *Busan*
Seung Hong Choi, *Seoul*
Dae-Seob Choi, *Jinju*
Hong-Seok Jang, *Seoul*
Yong Jeong, *Daejeon*
Chan Kyo Kim, *Seoul*
Se Hyung Kim, *Seoul*
Joong-Seok Kim, *Seoul*
Sang Eun Kim, *Seongnam*
Sung Joon Kwon, *Seoul*
Jeong Min Lee, *Seoul*
In Sook Lee, *Busan*
Noh Park, *Goyang*
Chang Min Park, *Seoul*
Sung Bin Park, *Seoul*
Deuk Jae Sung, *Seoul*
Choongsoo Shin, *Seoul*
Kwon-Ha Yoon, *Iksan*



Spain

Miguel A De Gregorio, *Zaragoza*
Antonio Luna, *Jaén*
Enrique Marco de Lucas, *Santander*
Fernando Ruiz Santiago, *Granada*



Sweden

Dmitry Grishenkov, *Stockholm*
Tie-Qiang Li, *Stockholm*



Switzerland

Nicolau Beckmann, *Basel*
Christian Boy, *Bern*
Giorgio Treglia, *Bellinzona*

Stephan Ulmer, *Kiel*



Thailand

Sirianong Namwongprom, *Chiang Mai*



Turkey

Kubilay Aydin, *Istanbul*
Ramazan Akdemir, *Sakarya*
Serhat Avcu, *Ankara*
Ayse Aralasmak, *Istanbul*
Oktay Algin, *Ankara*
Nevbahar Akcar, *Meselik*
Bilal Battal, *Ankara*
Zulkif Bozgeyik, *Elazig*
Nazan Ciledag, *Aakara*
Fuldem Y Donmez, *Ankara*
Gulgun Engin, *Istanbul*
Ahmet Y Goktay, *Izmir*
Oguzhan G Gumustas, *Bursa*
Kaan Gunduz, *Ankara*
Pelin Ozcan Kara, *Mersin*
Kivanc Kamburoglu, *Ankara*
Ozgur Kilickesmez, *Istanbul*
Furuzan Numan, *Istanbul*
Cem Onal, *Adana*
Ozgur Oztekin, *Izmir*
Seda Ozbek (Boruban), *Konya*
Selda Sarikaya, *Zonguldak*
Figen Taser, *Kutahya*
Baran Tokar, *Eskisehir*
Ender Uysal, *Istanbul*
Ensar Yekeler, *Istanbul*



United Kingdom

Indran Davagnanam, *London*
M DC Valdés Hernández, *Edinburgh*
Alan Jackson, *Manchester*
Suneil Jain, *Belfast*
Long R Jiao, *London*
Miltiadis Krokidis, *Cambridge*
Pradesh Kumar, *Liverpool*
Peter D Kuzmich, *Derby*
Georgios Plataniotis, *Brighton*
Vanessa Sluming, *Liverpool*



United States

Garima Agrawal, *Saint Louis*
James R Brasic, *Baltimore*
Rajendra D Badgaiyan, *Buffalo*
Ulas Bagci, *Bethesda*
Anat Biegon, *Stony Brook*
Ramon Casanova, *Winston Salem*
Wenli Cai, *Boston*
Zheng Chang, *Durham*
Corey J Chakarun, *Long Beach*
Kai Chen, *Los Angeles*
Hyun-Soon Chong, *Chicago*
Marco Cura, *Dallas*
Ravi R Desai, *Bensalem*
Delia DeBuc, *Miami*
Carlo N De Cecco, *Charleston*

Timm-Michael L Dickfeld, *Baltimore*
Subba R Digumarthy, *Boston*
Huy M Do, *Stanford*
Todd A Faasse, *Grand Rapids*
Salomao Faintuch, *Boston*
Girish M Fatterpekar, *New York*
Dhakshinamoorthy Ganeshan, *Houston*
Robert J Griffin, *Little Rock*
Andrew J Gunn, *Boston*
Sandeep S Hedgire, *Boston*
Timothy J Hoffman, *Columbia*
Mai-Lan Ho, *San Francisco*
Juebin Huang, *Jackson*
Abid Irshad, *Charleston*
Matilde Inglese, *New York*
El-Sayed H Ibrahim, *Jacksonville*
Paul R Julsrud, *Rochester*
Pamela T Johnson, *Baltimore*
Ming-Hung Kao, *Tempe*
Sunil Krishnan, *Houston*
Richard A Komoroski, *Cincinnati*
Sandi A Kwee, *Honolulu*
King Kim, *Ft. Lauderdale*
Guozheng Liu, *Worcester*
Yiyan Liu, *Newark*
Venkatesh Mani, *New York*
Lian-Sheng Ma, *Pleasanton*
Rachna Madan, *Boston*
Zeyad A Metwalli, *Houston*
Yilong Ma, *Manhasset*
Hui Mao, *Atlanta*
Feroze B Mohamed, *Philadelphia*
Gul Moonis, *Boston*
John L Noshier, *New Brunswick*
Rahmi Oklu, *Boston*
Aytekin Oto, *Chicago*
Bishnuhari Paudyal, *Philadelphia*
Rajul Pandya, *Youngstown*
Chong-Xian Pan, *Sacramento*
Jay J Pillai, *Baltimore*
Neal Prakash, *Duarte*
Reza Rahbar, *Boston*
Ali S Raja, *Boston*
Gustavo J Rodriguez, *El Paso*
David J Sahn, *Portland*
Steven Schild, *Scottsdale*
Ali R Sepahdari, *Los Angeles*
Li Shen, *Indianapolis*
JP Sheehan, *Charlottesville*
Atul B Shinagare, *Boston*
Sarabjeet Singh, *Boston*
Charles J Smith, *Columbia*
Kenji Suzuki, *Chicago*
Monvadi Srichai-Parsia, *Washington*
Sree H Tirumani, *Boston*
Hebert A Vargas, *New York*
Sachit Verma, *Philadelphia*
Yoichi Watanabe, *Minneapolis*
Li Wang, *Chapel Hill*
Carol C Wu, *Boston*
Shoujun Xu, *Houston*
Min Yao, *Cleveland*
Xiaofeng Yang, *Atlanta*
Qingbao Yu, *Albuquerque*
Aifeng Zhang, *Chicago*
Chao Zhou, *Bethlehem*
Hongming Zhuang, *Philadelphia*

REVIEW

- 371 Cerebellum and neurodegenerative diseases: Beyond conventional magnetic resonance imaging

Mormina E, Petracca M, Bommarito G, Piaggio N, Cocozza S, Inglese M

- 389 Lymph node imaging in initial staging of prostate cancer: An overview and update

Zarzour JG, Galgano S, McConathy J, Thomas JV, Rais-Bahrami S

CASE REPORT

- 400 MR neurography in intraosseous median nerve entrapment

Aggarwal A, Jana M, Kumar V, Srivastava DN, Garg K

ABOUT COVER

Editorial Board Member of *World Journal of Radiology*, Stefano Arcangeli, MD, Assistant Professor, Department of Radiotherapy, Azienda Ospedaliera S. Camillo-Forlanini, Rome 00152, Italy

AIM AND SCOPE

World Journal of Radiology (*World J Radiol*, *WJR*, online ISSN 1949-8470, DOI: 10.4329) is a peer-reviewed open access academic journal that aims to guide clinical practice and improve diagnostic and therapeutic skills of clinicians.

WJR covers topics concerning diagnostic radiology, radiation oncology, radiologic physics, neuroradiology, nuclear radiology, pediatric radiology, vascular/interventional radiology, medical imaging achieved by various modalities and related methods analysis. The current columns of *WJR* include editorial, frontier, diagnostic advances, therapeutics advances, field of vision, mini-reviews, review, topic highlight, medical ethics, original articles, case report, clinical case conference (clinicopathological conference), and autobiography.

We encourage authors to submit their manuscripts to *WJR*. We will give priority to manuscripts that are supported by major national and international foundations and those that are of great basic and clinical significance.

INDEXING/ABSTRACTING

World Journal of Radiology is now indexed in PubMed, PubMed Central, and Emerging Sources Citation Index (Web of Science).

FLYLEAF

I-III Editorial Board

EDITORS FOR THIS ISSUE

Responsible Assistant Editor: *Xiang Li*
Responsible Electronic Editor: *Ya-Jing Lu*
Proofing Editor-in-Chief: *Lian-Sheng Ma*

Responsible Science Editor: *Li-Jun Cui*
Proofing Editorial Office Director: *Xiu-Xia Song*

NAME OF JOURNAL
World Journal of Radiology

ISSN
 ISSN 1949-8470 (online)

LAUNCH DATE
 January 31, 2009

FREQUENCY
 Monthly

EDITORS-IN-CHIEF
Kai U Juergens, MD, Associate Professor, MRT und PET/CT, Nuklearmedizin Bremen Mitte, ZEMODI - Zentrum für morphologische und molekulare Diagnostik, Bremen 28177, Germany

Edwin JR van Beek, MD, PhD, Professor, Clinical Research Imaging Centre and Department of Medical Radiology, University of Edinburgh, Edinburgh EH16 4TJ, United Kingdom

Thomas J Vogl, MD, Professor, Reader in Health Technology Assessment, Department of Diagnostic and Interventional Radiology, Johann Wolfgang Goethe University of Frankfurt, Frankfurt 60590,

Germany

EDITORIAL BOARD MEMBERS
 All editorial board members resources online at <http://www.wjnet.com/1949-8470/editorialboard.htm>

EDITORIAL OFFICE
 Xiu-Xia Song, Director
World Journal of Radiology
 Baishideng Publishing Group Inc
 7901 Stoneridge Drive, Suite 501, Pleasanton, CA 94588, USA
 Telephone: +1-925-2238242
 Fax: +1-925-2238243
 E-mail: editorialoffice@wjnet.com
 Help Desk: <http://www.f6publishing.com/helpdesk>
<http://www.wjnet.com>

PUBLISHER
 Baishideng Publishing Group Inc
 7901 Stoneridge Drive, Suite 501, Pleasanton, CA 94588, USA
 Telephone: +1-925-2238242
 Fax: +1-925-2238243
 E-mail: bpgoffice@wjnet.com
 Help Desk: <http://www.f6publishing.com/helpdesk>
<http://www.wjnet.com>

PUBLICATION DATE
 October 28, 2017

COPYRIGHT
 © 2017 Baishideng Publishing Group Inc. Articles published by this Open-Access journal are distributed under the terms of the Creative Commons Attribution Non-commercial License, which permits use, distribution, and reproduction in any medium, provided the original work is properly cited, the use is non commercial and is otherwise in compliance with the license.

SPECIAL STATEMENT
 All articles published in journals owned by the Baishideng Publishing Group (BPG) represent the views and opinions of their authors, and not the views, opinions or policies of the BPG, except where otherwise explicitly indicated.

INSTRUCTIONS TO AUTHORS
<http://www.wjnet.com/bpg/gerinfo/204>

ONLINE SUBMISSION
<http://www.f6publishing.com>

Cerebellum and neurodegenerative diseases: Beyond conventional magnetic resonance imaging

Enricomaria Mormina, Maria Petracca, Giulia Bommarito, Niccolò Piaggio, Sirio Coccozza, Matilde Inglese

Enricomaria Mormina, Maria Petracca, Giulia Bommarito, Sirio Coccozza, Matilde Inglese, Department of Neurology, Icahn School of Medicine at Mount Sinai, New York, NY 10029, United States

Enricomaria Mormina, Neuroradiology Unit, Department of Biomedical Sciences and Morphological and Functional Images, University of Messina, 98100 Messina, Italy

Maria Petracca, Department of Neuroscience, Reproductive Sciences and Odontostomatology, University of Naples Federico II, 80138 Naples, Italy

Giulia Bommarito, Niccolò Piaggio, Matilde Inglese, Department of Neuroscience, Rehabilitation, Ophthalmology, Genetics and Maternal and Child Health (DINO GMI), University of Genoa, 16132 Genoa, Italy

Niccolò Piaggio, Department of Neuroradiology, San Martino Hospital, 16132 Genoa, Italy

Sirio Coccozza, Department of Advanced Biomedical Sciences, University of Naples Federico II, 80138 Naples, Italy

Author contributions: Inglese M takes responsibility for the integrity and accuracy of the review; Study concept and design: Mormina E, Petracca M and Inglese M; Literature review: All authors; Drafting and critical revision of the manuscript for important intellectual content: All authors; Study supervision: Inglese M.

Conflict-of-interest statement: No potential conflicts of interest. No financial support.

Open-Access: This article is an open-access article which was selected by an in-house editor and fully peer-reviewed by external reviewers. It is distributed in accordance with the Creative Commons Attribution Non Commercial (CC BY-NC 4.0) license, which permits others to distribute, remix, adapt, build upon this work non-commercially, and license their derivative works on different terms, provided the original work is properly cited and the use is non-commercial. See: <http://creativecommons.org/licenses/by-nc/4.0/>

Manuscript source: Invited manuscript

Correspondence to: Matilde Inglese, MD, PhD, Associate Professor, Director of Neurology Imaging Laboratory, Department of Neurology, Icahn School of Medicine at Mount Sinai, Annenberg 14, Box 1137, One Gustave L. Levy Place, New York, NY 10029, United States. matilde.inglese@mssm.edu
Telephone: +1-212-8249310
Fax: +1-212-3481310

Received: January 27, 2017
Peer-review started: February 12, 2017
First decision: April 17, 2017
Revised: July 18, 2017
Accepted: August 2, 2017
Article in press: August 2, 2017
Published online: October 28, 2017

Abstract

The cerebellum plays a key role in movement control and in cognition and cerebellar involvement is described in several neurodegenerative diseases. While conventional magnetic resonance imaging (MRI) is widely used for brain and cerebellar morphologic evaluation, advanced MRI techniques allow the investigation of cerebellar microstructural and functional characteristics. Volumetry, voxel-based morphometry, diffusion MRI based fiber tractography, resting state and task related functional MRI, perfusion, and proton MR spectroscopy are among the most common techniques applied to the study of cerebellum. In the present review, after providing a brief description of each technique's advantages and limitations, we focus on their application to the study of cerebellar injury in major neurodegenerative diseases, such as multiple sclerosis, Parkinson's and Alzheimer's disease and hereditary ataxia. A brief introduction to the pathological substrate of cerebellar involvement is provided for each disease, followed by the review of MRI studies exploring structural and functional cerebellar abnormalities and by a discussion of the clinical relevance of MRI measures of cerebellar damage in terms of both clinical status and cognitive performance.

Key words: Cerebellum; Neurodegenerative disease; Ataxia; Multiple sclerosis; Parkinson's disease; Diffusion magnetic resonance imaging; Tractography; Volumetry; Functional magnetic resonance imaging; Alzheimer's disease

© **The Author(s) 2017.** Published by Baishideng Publishing Group Inc. All rights reserved.

Core tip: The cerebellum is involved in movement control and cognition. Conventional and advanced magnetic resonance imaging (MRI) techniques are widely used for the morphologic evaluation and the microstructural and functional investigation of the cerebellum. In this review we show the state of the art of advanced MRI techniques in the investigation of cerebellum alterations, especially in patients affected by neurodegenerative diseases. In particular, we evaluated advantages, limitations and future perspective of these techniques in multiple sclerosis, Parkinson's disease and Parkinsonisms, Alzheimer's disease and hereditary ataxia, highlighting how the investigation of cerebellum may play a key role in the assessment of motor performance and clinical status of these diseases.

Mormina E, Petracca M, Bommarito G, Piaggio N, Cocozza S, Inglese M. Cerebellum and neurodegenerative diseases: Beyond conventional magnetic resonance imaging. *World J Radiol* 2017; 9(10): 371-388 Available from: URL: <http://www.wjgnet.com/1949-8470/full/v9/i10/371.htm> DOI: <http://dx.doi.org/10.4329/wjr.v9.i10.371>

INTRODUCTION

The cerebellum plays a key role in normal brain function and its structural and functional involvement in several neurological diseases is associated with the impairment of both motor and non-motor functions such as cognition, mood and behavior. Imaging studies have been challenged in the past by the complex cerebellar anatomical structure and by its location in the posterior fossa. The advent of high-field magnets and the development of new algorithms for image acquisition and analysis have, at least in part, improved the study of cerebellar structure and functions. This review provides a brief description of cerebellar macro- and microscopic anatomy and functions and focuses on the imaging methods and segmentation tools for the analysis of the cerebellum with emphasis on each method's advantages and limitations. Further, the clinical implications of the cerebellar involvement in neurological diseases such as multiple sclerosis, hereditary ataxias, Parkinson's and Alzheimer's disease are discussed.

Anatomy and function

The cerebellum is a large folded structure consisting of two cerebellar hemispheres, united by a central part known as vermis located in the posterior cranial fossa, lying dorsal to the brainstem and inferior occipital lobes.

It is separated from the cerebrum by a dura mater layer known as tentorium cerebelli and it is surrounded postero-laterally and infero-medially by venous structures, respectively transverse and sigmoid sinuses. The cerebellar cortex is tightly folded and composed by three layers: Molecular layer, Purkinje cell layer and granular layer. Each ridge or gyrus of gray matter is called folium. Undereath these layer of gray matter there is a central mass of white matter, also called corpus midollare or arbor vitae (tree of life), in which are embedded the three deep gray matter cerebellar nuclei: Fastigial nucleus, interposed nucleus (composed by the emboliform and globose nuclei) and dentate nucleus. Three white matter peduncles (superior, middle and inferior) connect the cerebellum to the brainstem, respectively to the midbrain, pons and medulla oblongata. In addition to the above reported macro- and microscopic description, cerebellar structure can be further characterized from a morphologic, phylogenetic and functional perspective. The morphologic classification describes, without any functional basis, a division into three lobes: Anterior, posterior and flocculonodular lobe, while the phylogenetic classification divides the cerebellum into archicerebellum (the most ancient portion), paleocerebellum (developed after archicerebellum) and neocerebellum (the newest portion). The functional classification divides the cerebellum in three regions: Vestibulocerebellum, spinocerebellum and cerebrocerebellum based on the location of the afferent and efferent neurons^[1,2]. The vestibulocerebellum corresponds to the flocculonodular lobe, with afferents neurons arising from vestibular nuclei (and some portion of visual cortex) and efferents neurons going to vestibular nuclei. It modulates gait balance and eye movements. The spinocerebellum is formed by the superior and inferior portion of the vermis (with the exception of the nodule) and by a bilateral paravermian portion, located on both sides of the vermis. The vermian part of the spinocerebellum has its afferent neurons arising from the spinal cord, vestibular, visual and acoustic nuclei and has its efferents neurons going through the fastigial nucleus. It modulates head and neck muscle movement as well as trunk and limb proximal portions. The paravermian part of the spinocerebellum has its afferents neurons arising from the spinal cord and trigeminal sensory nuclei, and its efferents neurons going through the interposed nucleus. It completes movement modulation performed by the vermian part, acting on limb distal portions. The cerebrocerebellum is composed by the two cerebellar hemispheres and receives afferent neurons from most of the neocortex (frontal, parietal, temporal, and occipital lobes) through the pons nuclei, sending its efferent neurons to thalamus and cerebral cortex through the dentate nucleus. Functional specificity is granted by the presence of multiple close-loop circuits between cerebral and cerebellar cortex, in which the same brain area that is the major target of output from the cerebro-cerebellar circuit it is also its major source of input^[3,4]. In each loop, a specific cortical area projects through the pontine nuclei to a distinct region

of the cerebellar cortex. A specific portion of the dentate nucleus projects then to a specific cortical area through a distinct thalamic region, thus closing the cerebro-cerebellar loop^[5,6]. According to studies conducted on primates, the dentate nucleus is topographically organized in a ventral portion, projecting to the prefrontal and posterior parietal cortex, and a dorsal portion, projecting to the motor cortex^[7]. Both motor and non-motor domains of the dentate also project to the striatum (input stage of basal ganglia processing), raising the hypothesis that cerebellum could also modulate basal ganglia facilitation of voluntary movements^[8]. The cerebrocerebellum is the largest part of the cerebellum and accounts for motor planning and motor learning. It is responsible for the transition from controlled to automatic movement: Once motor memories storage has been achieved in the cerebellar cortex, the execution of movements can be triggered by sparse high-level command from cerebral cortex^[9]. The ability of the cerebellum to adjust performance according to context, automatically integrating interoception with perception and internal models, does not apply only to movements controls but also to cognitive function, as proved by the occurrence of the cerebellar cognitive-affective syndrome following acute cerebellar lesions of the posterior lobe^[10]. In particular, lesions of the posterolateral hemispheres cause cognitive disturbances, while vermis lesions induce behavioral and affective alterations. Cerebrocerebellum is considered an essential modulator of cognitive abilities, such as language processing and visuospatial perception (respectively lateralized in the right and left cerebellar hemisphere), as well as high order functions as emotions, behaviors and personality. For example, thanks to its connection to the prefrontal cortex, the cerebellum is involved in the execution of abstract rules that govern response selection, regardless of whether they specifically relate to the selection of actions^[11,12].

MRI of the posterior cranial fossa

The posterior cranial fossa (PCF) is located between the tentorium cerebelli and foramen magnum and houses the cerebellum and the brainstem. For its peculiar conformation, small dimensions and contained structures, an accurate study by means of computed tomography (CT) and MRI had always represented a great challenge^[13-15]. However, several progresses have been made in this field to avoid the artifacts related to the X-ray beam hardening and the partial volume effects (which is non-linear) caused by the thickness and the irregularity of the skull-base bones. Specifically, the introduction of thin-section spiral multidetector CT, which allows the acquisition of isotropic voxel scans and the use of MRI scanners which allow the acquisition of multiplanar and multiparametric images have contributed to minimize PCF artifacts^[16-23]. Most of PCF artifacts are related to blood flow pulsation, inflow/outflow of cerebro-spinal fluid (CSF) and to the brain-bone-air interfaces^[24-30].

Artifacts related to vessels blood pulsation generate a signal that is displaced from its correct anatomical

position causing a wrong/inappropriate image, also called "ghost" artifacts^[31]. Transverse sinuses blood-flow related artifact, which often generate a false image projecting onto cerebellar parenchyma, may lead to an inaccurate or inappropriate interpretation of MR images. Artifacts related to the inflow and outflow of CSF inside PCF from the superior or inferior regions can be minimized by the use of fluid attenuated inversion recovery (FLAIR) images where the CSF signal is nulled out by setting a proper inversion pulse. Unfortunately, these artifacts can still be present if the inversion pulse is spatially selective, allowing a partial suppression^[30,32]. As shown by Baksi *et al.*^[30] and Lavdas *et al.*^[33] this type of artifact may mimic or hide a brain parenchymal lesion due to the presence, along with the phase encoding direction, of a redundant CSF signal.

The brain-bone-air interfaces artifact represents one of the magnetic susceptibility artifacts that are often present on gradient-echo sequences^[28], especially in regions like the skull base, petrous temporal bone, paranasal sinuses and orbits^[34,35].

It should be noted that some MRI sequences are more prone to specific artifacts than others: *i.e.*, gradient-echo for susceptibility artifacts (since this sequence does not use a refocusing 180° pulse and signal dephases fast due to field inhomogeneity), inversion recovery (*e.g.*, short tau inversion recovery and FLAIR) for pulsatile artifacts, or 2D time-of-flight for slow-flow artefactual gaps in non-dominant transverse sinus^[13,30,33,36]. Nonetheless, some of these artifacts are routinely exploited for diagnostic purposes: Susceptibility weighted images (and in general T2*w gradient-echo images) thanks to its capability of being susceptible to paramagnetic molecules, is able to recognize small amounts of blood degradation products better than other sequences and to distinguish between parenchymal calcifications and blood products^[37].

Although the combined use of MRI and CT is recommended for the diagnosis of PCF pathologies, MR is preferred to CT in order to evaluate soft tissue structures and to determinate their spatial relationship. While MRI provides higher accuracy in detecting bone marrow changes, brain parenchyma, meningeal infiltration, perineural and perivascular spread caused by tumors^[14,38,39], CT is more sensitive for the evaluation of bone structures, PFC tumoral and non-tumoral conditions^[14,40].

High and ultra-high field MRI

The possibility to study the brain at high and ultra-high field strength has become quite common after the United States FDA approval of MR magnets up to 4 Tesla (T) for clinical use. Currently, the term ultra-high field is used for MR scanners with a magnetic field strength higher than 3T. The application of high and ultra-high static magnetic field strength can improve the visualization of brain anatomy and the study of changes in brain structure and function in several neuropsychiatric diseases. For example, the higher signal-to-noise ratio (SNR) of 3T scanners allows not only to perform faster imaging compared to 1.5T scanners (doubling the strength of the

magnetic field would theoretically lead to a reduction of acquisition time of a factor of four), but also to acquire images at higher spatial resolution, that turns be very useful in the evaluation of small structures such as the cerebellum and the brainstem. It has been shown that higher spatial resolution is helpful in studying the cerebellar cortex, whose thickness is lower than cerebral thickness (< 0.5 mm vs the 3-4 mm, respectively)^[41,42].

In the research field, 7T MR scanners have proven to be of great use for the identification and the study of each cerebellar folia (which are approximately 260)^[43] and for the study of cerebellar cortical layers. Specifically, the granular and molecular cerebellar layers, whose thickness is approximately 240 μm , are well recognized and morphologically studied at 7T which has the unique advantage to allow an in-plane voxel size of 120 μm not possible at low-field MR scanners^[44]. It is important to bear in mind that higher magnetic fields bring the inherit heavy burden of several artifacts and limitations. For instance chemical shift imaging and susceptibility artifacts, are only some of the artifacts that will increase with high magnetic field. These phenomena, which may cause images misinterpretation, can also be exploited, leading for example to a better separation of metabolites in spectroscopy, a better performance in perfusion weighted imaging, or a better blood products detection. Further, when using high and ultra-high magnetic fields in humans, the specific absorption rate (SAR) should also be carefully evaluated, since it will be quadruplicate with the doubling of the field strength, limiting the use of some sequences and making some parameter modulation necessary in order not to exceed the SAR threshold limit given by International Electrotechnical Commission^[45].

MRI techniques available for the study of cerebellum

Conventional morphologic techniques

The remarkable wide range of MR sequences available for the study of the PCF and the cerebellum comes with the difficulty of making the optimal selection based on the clinical or research question. In a standard clinical study the MRI protocol should include a turbo spin-echo (TSE) T1weighted (T1w) sequence to assess shape and dimension of the cerebellum and of the PCF, TSE-T2w and FLAIR-T2w sequences to detect potential white matter (WM) lesions. The choice of an isotropic voxel (≤ 1 mm) should always be preferred when available or when a high-resolution multiplanar evaluation is needed. For example, it has been showed that, in comparison to TSE-T2/proton density sequences, isotropic 3D-FLAIR is more accurate in detecting not only white matter lesions but also cortical and infratentorial lesions in patients with multiple sclerosis (MS)^[46]. 3D FLAIR has advantages even when acquired at ultra-high magnetic field, such as in the study of Kilsdonk *et al*^[47] in which cortical gray matter (GM) lesions were better detected at 7T with 3D FLAIR than with GM-Specific 3D double inversion recovery (DIR) or with 2D-T2w and 3D-T1w. Finally, quantitative T1 and proton density (ρ) magnetic resonance imaging at 3T

provide a good visualization of deep cerebellar nuclei, like dentate nuclei at 1.5T^[48]. Similarly, susceptibility weighted imaging (SWI) allows a better detection of the dentate nuclei at 1.5T while higher magnetic field allows visualization of the dentate wall corrugation, which is the iron-poorer dorsal portion of it^[49].

Volumetric techniques

There is an ever-increasing interest in the evaluation of cerebellar volume as a potential correlate of motor and cognitive performance and as a biomarker of progression and/or treatment outcome in neurodegenerative disorders^[50].

Several computerized methods with specific advantages and limitations are available to perform cerebellar segmentation, lobule parcellation and thus to assess global cerebellar volume, regional or lobular volumes and GM and WM volume. Although manual volume segmentation is considered the "gold standard", this option is extremely time-consuming and its reliability may vary with the experience of the raters^[51]. Several semi-automatic computerized methods have been developed and validated in order to minimize operator-dependent limitation. We will focus on the methods that have been more extensively applied in clinical studies and will describe each method's advantages and limitations.

SUIT (spatially unbiased atlas template of the cerebellum and brainstem) is a Statistical Parametric mapping software (SPM) toolbox for MATLAB, based on a nonlinear coregistration of MRI images to a high-resolution cerebellum template obtained from images of healthy controls^[52]. This method allows the parcellation of the cerebellum in at least 28 lobules, thus measuring GM volume for each lobule and the global GM volume as the sum of all lobule volumes (Figure 1). SUIT has been applied to the study of several diseases such as multiple sclerosis (MS), autism spectrum disorder, attention deficit hyperactivity disorder, developmental dyslexia and primary craniocervical dystonia, and it has been shown that it has higher sensibility to volume changes than conventional whole-brain voxel-based morphometry (VBM) methods^[50,53,54]. The main advantage of SUIT is that it provides an optimal overlap of the cerebellar lobules, preserving anatomical details, and thanks to its cropping step avoids results bias from supratentorial structures^[50,53,54]. However, Bogovic *et al*^[51] reported that SUIT accuracy may decrease in patients with severe cerebellar atrophy especially with regard to lobule specific segmentation.

Cerebellar analysis toolkit (CATK) is based on a Bayesian framework of FMRIB's Integrated Registration and Segmentation Tool^[55]. Using hand-delineated examples, active appearance models are created in order to perform cerebellar labeling and segmentation. CATK has shown a high reliability (Intraclass Correlation Coefficients, ICCs, of 0.96 for test-retest) a good manual segmentation agreement (ICC 0.87) and a better performance than other softwares, such as SUIT (v 2.7) and Freesurfer when compared to manual segmentation

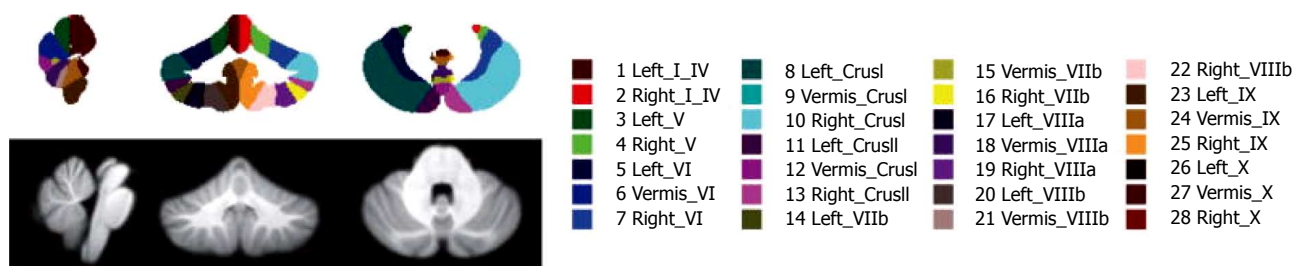


Figure 1 SUIE atlas (top) and template (bottom) showing the central cerebellar slice in the sagittal, coronal and axial planes. The atlas does not explicitly identify white matter apart from the dentate nuclei (from Ref. [55]).

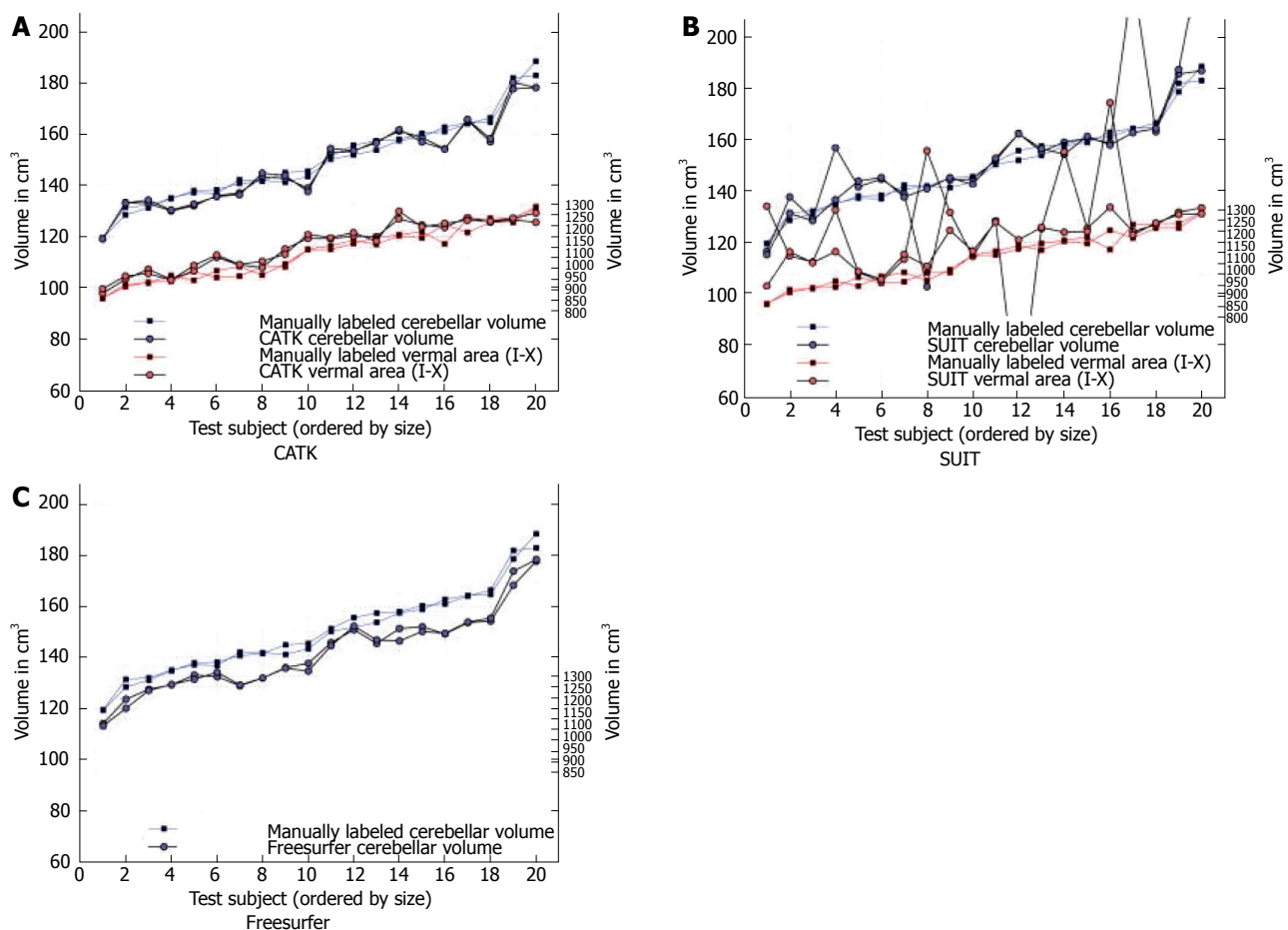


Figure 2 Comparative plots of total cerebellar volumes and combined vermal areas are shown against manually labeled examples, in 20 subjects with (A) CATK, (B) SUIE and (C) Freesurfer. Both test and retest are plotted, illustrating the repeatability of each method (from Ref. [55]).

(gold standard). However, the main limitation when compared to other softwares, is that CATK does not allow cerebellar hemisphere parcellation, although Price *et al.*^[55] in their paper stated a pending further improvement which would solve this issue and which would give higher image delineation (Figure 2).

ECCET is a semiautomatic toolkit based on a manually drawn region of interest ROI software. It is able to perform a fast semiautomatic segmentation after a manual outline drawing of few brainstem slices. It allows, when needed, manual editing in a 3D volume rendering mode (https://www.eccet.de/projects/neuro_en.html). This method has shown a good interobserver (ICC =

0.98, 95%CI = 0.74-0.99) and test-retest reliability (ICC = 0.99, 95%CI = 0.98-0.99) and the capability of avoiding some segmentation errors such as the inclusion of venous sinuses without the need of manual editing^[56].

Unfortunately, to date, all the above-mentioned softwares provide pipelines for one time point evaluation (cross-sectional), but not for longitudinal analysis along time. This gap has been fulfilled by Freesurfer, which is a software that allows a reliable automatic whole brain segmentation, with up to 40 subcortical structures, labelling each voxel in a normalized space of the brain volume^[57]. In addition to the cross-sectional analysis, Freesurfer comprises a longitudinal stream where each

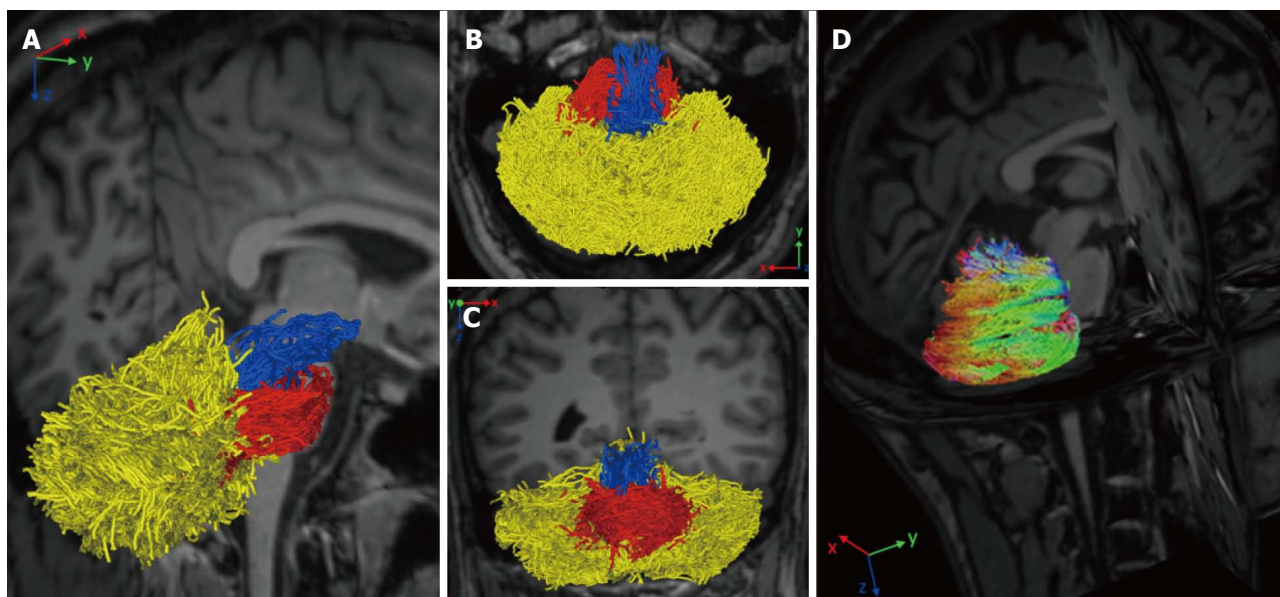


Figure 3 Reconstruction of cerebellar white matter tracts using constrained spherical deconvolution. Sagittal rotated view (A), superior axial view (B), and coronal view (C) show each fiber bundle manually colored: Superior cerebellar peduncle (blue), middle cerebellar peduncle (red), and hemispheric cerebellar tracts (yellow). The tridimensional sagittal rotated view shows color-coded cerebellar hemispheric streamlines according to the principal eigenvector's direction (with permission of Springer, from Ref. [63]).

time-point is co-registered to a subject-specific template by creating an average segmentation along time points, resulting in volume and GM thickness estimation^[57]. Although Freesurfer presents this important advantage, it does not allow sub-regional segmentation in cerebellar lobules^[55]. Moreover, manual editing of segmentation outputs is needed in order to improve volume evaluation reliability^[58]. Although the editing can be performed manually, resulting in a very time-consuming (up to 4h) and operator-dependent approach, Wang *et al.*^[58], in a recent paper, proposed an accurate and efficient new machine-learning based method in order to overcome this issue.

Diffusion weighted imaging and fiber tractography

Diffusion magnetic resonance imaging (dMRI) is a MRI technique able to detect water molecules diffusion inside brain tissue. While diffusion of water molecules in GM is isotropic, diffusion in WM is anisotropic, *i.e.*, it occurs in one main direction due to the presence of myelin barriers^[59]. The evaluation of diffusion in a three dimensional space and along at least 6 directions, allows the creation of a diffusion tensor matrix, which provides the bases of tractographic reconstruction of brain neural circuitry^[60]. Diffusion tensor imaging (DTI) and more advanced approaches (such as diffusion spectrum imaging or constrained spherical deconvolution) have been applied to determine cerebellar pathways and their connection with other supratentorial areas^[61-63] (Figure 3). Although conventional DTI techniques are the most used technique to reconstruct cerebellar pathways by means of tractography, they are also well known for their limitations in the study of connectivity. DTI, indeed, is limited by the inability to discriminate different fiber

populations with complex configurations at a voxel level (kissing fibers, bridging fibers, merging fibers, crossing fibers), thus leading to artefacts in fiber reconstructions and connectivity evaluations. Methods such as diffusion spectrum imaging and Q-ball imaging have been developed over the last few years to overcome these limitations; however, the more complex hardware set up and the longer acquisition times have limited so far their application in the clinical setting^[64]. Other promising techniques, such as diffusion kurtosis imaging (DKI), neurite orientation dispersion and density imaging (NODDI) and constrained spherical deconvolution can be performed within clinically feasible acquisition times^[65] (Figure 3). Moreover, all these techniques can be analyzed with both deterministic and probabilistic fiber reconstruction models. While deterministic models reconstruct streamlines (virtual fiber tracts) taking into account the principle eigenvector of fractional anisotropy (FA) in each voxel, probabilistic models generate a connectivity map from a larger numbers of possible pathways, obtaining the probability of each voxel to be connected to another^[66]. Regardless of the used approach, tractographic output can be used not only to reconstruct the spatial configuration of fiber tracts but also to measure diffusion parameters (*i.e.*, FA or mean diffusivity) at voxel level. However, it has been proved that, not only parameters' quantification but also the accuracy of tractographic results may be affected by the poor quality of the acquired data that can lead to the detection of false connections or to miss detection of a real connections between structures^[59]. Therefore, a better data quality, optimized in terms of SNR, spatial resolution, number of diffusion directions, and number and values of *b* values, with the choice of a proper tractography method, may improve the method performance avoiding

inaccuracy in structural connectivity analysis^[67]. Since cerebellar pathways tracking is particularly difficult due to the presence of sharp turning angles along their crossing, the assessment of cerebro-cerebellar and intra-cerebellar connectivity could especially benefit from data quality improvement^[61,63].

Resting state and task related fMRI

Functional MRI (fMRI) is based on the detection of the blood oxygen level-dependent (BOLD) changes that take place as a consequence of neuronal activity. An increase in neural activity leads to an increase in the arterial blood flow, in order to increase the activity itself. To this increase in the amount of oxygenated blood does not correspond a similar increase in oxygen extraction at the level of capillary bed, leading to a relative decrease of deoxyhemoglobin levels, that directly affects the MR signal.

fMRI experiments can be divided in task and rest-related. The first measure brain activity during a task performance, the second evaluate the interaction between different brain regions without the execution of any specific task, in a rest condition (resting-state fMRI - RS-fMRI).

With regard to task-based fMRI studies, two main experimental paradigms are commonly used^[68]. The first one is the so-called block design experiment, in which stimuli are presented to the subject in blocks of variable length alternated to blocks of rest, in which the stimulus is removed. MRI signals are then compared between the two conditions, in order to extrapolate the areas that show more activation during the execution of the task. The second is the event-related experimental design, in which the stimuli and the resting blocks are not alternated in a set sequence, but the administration, as well as the duration of the stimulus, are randomized.

RS-fMRI experiments can be analyzed using two major approaches. The first one is the seed-based approach, in which a region of interest is selected and the corresponding time-activity curve is extracted. Then, voxels with similar activation are searched whole brain, and are assumed to be functionally correlated to the chosen seed^[69]. The second method is the independent component analysis (ICA), a mathematical algorithm that allows to subdivide a multivariate and noisy signal in its subcomponents^[70]. In this approach, no a priori seeds are chosen, but the operator is asked to identify the component of interest, and discard those obtained from noise or physiological signals. ICA analysis has allowed the identification of preferential connections between specific cerebral structures, that take the name of resting state networks^[71]. Cerebellar lobules are not only hubs of several of these resting state networks (*i.e.*, lobule IX in the default mode network, crus I and II in the executive control network or lobule VI in the salience network)^[72], but also an entire and separate cerebellar network is recognized among the major resting state networks^[71].

With this knowledge, it is easy to understand how future improvement is warranted to increase the of

functional changes with respect of the cerebellar lobular anatomy. In particular, the possibility of increasing spatial resolution in fMRI experiments is a future challenge for investigating cerebellar functional connectivity due to the characteristic lobular anatomy. The increase in spatial resolution could further help in elucidating the exact functional lobular topography of the cerebellum, with regards to specific motor and cognitive functions^[73].

Proton magnetic resonance spectroscopy

Proton magnetic resonance spectroscopy (¹H-MRS) is an analytical method that allows the investigation of brain metabolites. Every metabolite at sufficient concentration level generates a specific peak in function of its resonance frequency^[74]. Since metabolic abnormalities occur earlier than structural MRI alterations, ¹H-MRS can provide a valid tool for early diagnosis and for monitoring of neurological diseases^[75].

The most commonly studied brain metabolites are the N-acetylaspartate, a marker of neuroaxonal integrity, choline containing compounds, a marker of membrane turnovers, creatine/phosphocreatine, a marker of energy metabolism, and myo-inositol, a marker of astroglial activation. From a quantification point of view, metabolites' levels are expressed as absolute quantifications or as ratios where the denominator is the creatine level which is assumed to be stable in normal as well as in many pathologic states^[76].

Although the infratentorial structures are often involved in neurodegenerative processes, strong B0 inhomogeneities due to nearby skull bone, scalp lipids and tissue/air interfaces constitute a technical challenge for the ¹H-MRS acquisition. In addition, the small size of cerebellum increases the risk of partial volume effects^[77], which can be accounted for by combining spectroscopic data with structural MRI segmentation^[78]. Nevertheless, ¹H-MRS of the infratentorial fossa is feasible^[79] and could provide an early biomarker of neuronal damage in cerebellar diseases, with even increased specificity when used in combination with other techniques^[80].

Perfusion MRI

Perfusion weighted imaging (PWI) allows the measurement of blood perfusion in brain tissue and it is categorized as: "minimally invasive" if requiring gadolinium injection (*i.e.*, dynamic susceptibility contrast MRI or DSC-MRI and dynamic contrast enhanced MRI or DCE-MRI) or "non-invasive" if no contrast agent is needed (*i.e.*, arterial spin labelling or ASL-MRI)^[81]. Data from either technique above is subsequently processed and normalized to estimate the well-known perfusion values: cerebral blood flow (CBF), cerebral blood volume (CBV), mean transit time (MTT), Ktrans and *etc.*, which are all representable on parametric color maps.

Cerebellar tissue is subject to a great blood supply, and measurement of local variations of blood request/availability is clinically relevant in the assessment of neurodegenerative diseases. Specifically, cerebral blood flow (CBF) alterations (*i.e.*, general or local CBF

reduction) appear to precede structural abnormalities (for example: atrophy). Moreover, the cerebellum has been used as a reference region for intensity normalization of "relative" Cerebral Blood Volume (rCBV), based on the assumption that its CBV is not affected in neurocognitive disorders^[82]. Although hard to eradicate, this assumption is nowadays obsolete, as alternative reference regions have recently been proposed and validated^[83].

With respect to the study of the cerebellum and the PCF, DSC-MRI provides higher spatial resolution, high sensitivity in transit time and whole-brain coverage in shorter scan times, and it is preferred in all situations where a fast assessment is required. DCE-MRI has the advantage of reducing artifacts especially for the measurement of CBV and Ktrans. ASL-MRI is often preferred in the study of neurodegenerative diseases for its complete lack of invasiveness, vessel selective capability^[84] and the best accuracy in absolute tissue perfusion quantification^[81]. Particular care in placing the "labeling plane" is essential to avoid artifacts in the lower cerebellar sections^[85]. Another limit of ASL-MRI is WM assessment, which is particularly challenging due to the low blood transit and the consequent low SNR^[86].

Unfortunately, despite the theoretical indications of each method, in the routine clinical settings, is the availability and practicality of the techniques that forces the choice, rather than its potential performance. This could explain the more frequent use of DSC and DCE imaging, faster, easy to perform and widely installed on most clinical scanners, compared to the use of ASL.

MRI AND CLINICAL APPLICATIONS ON NEURODEGENERATIVE DISEASES

Multiple sclerosis

Multiple Sclerosis (MS) is an inflammatory/demyelinating disease of the central nervous system (CNS) characterized by heterogeneous symptoms and signs that can present a relapsing remitting (RR) or a progressive course. In 1877 Jean Martin Charcot first described the disease as a triad of symptoms consisting of nystagmus, dysarthria and ataxia^[87], thus underlining the dominant role of cerebellar deficits. Not only is the cerebellum frequently involved by the disease pathological processes but the presence of MRI visible infratentorial lesions provides high specificity to the diagnostic criteria for MS^[88]. Indeed, 31% of patients with a clinically isolated syndrome (CIS) present with at least one infratentorial lesion and about 20.5% with a cerebellar lesion. The detection of a cerebellar lesion at onset is associated with an increased risk of conversion to MS^[89]. In patients with a clinically defined MS, cerebellar lesions have been described in up to 49% of cases and patients with a progressive form have an increased number of PCF lesions when compared to patients with a RR type^[90]. Disease pathology involves not only the cerebellar WM but also the GM; in fact, cortical cerebellar lesions are

observed in patients with MS, even at the early stages of the disease, and correlate with the cerebellar functional score of the expanded disability status scale (EDSS)^[91]. Longitudinal studies have shown cerebellar GM volume loss and an increased number of cortical lesions in both CIS, RR and progressive patients^[92,93].

Volumetry changes

Along with cerebral atrophy, also cerebellar volume loss occurs in patients with MS, at all the disease stages. Edwards and coworkers found reduced global cerebellar volumes in patients with a secondary progressive (SP) form when compared to RR patients, and in both groups when compared to healthy controls^[94]. However, in a more recent study, when compared to healthy controls only MS patients with a SP form, but not RR or patients with benign MS, showed lower cerebellar volumes^[50]. When cerebellar WM and GM are considered separately, study results are discordant. Ramasamy *et al.*^[95] found a reduced cerebellar WM but not GM volume in CIS and MS patients when compared to healthy controls. However, Anderson and coworkers detected a reduced cerebellar GM volume in RR and SP MS patients versus controls and only a trend of significance, when comparing WM volumes, between SP MS and controls^[96]. In the latter study, cerebellar GM and WM volumes were related with performance at the nine-hole peg test, highlighting the clinical relevance of measures of cerebellar volumes. A greater loss of GM in patients with a progressive course and its correlation with measures of clinical outcome are findings mirroring the process at the whole brain level.

Structural connectivity changes

DTI has been widely used for the study of cerebellar WM, in particular to evaluate the damage of the cerebellar peduncles and its clinical impact. Anderson *et al.*^[97] found reduced FA and increased radial diffusivity values in the middle cerebellar peduncle in patients with primary progressive (PP) MS; DTI metrics correlated with clinical impairment both of the upper and lower limbs. A study on a cohort of patients at different stages of the disease revealed greater mean, axial and radial diffusivity and reduced FA in MS patients, when compared to healthy controls, at the level of the middle and superior cerebellar peduncles; moreover, when compared to cerebellar peduncles T2 lesion load or atrophy, diffusivity measures better distinguished between patients with a worse EDSS score^[98]. Disability in RR patients also correlated with the FA values of the cerebellar normal appearing WM^[99].

Functional MR changes

MS is characterized by a reorganization of the functional connectivity. Functional MR studies with motor tasks revealed an increased activation in several cortical areas within the sensorimotor network, including the cerebellum, in patients when compared to healthy controls^[100,101] (Figure 4). The altered functional cerebellar connectivity could represent a compensatory mechanism to WM

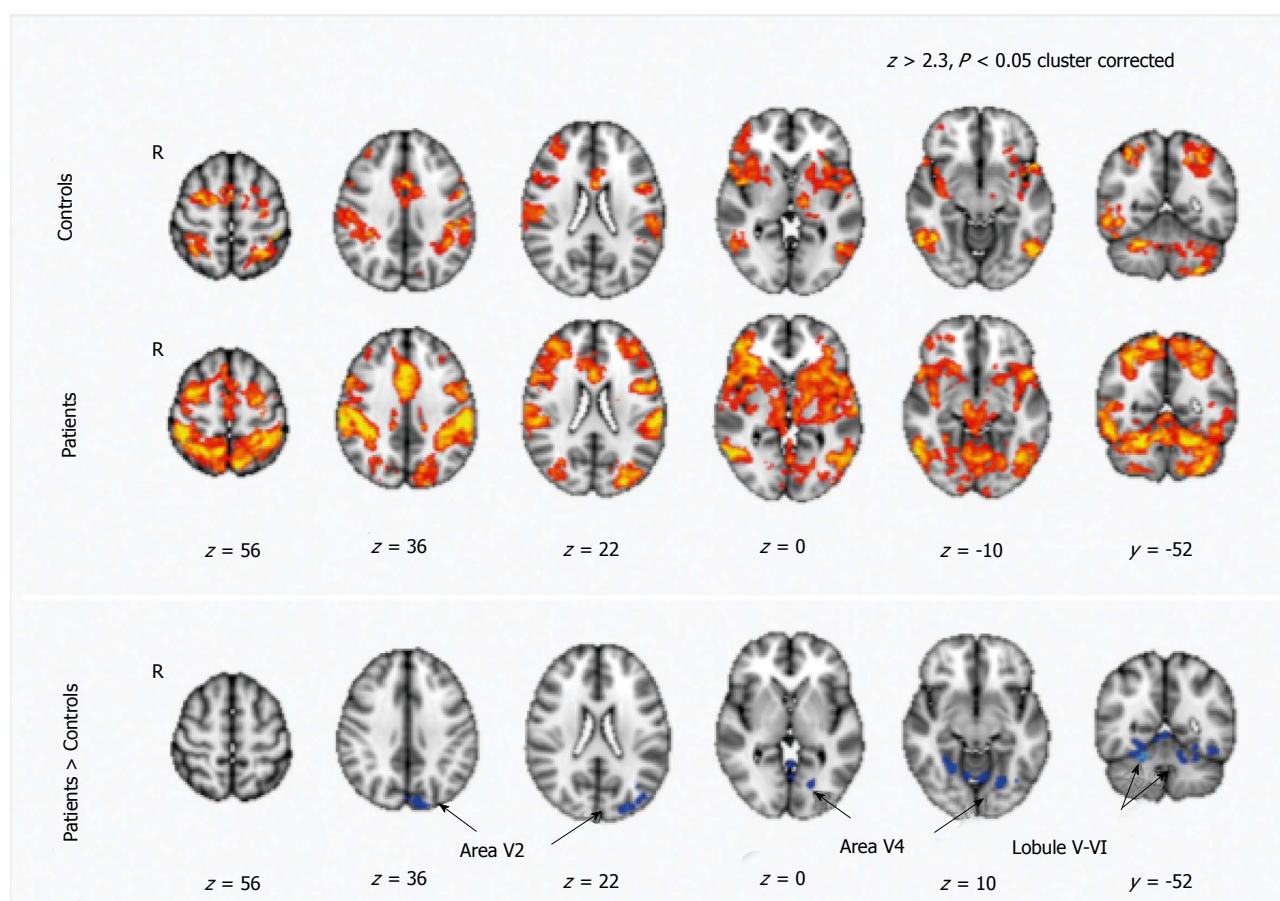


Figure 4 Motor training-dependent functional magnetic resonance imaging signal changes in healthy volunteers and in MS patients. Maps of training-related functional magnetic resonance imaging signal changes are reported in healthy volunteers (indicated as controls) and in patients ($Z > 2.3$, $P < 0.05$, cluster corrected). Comparison between patients and controls show a higher signal reduction in the patients in regions corresponding to the secondary visual areas (V2 and V4) and in the cerebellum (lobule V-VI) (from Ref. [100]). V5: Visual cortex; R5: Right hemisphere; fMRI: Functional magnetic resonance imaging.

damage; accordingly, in RR MS patients a damage in the dentatorubrothalamic tract, assessed by means of DTI, was related to an increased functional connectivity between right sensorimotor cortex and cerebellum^[101]. The cerebellum activation is also increased in patients with greater perceived fatigue where fatigue is conceived as a correlate of an increased resource demand for motor activities^[102].

Cerebellum and cognitive impairment

Besides the classical motor clinical features associated with cerebellar dysfunction, lately more attention has been focused on the role of cerebellum in cognitive impairment. MS patients with cerebellar signs perform worse at the symbol digit modalities test (SDMT) and the paced auditory serial addition test (PASAT); moreover, the PASAT execution is predicted by cerebellar lesion volume^[103]. In particular the posterior cerebellum has been implicated in cognitive processing; in MS patients, a reduced posterior volume predicted a worse cognitive performance^[50]. Information processing speed impairment has been associated with GM atrophy of the posterior lobules, especially at the level of the vermis VI^[104]. As with

motor tasks, a functional reorganization could also occur in response to the impairment of cognitive processes. Recently, a greater functional connectivity of the dentate nucleus with frontal and parietal cortical areas was detected in MS patients versus controls^[105,106] and the increased connectivity was related to a better cognitive performance. Moreover, an increased connectivity between anterior cingulate cortex and cerebellum was also associated with a better performance at PASAT in CIS, RR and SP patients versus controls and authors suggested an adaptive mechanism^[107].

Dentate nuclei hyperintensity

The hyperintense signal on T1-weighted images at the level of dentate nucleus has been detected in almost 50% of patients with a secondary progressive phase of the disease, in contrast to what found in the RR or PP form^[108]. Although this change in signal could be related to the reduction in the number and axosomatic synapses in the dentate nucleus as documented by pathological studies^[109], an association between the nuclei hyperintensity in T1-weighted images and Gadolinium retention has recently received greater attention^[110].

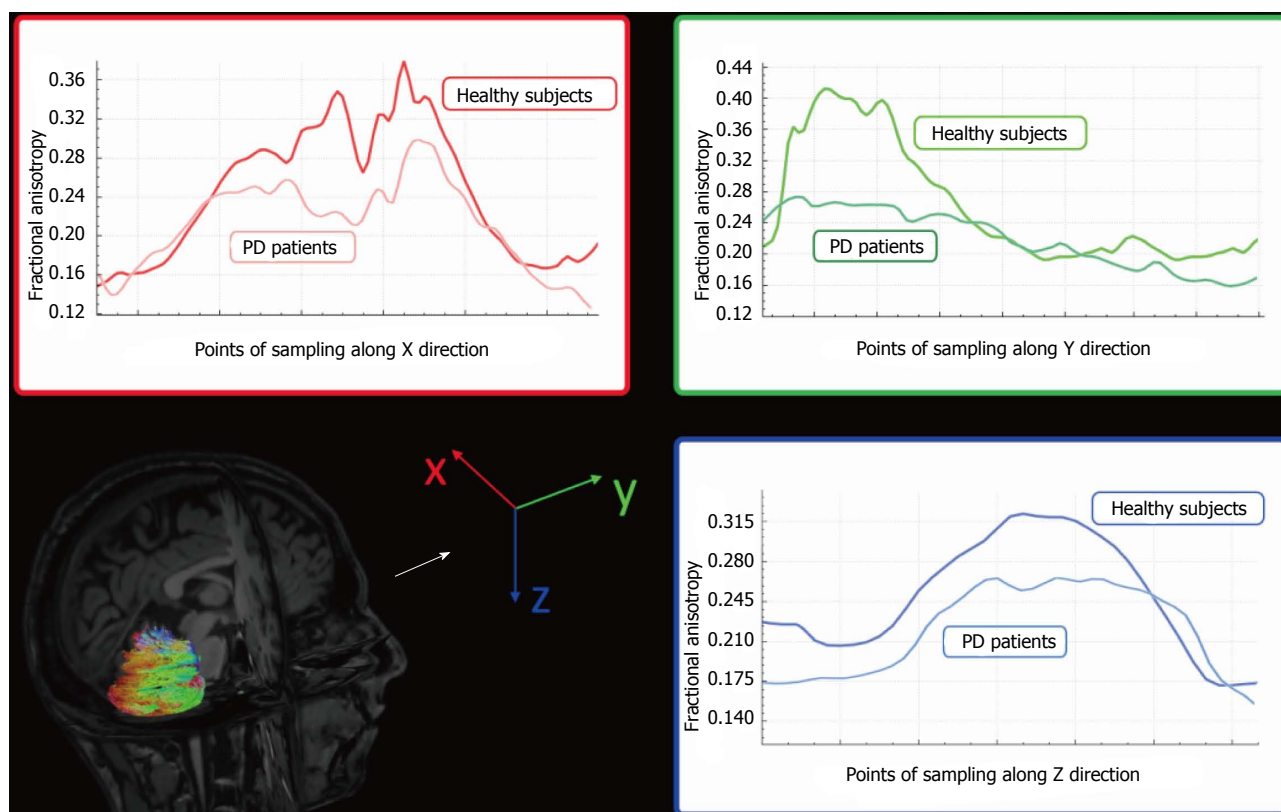


Figure 5 Graphic representations of Fractional Anisotropy mean decrement along X (red), Y (green), and Z (blue) direction samplings of Parkinson's disease patients compared to healthy subjects. Colors follow principal eigenvector's directions (with permission of Springer, from Ref. [63]). PD: Parkinson's disease.

PARKINSON'S DISEASE AND OTHER MOVEMENT DISORDERS

Parkinson's disease

Parkinson's disease (PD) is a neurodegenerative disorder pathologically characterized by the loss of dopaminergic neurons of the pars compacta of the substantia nigra; clinical features include motor, in particular rest tremor, bradykinesia and rigidity, and non-motor symptoms. The role of cerebellum in the physiopathology of this frequent neurodegenerative disorder has received increasing interest. Studies on monkeys discovered direct anatomical connections between cerebellum and basal ganglia, in particular with the subthalamic nuclei and the striatum^[8,111]. Such findings have been confirmed with a DTI study in humans^[112]. Interestingly, patients receiving deep brain stimulation had a clinical benefit when the electrode was positioned nearby one of these basal ganglia-cerebellum connections, in particular the dentato-thalamic tract.

Volumetry changes

Cerebellar atrophy has been documented in patients with PD. MRI morphometric studies have shown cerebellar volume loss at the level of the left cerebellum when compared to controls^[113], and at the level of the right quadrangular lobe and declive in patients with tremor compared to those without, thus suggesting a possible role of cerebellum in the genesis of rest tremor^[114]. A more

recent study confirmed cerebellar GM atrophy, which correlated with a reduced connectivity between cerebellum and sensorimotor, dorsal attention and default networks and an increased connectivity with the frontoparietal network^[115]. Altogether these results confirm the role of cerebellum in the physiopathology of motor symptoms in PD. Atrophy occurs since cerebellum is involved in the neurodegenerative pathological process of the disease, with the accumulation of α -synuclein and neuronal loss.

Structural connectivity changes

DTI studies have detected decreased FA in the cerebellar hemispheres of patients with PD when compared to healthy controls (Figure 5)^[63,116]. Although no differences in DTI parameters in superior and middle cerebellar peduncles have been detected between patients with PD and healthy subjects^[63], DTI metrics of the superior cerebellar peduncles could be helpful in differentiating PD and other parkinsonism, such as progressive supranuclear palsy (PSP)^[117].

Functional MR changes

Cerebellar hyperactivation has been showed and confirmed in several studies on patients with PD, both with akinesia-rigidity subtype and with tremor subtype. Whether the contribution of cerebellum is mostly an adaptive mechanism or a primary pathologic change of the disease is still a matter of debate. In a resting-state fMRI study, Wu *et al.*^[118] observed an increased activation

in the cerebellum in PD patients versus healthy controls; moreover, the altered pattern of activation was normalized after levodopa administration. A substitutive hyperactivity of the cerebello-thalamo-cortical circuit has been proposed as a mechanism to compensate the hypoactivation of the striato-thalamo-cortical circuit in hypokinetic patients; however, for PD tremor subtype, a dysfunction in the cerebello-thalamo-cortical circuit has been advanced as a physiopathologic mechanism for rest tremor^[118,119].

Multiple systemic atrophy

Multiple systemic atrophy (MSA) is a movement disorder, with a poor prognosis, which has two clinical phenotypes: one with a prominent akinetic-rigid parkinsonism (parkinsonian variant, MSA-P) and the other with a progressive ataxia (cerebellar variant, MSA-C). It has been suggested that imaging of cerebellum could be useful in the differential diagnosis of MSA. Atrophy of the middle cerebellar peduncles is frequent in patients with MSA and reduced volume of basal ganglia, middle and inferior cerebellar peduncles and pons have been found in the parkinsonian subtype of MSA, when compared with controls and PD patients^[120]. Moreover, both MSA-P and MSA-C patients were found to have higher MD values in cerebellar hemispheres when compared to PD and PSP patients^[121]. Brainstem and middle cerebellar peduncles atrophy have also been found to be very specific for the cerebellar subtype of MSA when compared to idiopathic late-onset cerebellar ataxia^[122].

Dystonia

Dystonia is a disorder characterized by sustained and abnormal spontaneous muscle contractions. It can be classified according to the etiology (inherited or acquired) or the topographic distribution. Cerebellar dysfunction has been implicated in the physiopathology of dystonia. Morphological cerebellar abnormalities have been reported in 14% of patients with cervical or segmental dystonia^[123]. Focal cerebellar lesions have been associated with dystonia and cerebellar atrophy has been described in patients with writer's cramp^[124]. Besides morphological studies, several functional studies have shown an increased activation in cerebellum in patients with writer's cramp^[125] and in patients with blepharospasm^[126].

Hereditary ataxias

Ataxias are an heterogeneous group of conditions characterized by slowly progressive incoordination of gait, often associated with a reduction of coordination of hands, speech, and oculomotor signs^[127]. Ataxias can be subdivided, basing on the etiology behind the development of the condition, in three major groups: acquired ataxias, nonhereditary degenerative ataxias and hereditary ataxias (HA), which can be further divided in dominant and recessive^[127]. Spinocerebellar ataxia type 3 (SCA3) is the most frequent type of dominant ataxia, followed by SCA2 and SCA6, while Friedreich Ataxia (FRDA) and ataxia-telangiectasia (AT) are respectively the first and the second most

common type of recessive ataxias, with FRDA that is, independently from the inheritance, the most frequent ataxia in terms of incidence^[128].

Volumetry changes

Atrophy of the cerebellar cortex is not a distinguish feature of all the HA. Different patterns of atrophy can be identified, depending on the degree of cerebellar atrophy and the involvement of midbrain structures. In particular, SCA3 and SCA2 are characterized by the presence of cortical, cerebellar and pons atrophy^[129]. On the other hand, SCA6 shows a pattern of pure cortical cerebellar atrophy, with a relative sparing of midbrain structures^[130]. With regard to recessive ataxias, FRDA is characterized by a prominent spinal cord atrophy^[131] compared to cerebellar cortical structures^[132], with atrophy that, when significant, affects mainly the lateral cerebellar hemispheres^[133]. Finally, AT is characterized by superior cerebellar hemispheres atrophy, in particular of the vermis, which appears hypoplastic in its inferior portion^[134-137].

Structural connectivity changes

Unlike volumetric measures, almost all the major HA show similar microstructural changes affecting infratentorial WM tracts. Indeed, SCA3 patients showed a significant FA reduction in different cerebellar areas, including both anterior and posterior cerebellar lobes, nodule, culmen, dentate, fastigial, lingual, and all three cerebellar peduncles, as well as in pons and midbrain^[138]. These abnormalities were correlated with clinical variables, such as scale for the assessment and rating of ataxia (SARA) scores or disease duration^[138,139]. In SCA2, significant microstructural changes were present in cerebellar WM, brainstem and cerebellar peduncle^[140,141], with changes in the mode of anisotropy that were lower in SCA2 patients compared to healthy controls in a longitudinal evaluation^[141]. Unlike in SCA3, no correlation with clinical variables emerged for these infratentorial clusters of microstructural changes in SCA2. In FRDA, microstructural changes were found to affect predominantly cerebellar peduncles^[142-145], as well as cerebellar hemispheres and vermis^[144] and to be associated with clinical disability^[142-144]. Finally, in AT patients a reduction of mean diffusivity was reported within cerebellar peduncle regions^[146] (Figure 6).

Functional MR changes

Similar to structural connectivity, functional connectivity changes are present in almost all HA. However, these modifications are not limited to a somehow expected reduction of FC in HA patients compared to healthy controls, but also increase in FC are reported in some HA, probably due to compensatory phenomena, reflecting the known heterogeneity of this group of conditions. Indeed, a significant increase of activation of the ventral part of the dentate nuclei, but not of the cerebellar cortex, was found during an hand-movement task fMRI experiment in SCA3 patients compared to healthy controls, suggesting a

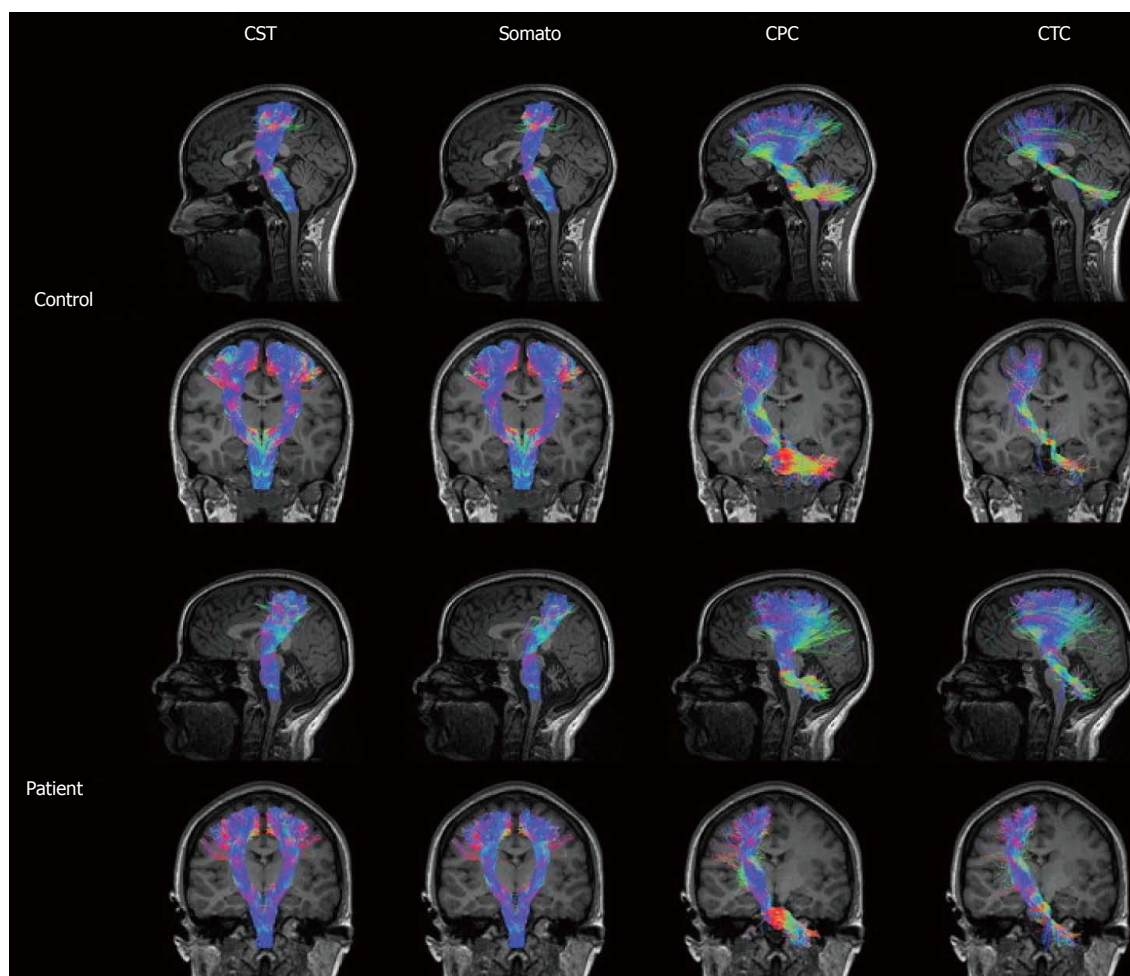


Figure 6 Somatosensory motor tracts in a representative control and ataxia telangiectasia (A-T) subject (age 23). Control tracts are displayed in the first and second rows comprising the left sagittal (first row) tracts, left and right coronal (second row) corticospinal (CST) and somatosensory tracts, and left coronal (second row) cortico-ponto-cerebellar (CPC) and cerebellar-thalamo-cortical (CTC) tracts. Patient tracts are displayed in the third and fourth rows comprising the left sagittal (third row) tracts, left and right coronal (fourth row) CST and somatosensory tracts, and left coronal (fourth row) CPC and CTC tracts. Tract colors are based on the direction of water diffusion (Blue: Ascending–descending diffusion; Red: Left–right diffusion; Green: Anterior–posterior diffusion). Compared to motor pathways in age matched controls, A-T CST and somatosensory pathways display a morphological thinning of tracts at the level of the thalamus in the coronal view. In addition, A-T CPC and CTC pathways display morphological thinning of tracts in the cerebellum at the position of the medial cerebellar peduncles (from Ref. [147]).

compensatory phenomenon of the *cerebrocerebellum* to a prominent damage of the *spinocerebellum*^[147]. Moreover, a recent fMRI study, involving a bilateral audiopaced thumb movements paradigm, showed a diminished movement synchronization in SCA3 patients^[148] that would suggest the presence of functional reorganization of the motor network and a potential role of fMRI as a tool to monitor the disease^[148]. In SCA2, a seed-based fMRI analysis showed a decreased putaminal connection with the pons, together with a decreased connectivity between the rostral sensorimotor area and both cerebellum and pons^[149]. Furthermore, a decrease of the functional connectivity of the cerebellar components of the default mode, executive and right fronto-parietal networks was described in SCA2, unrelated to the cortical gray matter volume loss^[150], with some authors that showed a significant correlation between both motor and neuropsychological scores and the abnormal cerebellar functional connectivity strength^[151]. In SCA6 patients, a significantly higher activation at the level of the lobules V and VI, as well as in the dentate

nuclei, was detected compared to controls when performing a hand-movement task fMRI experiment^[147]. Likewise, in FRDA patients the same motor task showed a higher activation mainly prominent at the level of lobules V and VI and dentate nuclei, compared to healthy control^[147]. Furthermore, a working memory task fMRI experiment showed that FRDA patients had a decrease functional connectivity between cerebellum and prefrontal areas, with a correlation between disease severity and cerebellar dysfunction^[152].

Alzheimer's disease

Alzheimer's disease (AD) is the most common cause of dementia and it is preceded by a prodromal phase, called mild cognitive impairment (MCI), characterized by a deficit in one or more cognitive domains. The role of cerebellum involvement in AD is controversial. While a volumetric MRI study in patients with AD, MCI and healthy controls found a volume loss at the level of the posterior cerebellar lobes in AD patients compared to healthy

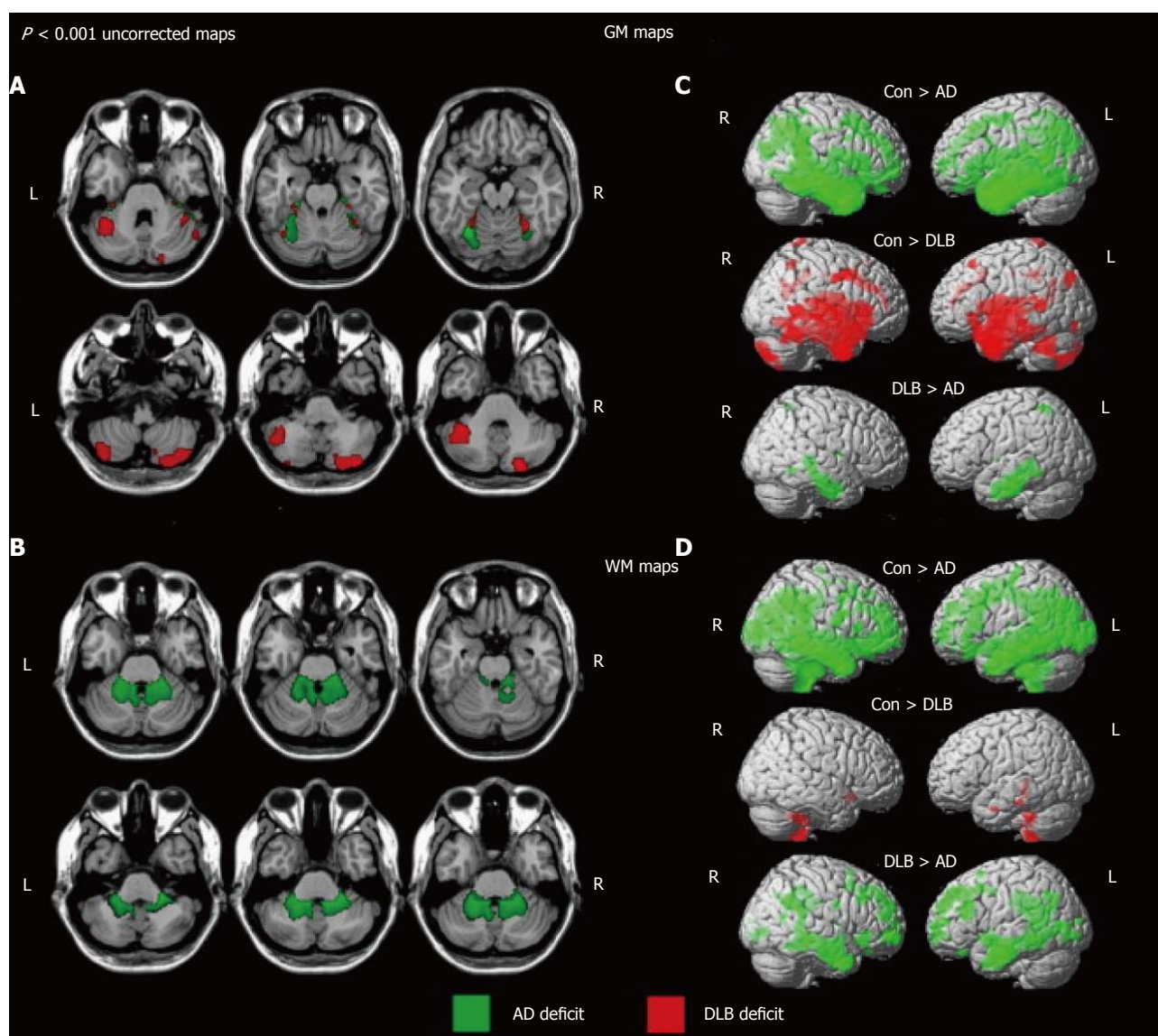


Figure 7 Significant cerebellar GM and WM loss in Alzheimer's disease. A: Significant cerebellar GM loss in Alzheimer's disease (green) and dementia with Lewy bodies (red) relative to healthy older subjects; B: Significant cerebellar WM loss in AD relative to healthy older subjects; C and D: Whole brain maps depicting significant regions of GM (C) and WM (D) loss between groups. Results superimposed on a MRI T1 brain template image (L = left, R = right). AD: Alzheimer's disease; DLB: Dementia with Lewy bodies (from Ref. [154]). GM: Gray matter; WM: White matter.

controls, no significant differences were showed between patients with MCI and healthy controls^[153]. Another study detected a regional GM atrophy in cerebellar lobule VI in patients with AD^[154] (Figure 7). These findings were not confirmed^[155] in a more recent study, suggesting that the decrease of cerebellar volume could be influenced by the patients' age. This is supported by the findings of cerebellar atrophy in patients with a late-onset, but not early-onset AD^[156] and by the presence of cerebellar atrophy in cognitively preserved old subjects^[157].

CONCLUSION

The cerebellum plays a key role in the control of motor and cognitive functions due to the multiple connections to the forebrain, the thalamus, and the spinal cord. However, the cerebellar complex anatomical structure and its

location in the posterior fossa represent a challenge for *in vivo* structural and cerebellar neuroimaging. The recent advancement in MRI hardware and software and the development of more accurate and robust algorithms for image analysis have improved the structural and functional assessment of the cerebellum. This is of paramount importance due to the frequent and early involvement of the cerebellum in several neurodegenerative diseases. Therefore, MRI measures of cerebellar structure and function could serve as early and sensitive marker of disease progression and help monitor response to current or experimental treatments.

REFERENCES

- 1 Nieuwenhuys R, Voogd J, Huijzen Cv. The human central nervous system. 4th ed. New York: Springer, 2008: 807-840 [DOI: 10.1007/97

- 8-3-540-34686-9]
- 2 **Barahona ML MJ**, Querol Pascual R, Alvarez-Linera Prado J, Gañan Presmanes Y, Fernández Gil MÁ. Structural and Functional anatomy of cerebellum. More than a motor conception. Poster No: C-0497 Congress: ECR 2011 Type: Educational Exhibit 2011 [DOI: 10.1594/ecr2011/C-0497]
 - 3 **Glickstein M**, May JG 3rd, Mercier BE. Corticopontine projection in the macaque: the distribution of labelled cortical cells after large injections of horseradish peroxidase in the pontine nuclei. *J Comp Neurol* 1985; **235**: 343-359 [PMID: 3998215 DOI: 10.1002/cne.902350306]
 - 4 **Schmahmann JD**. From movement to thought: anatomic substrates of the cerebellar contribution to cognitive processing. *Hum Brain Mapp* 1996; **4**: 174-198 [PMID: 20408197 DOI: 10.1002/(SICI)1097-0193(1996)4:3<174::AID-HBM3>3.0.CO;2-0]
 - 5 **Strick PL**, Dum RP, Fiez JA. Cerebellum and nonmotor function. *Annu Rev Neurosci* 2009; **32**: 413-434 [PMID: 19555291 DOI: 10.1146/annurev.neuro.31.060407.125606]
 - 6 **Milardi D**, Arrigo A, Anastasi G, Cacciola A, Marino S, Mormina E, Calamuneri A, Bruschetta D, Cutroneo G, Trimarchi F, Quartarone A. Extensive Direct Subcortical Cerebellum-Basal Ganglia Connections in Human Brain as Revealed by Constrained Spherical Deconvolution Tractography. *Front Neuroanat* 2016; **10**: 29 [PMID: 27047348 DOI: 10.3389/fnana.2016.00029]
 - 7 **Dum RP**, Strick PL. An unfolded map of the cerebellar dentate nucleus and its projections to the cerebral cortex. *J Neurophysiol* 2003; **89**: 634-639 [PMID: 12522208 DOI: 10.1152/jn.00626.2002]
 - 8 **Hoshi E**, Tremblay L, Féger J, Carras PL, Strick PL. The cerebellum communicates with the basal ganglia. *Nat Neurosci* 2005; **8**: 1491-1493 [PMID: 16205719 DOI: 10.1038/nm1544]
 - 9 **Marr D**. A theory of cerebellar cortex. *J Physiol* 1969; **202**: 437-470 [PMID: 5784296 DOI: 10.1113/jphysiol.1969.sp008820]
 - 10 **Schmahmann JD**, Sherman JC. The cerebellar cognitive affective syndrome. *Brain* 1998; **121** (Pt 4): 561-579 [PMID: 9577385 DOI: 10.1093/brain/121.4.561]
 - 11 **Balsters JH**, Ramnani N. Symbolic representations of action in the human cerebellum. *Neuroimage* 2008; **43**: 388-398 [PMID: 18692577 DOI: 10.1016/j.neuroimage.2008.07.010]
 - 12 **Balsters JH**, Ramnani N. Cerebellar plasticity and the automation of first-order rules. *J Neurosci* 2011; **31**: 2305-2312 [PMID: 21307266 DOI: 10.1523/JNEUROSCI.4358-10.2011]
 - 13 **Raut AA**, Naphade PS, Chawla A. Imaging of skull base: Pictorial essay. *Indian J Radiol Imaging* 2012; **22**: 305-316 [PMID: 23833423 DOI: 10.4103/0971-3026.111485]
 - 14 **Borges A**. Imaging of the central skull base. *Neuroimaging Clin N Am* 2009; **19**: 669-696 [PMID: 19959012 DOI: 10.1016/j.nic.2009.11.001]
 - 15 **Laine FJ**, Nadel L, Braun IF. CT and MR imaging of the central skull base. Part 2. Pathologic spectrum. *Radiographics* 1990; **10**: 797-821 [PMID: 2217972 DOI: 10.1148/radiographics.10.5.2217972]
 - 16 **Ertl-Wagner B**, Eftimov L, Blume J, Bruening R, Becker C, Cormack J, Brueckmann H, Reiser M. Cranial CT with 64-, 16-, 4- and single-slice CT systems-comparison of image quality and posterior fossa artifacts in routine brain imaging with standard protocols. *Eur Radiol* 2008; **18**: 1720-1726 [PMID: 18389247 DOI: 10.1007/s00330-008-0937-6]
 - 17 **Jones TR**, Kaplan RT, Lane B, Atlas SW, Rubin GD. Single- versus multi-detector row CT of the brain: quality assessment. *Radiology* 2001; **219**: 750-755 [PMID: 11376264 DOI: 10.1148/radiology.219.3.r01jn47750]
 - 18 **Kamalian S**, Atkinson WL, Florin LA, Pomerantz SR, Lev MH, Romero JM. Emergency department CT screening of patients with nontraumatic neurological symptoms referred to the posterior fossa: comparison of thin versus thick slice images. *Emerg Radiol* 2014; **21**: 251-256 [PMID: 24469596 DOI: 10.1007/s10140-014-1194-4]
 - 19 **Rozeik C**, Kotterer O, Preiss J, Schütz M, Dingler W, Deininger HK. Cranial CT artifacts and gantry angulation. *J Comput Assist Tomogr* 1991; **15**: 381-386 [PMID: 2026796 DOI: 10.1097/00004728-199105000-00007]
 - 20 **Levy JM**, Hupke R. Composite addition technique: a new method in CT scanning of the posterior fossa. *AJNR Am J Neuroradiol* 1991; **12**: 686-688 [PMID: 1882744]
 - 21 **Moström U**, Ytterbergh C. Artifacts in computed tomography of the posterior fossa: a comparative phantom study. *J Comput Assist Tomogr* 1986; **10**: 560-566 [PMID: 3734195 DOI: 10.1097/00004728-198607000-00002]
 - 22 **Glover GH**, Pelc NJ. Nonlinear partial volume artifacts in x-ray computed tomography. *Med Phys* 1980; **7**: 238-248 [PMID: 7393149 DOI: 10.1118/1.594678]
 - 23 **Joseph PM**, Spital RD. A method for correcting bone induced artifacts in computed tomography scanners. *J Comput Assist Tomogr* 1978; **2**: 100-108 [PMID: 670461 DOI: 10.1097/00004728-197801000-00017]
 - 24 **Morelli JN**, Runge VM, Ai F, Attenberger U, Vu L, Schmeets SH, Nitz WR, Kirsch JE. An image-based approach to understanding the physics of MR artifacts. *Radiographics* 2011; **31**: 849-866 [PMID: 21571661 DOI: 10.1148/rg.313105115]
 - 25 **Hwang DY**, Silva GS, Furie KL, Greer DM. Comparative sensitivity of computed tomography vs. magnetic resonance imaging for detecting acute posterior fossa infarct. *J Emerg Med* 2012; **42**: 559-565 [PMID: 22305149 DOI: 10.1016/j.jemermed.2011.05.101]
 - 26 **Young IR**, Bydder GM, Hall AS, Steiner RE, Worthington BS, Hawkes RC, Holland GN, Moore WS. The role of NMR imaging in the diagnosis and management of acoustic neuroma. *AJNR Am J Neuroradiol* 1983; **4**: 223-224 [PMID: 6410706 DOI: 10.1097/00004728-198302000-00049]
 - 27 **Wilms G**, Decrop E, Plets C, Demaerel P, Marchal G, Van Hecke P, Baert AL. Magnetic resonance imaging in acoustic neurinoma. Comparison with CT. *J Belge Radiol* 1989; **72**: 151-158 [PMID: 2793814]
 - 28 **Wenz F**, Hess T, Knopp MV, Weisser G, Blüml S, Schad LR, Hawighorst H, van Kaick G. 3D MPRAGE evaluation of lesions in the posterior cranial fossa. *Magn Reson Imaging* 1994; **12**: 553-558 [PMID: 8057759 DOI: 10.1016/0730-725X(94)92449-X]
 - 29 **Kallmes DF**, Hui FK, Mugler JP 3rd. Suppression of cerebrospinal fluid and blood flow artifacts in FLAIR MR imaging with a single-slab three-dimensional pulse sequence: initial experience. *Radiology* 2001; **221**: 251-255 [PMID: 11568348 DOI: 10.1148/radiol.2211001712]
 - 30 **Bakshi R**, Caruthers SD, Janardhan V, Wasay M. Intraventricular CSF pulsation artifact on fast fluid-attenuated inversion-recovery MR images: analysis of 100 consecutive normal studies. *AJNR Am J Neuroradiol* 2000; **21**: 503-508 [PMID: 10730642]
 - 31 **Winkelmann R**, Börmert P, Dössel O. Ghost artifact removal using a parallel imaging approach. *Magn Reson Med* 2005; **54**: 1002-1009 [PMID: 16155885 DOI: 10.1002/mrm.20640]
 - 32 **Rydborg JN**, Hammond CA, Grimm RC, Erickson BJ, Jack CR Jr, Huston J 3rd, Riederer SJ. Initial clinical experience in MR imaging of the brain with a fast fluid-attenuated inversion-recovery pulse sequence. *Radiology* 1994; **193**: 173-180 [PMID: 8090888 DOI: 10.1148/radiology.193.1.8090888]
 - 33 **Lavdas E**, Tsougos I, Kogia S, Gratsias G, Svolos P, Roka V, Fezoulidis IV, Kapsalaki E. T2 FLAIR artifacts at 3-T brain magnetic resonance imaging. *Clin Imaging* 2014; **38**: 85-90 [PMID: 24359643 DOI: 10.1016/j.clinimag.2013.10.004]
 - 34 **Schaefer PW**, Grant PE, Gonzalez RG. Diffusion-weighted MR imaging of the brain. *Radiology* 2000; **217**: 331-345 [PMID: 11058626 DOI: 10.1148/radiology.217.2.r00nv24331]
 - 35 **Holodny AI**, Ollenschlager M. Diffusion imaging in brain tumors. *Neuroimaging Clin N Am* 2002; **12**: 107-124, x [PMID: 11998248 DOI: 10.1016/S1052-5149(03)00072-8]
 - 36 **Ayanzen RH**, Bird CR, Keller PJ, McCully FJ, Theobald MR, Heiserman JE. Cerebral MR venography: normal anatomy and potential diagnostic pitfalls. *AJNR Am J Neuroradiol* 2000; **21**: 74-78 [PMID: 10669228]
 - 37 **Wu Z**, Mittal S, Kish K, Yu Y, Hu J, Haacke EM. Identification of calcification with MRI using susceptibility-weighted imaging: a case study. *J Magn Reson Imaging* 2009; **29**: 177-182 [PMID: 19097156 DOI: 10.1002/jmri.21617]
 - 38 **Lesser FD**, Derbyshire SG, Lewis-Jones H. Can computed tomography and magnetic resonance imaging differentiate between malignant pathology and osteomyelitis in the central skull base? *J Laryngol Otol* 2015; **129**: 852-859 [PMID: 26314320 DOI: 10.1017/

- S0022215115001991]
- 39 **Fischbein NJ**, Kaplan MJ. Magnetic resonance imaging of the central skull base. *Top Magn Reson Imaging* 1999; **10**: 325-346 [PMID: 10643825 DOI: 10.1097/00002142-199910000-00005]
- 40 **Curtin HD**, Chavali R. Imaging of the skull base. *Radiol Clin North Am* 1998; **36**: 801-817, v-vi [PMID: 9747190 DOI: 10.1016/S0033-8389(05)70065-8]
- 41 **Marques JP**, Gruetter R, van der Zwaag W. In vivo structural imaging of the cerebellum, the contribution of ultra-high fields. *Cerebellum* 2012; **11**: 384-391 [PMID: 20596807 DOI: 10.1007/s12311-010-0189-2]
- 42 **Hawkes R**, Blyth S, Chockkan V, Tano D, Ji Z, Mascher C. Structural and molecular compartmentation in the cerebellum. *Can J Neurol Sci* 1993; **20** Suppl 3: S29-S35 [PMID: 8334590]
- 43 **Manto M**. The cerebellum, cerebellar disorders, and cerebellar research—two centuries of discoveries. *Cerebellum* 2008; **7**: 505-516 [PMID: 18855093 DOI: 10.1007/s12311-008-0063-7]
- 44 **Marques JP**, van der Zwaag W, Granziera C, Krueger G, Gruetter R. Cerebellar cortical layers: in vivo visualization with structural high-field-strength MR imaging. *Radiology* 2010; **254**: 942-948 [PMID: 20177104 DOI: 10.1148/radiol.09091136]
- 45 **Tanenbaum LN**. Clinical 3T MR imaging: mastering the challenges. *Magn Reson Imaging Clin N Am* 2006; **14**: 1-15 [PMID: 16530631 DOI: 10.1016/j.mric.2005.12.004]
- 46 **Gramsch C**, Nensa F, Kastrup O, Maderwald S, Deuschl C, Ringelstein A, Schelhorn J, Forsting M, Schlamann M. Diagnostic value of 3D fluid attenuated inversion recovery sequence in multiple sclerosis. *Acta Radiol* 2015; **56**: 622-627 [PMID: 24867222 DOI: 10.1177/0284185114534413]
- 47 **Kilsdonk ID**, de Graaf WL, Soriano AL, Zwanenburg JJ, Visser F, Kuijjer JP, Geurts JJ, Pouwels PJ, Polman CH, Castelijn JA, Luijten PR, Barkhof F, Wattjes MP. Multicontrast MR imaging at 7T in multiple sclerosis: highest lesion detection in cortical gray matter with 3D-FLAIR. *AJNR Am J Neuroradiol* 2013; **34**: 791-796 [PMID: 23042930 DOI: 10.3174/ajnr.A3289]
- 48 **Deoni SC**, Catani M. Visualization of the deep cerebellar nuclei using quantitative T1 and rho magnetic resonance imaging at 3 Tesla. *Neuroimage* 2007; **37**: 1260-1266 [PMID: 17702607 DOI: 10.1016/j.neuroimage.2007.06.036]
- 49 **Maderwald S**, Thürling M, Küper M, Theysohn N, Müller O, Beck A, Aurich V, Ladd ME, Timmann D. Direct visualization of cerebellar nuclei in patients with focal cerebellar lesions and its application for lesion-symptom mapping. *Neuroimage* 2012; **63**: 1421-1431 [PMID: 22892334 DOI: 10.1016/j.neuroimage.2012.07.063]
- 50 **D'Ambrosio A**, Pagani E, Riccitelli GC, Colombo B, Rodegher M, Falini A, Comi G, Filippi M, Rocca MA. Cerebellar contribution to motor and cognitive performance in multiple sclerosis: An MRI sub-regional volumetric analysis. *Mult Scler* 2017; **23**: 1194-1203 [PMID: 27760859 DOI: 10.1177/1352458516674567]
- 51 **Bogovic JA**, Jedynak B, Rigg R, Du A, Landman BA, Prince JL, Ying SH. Approaching expert results using a hierarchical cerebellum parcellation protocol for multiple inexperienced human raters. *Neuroimage* 2013; **64**: 616-629 [PMID: 22975160 DOI: 10.1016/j.neuroimage.2012.08.075]
- 52 **Diedrichsen J**. A spatially unbiased atlas template of the human cerebellum. *Neuroimage* 2006; **33**: 127-138 [PMID: 16904911 DOI: 10.1016/j.neuroimage.2006.05.056]
- 53 **Stoodley CJ**. Distinct regions of the cerebellum show gray matter decreases in autism, ADHD, and developmental dyslexia. *Front Syst Neurosci* 2014; **8**: 92 [PMID: 24904314 DOI: 10.3389/fnsys.2014.00092]
- 54 **Piccinin CC**, Santos MC, Piovesana LG, Campos LS, Guimarães RP, Campos BM, Torres FR, França MC, Amato-Filho AC, Lopes-Cendes I, Cendes F, D'Abreu A. Infratentorial gray matter atrophy and excess in primary craniocervical dystonia. *Parkinsonism Relat Disord* 2014; **20**: 198-203 [PMID: 24262871 DOI: 10.1016/j.parkreldis.2013.10.026]
- 55 **Price M**, Cardenas VA, Fein G. Automated MRI cerebellar size measurements using active appearance modeling. *Neuroimage* 2014; **103**: 511-521 [PMID: 25192657 DOI: 10.1016/j.neuroimage.2014.08.047]
- 56 **Weier K**, Beck A, Magon S, Amann M, Naegelin Y, Penner IK, Thürling M, Aurich V, Derfuss T, Radue EW, Stippich C, Kappos L, Timmann D, Sprenger T. Evaluation of a new approach for semi-automatic segmentation of the cerebellum in patients with multiple sclerosis. *J Neurol* 2012; **259**: 2673-2680 [PMID: 22711160 DOI: 10.1007/s00415-012-6569-4]
- 57 **Reuter M**, Schmansky NJ, Rosas HD, Fischl B. Within-subject template estimation for unbiased longitudinal image analysis. *Neuroimage* 2012; **61**: 1402-1418 [PMID: 22430496 DOI: 10.1016/j.neuroimage.2012.02.084]
- 58 **Wang JY**, Ngo MM, Hessel D, Hagerman RJ, Rivera SM. Robust Machine Learning-Based Correction on Automatic Segmentation of the Cerebellum and Brainstem. *PLoS One* 2016; **11**: e0156123 [PMID: 27213683 DOI: 10.1371/journal.pone.0156123]
- 59 **Knösche TR**, Anwender A, Liptrot M, Dyrby TB. Validation of tractography: Comparison with manganese tracing. *Hum Brain Mapp* 2015; **36**: 4116-4134 [PMID: 26178765 DOI: 10.1002/hbm.22902]
- 60 **Le Bihan D**. Diffusion MRI: what water tells us about the brain. *EMBO Mol Med* 2014; **6**: 569-573 [PMID: 24705876 DOI: 10.1002/emmm.201404055]
- 61 **Keser Z**, Hasan KM, Mwangi BI, Kamali A, Ucisik-Keser FE, Riascos RF, Yozbatiran N, Francisco GE, Narayana PA. Diffusion tensor imaging of the human cerebellar pathways and their interplay with cerebral macrostructure. *Front Neuroanat* 2015; **9**: 41 [PMID: 25904851 DOI: 10.3389/fnana.2015.00041]
- 62 **Mormina E**, Briguglio M, Morabito R, Arrigo A, Marino S, Di Rosa G, Micalizzi A, Valente EM, Salpietro V, Vinci SL, Longo M, Granata F. A rare case of cerebellar agenesis: a probabilistic Constrained Spherical Deconvolution tractographic study. *Brain Imaging Behav* 2016; **10**: 158-167 [PMID: 25832852 DOI: 10.1007/s11682-015-9377-5]
- 63 **Mormina E**, Arrigo A, Calamuneri A, Granata F, Quartarone A, Ghilardi MF, Inglese M, Di Rocco A, Milardi D, Anastasi GP, Gaeta M. Diffusion tensor imaging parameters' changes of cerebellar hemispheres in Parkinson's disease. *Neuroradiology* 2015; **57**: 327-334 [PMID: 25479963 DOI: 10.1007/s00234-014-1473-5]
- 64 **Mormina E**, Longo M, Arrigo A, Alafaci C, Tomasello F, Calamuneri A, Marino S, Gaeta M, Vinci SL, Granata F. MRI Tractography of Corticospinal Tract and Arcuate Fasciculus in High-Grade Gliomas Performed by Constrained Spherical Deconvolution: Qualitative and Quantitative Analysis. *AJNR Am J Neuroradiol* 2015; **36**: 1853-1858 [PMID: 26113071 DOI: 10.3174/ajnr.A4368]
- 65 **Neto Henriques R**, Correia MM, Nunes RG, Ferreira HA. Exploring the 3D geometry of the diffusion kurtosis tensor—impact on the development of robust tractography procedures and novel biomarkers. *Neuroimage* 2015; **111**: 85-99 [PMID: 25676915 DOI: 10.1016/j.neuroimage.2015.02.004]
- 66 **Jenabi M**, Peck KK, Young RJ, Brennan N, Holodny AI. Identification of the Corticobulbar Tracts of the Tongue and Face Using Deterministic and Probabilistic DTI Fiber Tracking in Patients with Brain Tumor. *AJNR Am J Neuroradiol* 2015; **36**: 2036-2041 [PMID: 26251424 DOI: 10.3174/ajnr.A4430]
- 67 **Behrens TE**, Berg HJ, Jbabdi S, Rushworth MF, Woolrich MW. Probabilistic diffusion tractography with multiple fibre orientations: What can we gain? *Neuroimage* 2007; **34**: 144-155 [PMID: 17070705 DOI: 10.1016/j.neuroimage.2006.09.018]
- 68 **Gore JC**. Principles and practice of functional MRI of the human brain. *J Clin Invest* 2003; **112**: 4-9 [PMID: 12840051 DOI: 10.1172/JCI19010]
- 69 **Biswal B**, Yetkin FZ, Haughton VM, Hyde JS. Functional connectivity in the motor cortex of resting human brain using echo-planar MRI. *Magn Reson Med* 1995; **34**: 537-541 [PMID: 8524021 DOI: 10.1002/mrm.1910340409]
- 70 **Damoiseaux JS**, Rombouts SA, Barkhof F, Scheltens P, Stam CJ, Smith SM, Beckmann CF. Consistent resting-state networks across healthy subjects. *Proc Natl Acad Sci USA* 2006; **103**: 13848-13853 [PMID: 16945915 DOI: 10.1073/pnas.0601417103]
- 71 **Smith SM**, Fox PT, Miller KL, Glahn DC, Fox PM, Mackay CE, Filippini N, Watkins KE, Toro R, Laird AR, Beckmann CF. Correspondence of the brain's functional architecture during activation

- and rest. *Proc Natl Acad Sci USA* 2009; **106**: 13040-13045 [PMID: 19620724 DOI: 10.1073/pnas.0905267106]
- 72 **Habas C**, Kamdar N, Nguyen D, Prater K, Beckmann CF, Menon V, Greicius MD. Distinct cerebellar contributions to intrinsic connectivity networks. *J Neurosci* 2009; **29**: 8586-8594 [PMID: 19571149 DOI: 10.1523/JNEUROSCI.1868-09.2009]
- 73 **Yacoub E**, Shmuel A, Pfeuffer J, Van De Moortele PF, Adriany G, Andersen P, Vaughan JT, Merkle H, Ugurbil K, Hu X. Imaging brain function in humans at 7 Tesla. *Magn Reson Med* 2001; **45**: 588-594 [PMID: 11283986 DOI: 10.1002/mrm.1080]
- 74 **Jansen JF**, Backes WH, Nicolay K, Kooi ME. 1H MR spectroscopy of the brain: absolute quantification of metabolites. *Radiology* 2006; **240**: 318-332 [PMID: 16864664 DOI: 10.1148/radiol.2402050314]
- 75 **Oz G**, Alger JR, Barker PB, Bartha R, Bizzi A, Boesch C, Bolan PJ, Brindle KM, Cudalbu C, Dinçer A, Dydak U, Emir UE, Frahm J, González RG, Gruber S, Gruetter R, Gupta RK, Heerschap A, Henning A, Hetherington HP, Howe FA, Hüppi PS, Hurd RE, Kantarci K, Klomp DW, Kreis R, Kruiskamp MJ, Leach MO, Lin AP, Luijten PR, Marjańska M, Maudsley AA, Meyerhoff DJ, Mountford CE, Nelson SJ, Pamir MN, Pan JW, Peet AC, Poptani H, Posse S, Pouwels PJ, Ratai EM, Ross BD, Scheenen TW, Schuster C, Smith IC, Soher BJ, Tkáč I, Vigneron DB, Kauppinen RA; MRS Consensus Group. Clinical proton MR spectroscopy in central nervous system disorders. *Radiology* 2014; **270**: 658-679 [PMID: 24568703 DOI: 10.1148/radiol.13130531]
- 76 **Li BS**, Wang H, Gonen O. Metabolite ratios to assumed stable creatine level may confound the quantification of proton brain MR spectroscopy. *Magn Reson Imaging* 2003; **21**: 923-928 [PMID: 14599543 DOI: 10.1016/S0730-725X(03)00181-4]
- 77 **Mascalchi M**, Brugnoli R, Guerrini L, Belli G, Nistri M, Politi LS, Gavazzi C, Lolli F, Argenti G, Villari N. Single-voxel long TE 1H-MR spectroscopy of the normal brainstem and cerebellum. *J Magn Reson Imaging* 2002; **16**: 532-537 [PMID: 12412029 DOI: 10.1002/jmri.10189]
- 78 **Weber-Fahr W**, Ende G, Braus DF, Bachert P, Soher BJ, Henn FA, Büchel C. A fully automated method for tissue segmentation and CSF-correction of proton MRSI metabolites corroborates abnormal hippocampal NAA in schizophrenia. *Neuroimage* 2002; **16**: 49-60 [PMID: 11969317 DOI: 10.1006/nimg.2002.1057]
- 79 **Currie S**, Hadjivassiliou M, Wilkinson ID, Griffiths PD, Hoggard N. Magnetic resonance spectroscopy of the normal cerebellum: what degree of variability can be expected? *Cerebellum* 2013; **12**: 205-211 [PMID: 22987337 DOI: 10.1007/s12311-012-0415-1]
- 80 **Sajja BR**, Wolinsky JS, Narayana PA. Proton magnetic resonance spectroscopy in multiple sclerosis. *Neuroimaging Clin N Am* 2009; **19**: 45-58 [PMID: 19064199 DOI: 10.1016/j.nic.2008.08.002]
- 81 **Jahng GH**, Li KL, Ostergaard L, Calamante F. Perfusion magnetic resonance imaging: a comprehensive update on principles and techniques. *Korean J Radiol* 2014; **15**: 554-577 [PMID: 25246817 DOI: 10.3348/kjr.2014.15.5.554]
- 82 **Talbot PR**, Lloyd JJ, Snowden JS, Neary D, Testa HJ. Choice of reference region in the quantification of single-photon emission tomography in primary degenerative dementia. *Eur J Nucl Med* 1994; **21**: 503-508 [PMID: 8082664 DOI: 10.1007/BF00173036]
- 83 **Lacalle-Aurioles M**, Alemán-Gómez Y, Guzmán-De-Villoria JA, Cruz-Orduña I, Olazarán J, Mateos-Pérez JM, Martino ME, Desco M. Is the cerebellum the optimal reference region for intensity normalization of perfusion MR studies in early Alzheimer's disease? *PLoS One* 2013; **8**: e81548 [PMID: 24386081 DOI: 10.1371/journal.pone.0081548]
- 84 **Hartkamp NS**, Petersen ET, De Vis JB, Bokkers RP, Hendrikse J. Mapping of cerebral perfusion territories using territorial arterial spin labeling: techniques and clinical application. *NMR Biomed* 2013; **26**: 901-912 [PMID: 22807022 DOI: 10.1002/nbm.2836]
- 85 **Grade M**, Hernandez Tamames JA, Pizzini FB, Achten E, Golay X, Smits M. A neuroradiologist's guide to arterial spin labeling MRI in clinical practice. *Neuroradiology* 2015; **57**: 1181-1202 [PMID: 26351201 DOI: 10.1007/s00234-015-1571-z]
- 86 **van Gelderen P**, de Zwart JA, Duyn JH. Pitfalls of MRI measurement of white matter perfusion based on arterial spin labeling. *Magn Reson Med* 2008; **59**: 788-795 [PMID: 18383289 DOI: 10.1002/mrm.21515]
- 87 **Compston A**, Lassmann H, McDonald I. Chapter 1 - The story of multiple sclerosis. In: McAlpine's Multiple Sclerosis (Fourth Edition). Edinburgh: Churchill Livingstone, 2006: 3-68 [DOI: 10.1016/B978-0-443-07271-0.50003-3]
- 88 **Tintore M**, Otero-Romero S, Río J, Arrambide G, Pujal B, Tur C, Galán I, Comabella M, Nos C, Arévalo MJ, Vidal-Jordana A, Castelló J, Rodríguez-Acevedo B, Midaglia L, Mitjana R, Auger C, Sastre-Garriga J, Rovira À, Montalban X. Contribution of the symptomatic lesion in establishing MS diagnosis and prognosis. *Neurology* 2016; **87**: 1368-1374 [PMID: 27566747 DOI: 10.1212/WNL.0000000000003144]
- 89 **Fazekas F**, Offenbacher H, Fuchs S, Schmidt R, Niederkorn K, Horner S, Lechner H. Criteria for an increased specificity of MRI interpretation in elderly subjects with suspected multiple sclerosis. *Neurology* 1988; **38**: 1822-1825 [PMID: 3057397]
- 90 **Ormerod IE**, Miller DH, McDonald WI, du Boulay EP, Rudge P, Kendall BE, Moseley IF, Johnson G, Tofts PS, Halliday AM. The role of NMR imaging in the assessment of multiple sclerosis and isolated neurological lesions. A quantitative study. *Brain* 1987; **110** (Pt 6): 1579-1616 [PMID: 3427402]
- 91 **Favaretto A**, Lazzarotto A, Poggiali D, Rolma G, Causin F, Rinaldi F, Perini P, Gallo P. MRI-detectable cortical lesions in the cerebellum and their clinical relevance in multiple sclerosis. *Mult Scler* 2016; **22**: 494-501 [PMID: 26163070 DOI: 10.1177/1352458515594043]
- 92 **Calabrese M**, Reynolds R, Magliozzi R, Castellaro M, Morra A, Scalfari A, Farina G, Romualdi C, Gajofatto A, Pitteri M, Benedetti MD, Monaco S. Regional Distribution and Evolution of Gray Matter Damage in Different Populations of Multiple Sclerosis Patients. *PLoS One* 2015; **10**: e0135428 [PMID: 26267665 DOI: 10.1371/journal.pone.0135428]
- 93 **Bendfeldt K**, Kuster P, Traud S, Egger H, Winkhofer S, Mueller-Lenke N, Naegelin Y, Gass A, Kappos L, Matthews PM, Nichols TE, Radue EW, Borgwardt SJ. Association of regional gray matter volume loss and progression of white matter lesions in multiple sclerosis - A longitudinal voxel-based morphometry study. *Neuroimage* 2009; **45**: 60-67 [PMID: 19013533 DOI: 10.1016/j.neuroimage.2008.10.006]
- 94 **Edwards SG**, Gong QY, Liu C, Zvartau ME, Jaspan T, Roberts N, Blumhardt LD. Infratentorial atrophy on magnetic resonance imaging and disability in multiple sclerosis. *Brain* 1999; **122** (Pt 2): 291-301 [PMID: 10071057]
- 95 **Ramasamy DP**, Benedict RH, Cox JL, Fritz D, Abdelrahman N, Hussein S, Minagar A, Dwyer MG, Zivadinov R. Extent of cerebellum, subcortical and cortical atrophy in patients with MS: a case-control study. *J Neurol Sci* 2009; **282**: 47-54 [PMID: 19201003 DOI: 10.1016/j.jns.2008.12.034]
- 96 **Anderson VM**, Fisniku LK, Altmann DR, Thompson AJ, Miller DH. MRI measures show significant cerebellar gray matter volume loss in multiple sclerosis and are associated with cerebellar dysfunction. *Mult Scler* 2009; **15**: 811-817 [PMID: 19465449 DOI: 10.1177/1352458508101934]
- 97 **Anderson VM**, Wheeler-Kingshott CA, Abdel-Aziz K, Miller DH, Toosy A, Thompson AJ, Ciccarelli O. A comprehensive assessment of cerebellar damage in multiple sclerosis using diffusion tractography and volumetric analysis. *Mult Scler* 2011; **17**: 1079-1087 [PMID: 21511688 DOI: 10.1177/1352458511403528]
- 98 **Preziosa P**, Rocca MA, Mesaros S, Pagani E, Drulovic J, Stosic-Opincal T, Dackovic J, Copetti M, Caputo D, Filippi M. Relationship between damage to the cerebellar peduncles and clinical disability in multiple sclerosis. *Radiology* 2014; **271**: 822-830 [PMID: 24555637 DOI: 10.1148/radiol.13132142]
- 99 **Deppe M**, Tabelow K, Krämer J, Tenberge JG, Schiffler P, Bittner S, Schwindt W, Zipp F, Wiendl H, Meuth SG. Evidence for early, non-lesional cerebellar damage in patients with multiple sclerosis: DTI measures correlate with disability, atrophy, and disease duration. *Mult Scler* 2016; **22**: 73-84 [PMID: 25921041 DOI: 10.1177/1352458515579439]
- 100 **Tomassini V**, d'Ambrosio A, Petsas N, Wise RG, Sbardella E, Allen M, Tona F, Fanelli F, Foster C, Cami M, Gallo A, Pantano P, Pozzilli C. The effect of inflammation and its reduction on brain plasticity

- in multiple sclerosis: MRI evidence. *Hum Brain Mapp* 2016; **37**: 2431-2445 [PMID: 26991559 DOI: 10.1002/hbm.23184]
- 101 **Rocca MA**, Pagani E, Absinta M, Valsasina P, Falini A, Scotti G, Comi G, Filippi M. Altered functional and structural connectivities in patients with MS: a 3-T study. *Neurology* 2007; **69**: 2136-2145 [PMID: 18056577 DOI: 10.1212/01.wnl.0000295504.92020.ca]
- 102 **Pardini M**, Bonzano L, Roccatagliata L, Mancardi GL, Bove M. The fatigue-motor performance paradox in multiple sclerosis. *Sci Rep* 2013; **3**: 2001 [PMID: 23774178 DOI: 10.1038/srep02001]
- 103 **Weier K**, Penner IK, Magon S, Amann M, Naegelin Y, Andelova M, Derfuss T, Stippich C, Radue EW, Kappos L, Sprenger T. Cerebellar abnormalities contribute to disability including cognitive impairment in multiple sclerosis. *PLoS One* 2014; **9**: e86916 [PMID: 24466290 DOI: 10.1371/journal.pone.0086916]
- 104 **Damasceno A**, Damasceno BP, Cendes F. The clinical impact of cerebellar grey matter pathology in multiple sclerosis. *PLoS One* 2014; **9**: e96193 [PMID: 24789257 DOI: 10.1371/journal.pone.0096193]
- 105 **Yeoman LJ**, Howarth L, Britten A, Cotterill A, Adam EJ. Gantry angulation in brain CT: dosage implications, effect on posterior fossa artifacts, and current international practice. *Radiology* 1992; **184**: 113-116 [PMID: 1609066 DOI: 10.1148/radiology.184.1.1609066]
- 106 **Sbardella E**, Upadhyay N, Tona F, Prosperini L, De Giglio L, Petsas N, Pozzilli C, Pantano P. Dentate nucleus connectivity in adult patients with multiple sclerosis: functional changes at rest and correlation with clinical features. *Mult Scler* 2017; **23**: 546-555 [PMID: 27411700 DOI: 10.1177/1352458516657438]
- 107 **Loitfelder M**, Filippi M, Rocca M, Valsasina P, Ropele S, Jehna M, Fuchs S, Schmidt R, Neuper C, Fazekas F, Enzinger C. Abnormalities of resting state functional connectivity are related to sustained attention deficits in MS. *PLoS One* 2012; **7**: e42862 [PMID: 22912754 DOI: 10.1371/journal.pone.0042862]
- 108 **Roccatagliata L**, Vuolo L, Bonzano L, Pichiecchio A, Mancardi GL. Multiple sclerosis: hyperintense dentate nucleus on unenhanced T1-weighted MR images is associated with the secondary progressive subtype. *Radiology* 2009; **251**: 503-510 [PMID: 19401576 DOI: 10.1148/radiol.2511081269]
- 109 **Albert M**, Barrantes-Freer A, Lohrberg M, Antel JP, Prineas JW, Palkovits M, Wolff JR, Brück W, Stadelmann C. Synaptic pathology in the cerebellar dentate nucleus in chronic multiple sclerosis. *Brain Pathol* 2016; Epub ahead of print [PMID: 27706868 DOI: 10.1111/bpa.12450]
- 110 **Tedeschi E**, Palma G, Canna A, Cocozza S, Russo C, Borrelli P, Lanzillo R, Angelini V, Postiglione E, Morra VB, Salvatore M, Brunetti A, Quarantelli M. In vivo dentate nucleus MRI relaxometry correlates with previous administration of Gadolinium-based contrast agents. *Eur Radiol* 2016; **26**: 4577-4584 [PMID: 26905870 DOI: 10.1007/s00330-016-4245-2]
- 111 **Bostan AC**, Dum RP, Strick PL. The basal ganglia communicate with the cerebellum. *Proc Natl Acad Sci USA* 2010; **107**: 8452-8456 [PMID: 20404184 DOI: 10.1073/pnas.1000496107]
- 112 **Sweet JA**, Walter BL, Gunalan K, Chaturvedi A, McIntyre CC, Miller JP. Fiber tractography of the axonal pathways linking the basal ganglia and cerebellum in Parkinson disease: implications for targeting in deep brain stimulation. *J Neurosurg* 2014; **120**: 988-996 [PMID: 24484226 DOI: 10.3171/2013.12.JNS131537]
- 113 **Borghammer P**, Østergaard K, Cumming P, Gjedde A, Rodell A, Hall N, Chakravarty MM. A deformation-based morphometry study of patients with early-stage Parkinson's disease. *Eur J Neurol* 2010; **17**: 314-320 [PMID: 19912319 DOI: 10.1111/j.1468-1331.2009.02807.x]
- 114 **Benninger DH**, Thees S, Kollias SS, Bassetti CL, Waldvogel D. Morphological differences in Parkinson's disease with and without rest tremor. *J Neurol* 2009; **256**: 256-263 [PMID: 19219572 DOI: 10.1007/s00415-009-0092-2]
- 115 **O'Callaghan C**, Hornberger M, Balsters JH, Halliday GM, Lewis SJ, Shine JM. Cerebellar atrophy in Parkinson's disease and its implication for network connectivity. *Brain* 2016; **139**: 845-855 [PMID: 26794597 DOI: 10.1093/brain/awv399]
- 116 **Zhang K**, Yu C, Zhang Y, Wu X, Zhu C, Chan P, Li K. Voxel-based analysis of diffusion tensor indices in the brain in patients with Parkinson's disease. *Eur J Radiol* 2011; **77**: 269-273 [PMID: 19692193 DOI: 10.1016/j.ejrad.2009.07.032]
- 117 **Nicoletti G**, Caligiuri ME, Cherubini A, Morelli M, Novellino F, Arabia G, Salsone M, Quattrone A. A Fully Automated, Atlas-Based Approach for Superior Cerebellar Peduncle Evaluation in Progressive Supranuclear Palsy Phenotypes. *AJNR Am J Neuroradiol* 2017; **38**: 523-530 [PMID: 28034996 DOI: 10.3174/ajnr.A5048]
- 118 **Wu T**, Long X, Zang Y, Wang L, Hallett M, Li K, Chan P. Regional homogeneity changes in patients with Parkinson's disease. *Hum Brain Mapp* 2009; **30**: 1502-1510 [PMID: 18649351 DOI: 10.1002/hbm.20622]
- 119 **Dirkx MF**, den Ouden H, Aarts E, Timmer M, Bloem BR, Toni I, Helmich RC. The Cerebral Network of Parkinson's Tremor: An Effective Connectivity fMRI Study. *J Neurosci* 2016; **36**: 5362-5372 [PMID: 27170132 DOI: 10.1523/JNEUROSCI.3634-15.2016]
- 120 **Planetta PJ**, Kurani AS, Shukla P, Prodoehl J, Corcos DM, Comella CL, McFarland NR, Okun MS, Vaillancourt DE. Distinct functional and macrostructural brain changes in Parkinson's disease and multiple system atrophy. *Hum Brain Mapp* 2015; **36**: 1165-1179 [PMID: 25413603 DOI: 10.1002/hbm.22694]
- 121 **Nicoletti G**, Rizzo G, Barbagallo G, Tonon C, Condino F, Manners D, Messina D, Testa C, Arabia G, Gambardella A, Lodi R, Quattrone A. Diffusivity of cerebellar hemispheres enables discrimination of cerebellar or parkinsonian multiple system atrophy from progressive supranuclear palsy-Richardson syndrome and Parkinson disease. *Radiology* 2013; **267**: 843-850 [PMID: 23329659 DOI: 10.1148/radiol.12120364]
- 122 **Lin DJ**, Hermann KL, Schmahmann JD. The Diagnosis and Natural History of Multiple System Atrophy, Cerebellar Type. *Cerebellum* 2016; **15**: 663-679 [PMID: 26467153 DOI: 10.1007/s12311-015-0728-y]
- 123 **Batla A**, Sánchez MC, Erro R, Ganos C, Stamelou M, Balint B, Brügger F, Antelmi E, Bhatia KP. The role of cerebellum in patients with late onset cervical/segmental dystonia?--evidence from the clinic. *Parkinsonism Relat Disord* 2015; **21**: 1317-1322 [PMID: 26385708 DOI: 10.1016/j.parkreldis.2015.09.013]
- 124 **Delmaire C**, Vidailhet M, Elbaz A, Bourdain F, Bleton JP, Sangla S, Meunier S, Terrier A, LeHéry S. Structural abnormalities in the cerebellum and sensorimotor circuit in writer's cramp. *Neurology* 2007; **69**: 376-380 [PMID: 17646630 DOI: 10.1212/01.wnl.0000266591.49624.1a]
- 125 **Preibisch C**, Berg D, Hofmann E, Solymosi L, Naumann M. Cerebral activation patterns in patients with writer's cramp: a functional magnetic resonance imaging study. *J Neurol* 2001; **248**: 10-17 [PMID: 11266013]
- 126 **Baker RS**, Andersen AH, Morecraft RJ, Smith CD. A functional magnetic resonance imaging study in patients with benign essential blepharospasm. *J Neuroophthalmol* 2003; **23**: 11-15 [PMID: 12616082]
- 127 **Klockgether T**. Update on degenerative ataxias. *Curr Opin Neurol* 2011; **24**: 339-345 [PMID: 21734495 DOI: 10.1097/WCO.0b013e32834875ba]
- 128 **Ruano L**, Melo C, Silva MC, Coutinho P. The global epidemiology of hereditary ataxia and spastic paraplegia: a systematic review of prevalence studies. *Neuroepidemiology* 2014; **42**: 174-183 [PMID: 24603320 DOI: 10.1159/000358801]
- 129 **Bürk K**, Abele M, Fetter M, Dichgans J, Skalej M, Laccone F, Didierjean O, Brice A, Klockgether T. Autosomal dominant cerebellar ataxia type I clinical features and MRI in families with SCA1, SCA2 and SCA3. *Brain* 1996; **119** (Pt 5): 1497-1505 [PMID: 8931575 DOI: 10.1093/brain/119.5.1497]
- 130 **Schulz JB**, Borkert J, Wolf S, Schmitz-Hübsch T, Rakowicz M, Mariotti C, Schöls L, Timmann D, van de Warrenburg B, Dürr A, Pandolfo M, Kang JS, Mandly AG, Nägele T, Grisoli M, Boguslawska R, Bauer P, Klockgether T, Hauser TK. Visualization, quantification and correlation of brain atrophy with clinical symptoms in spinocerebellar ataxia types 1, 3 and 6. *Neuroimage* 2010; **49**: 158-168 [PMID: 19631275 DOI: 10.1016/j.neuroimage.2009.07.027]
- 131 **Klockgether T**, Petersen D, Grodd W, Dichgans J. Early onset cerebellar ataxia with retained tendon reflexes. Clinical, electrophysiological and MRI observations in comparison with Friedreich's ataxia. *Brain* 1991;

- 114 (Pt 4): 1559-1573 [PMID: 1884166 DOI: 10.1093/brain/114.4.1559]
- 132 **Mascalchi M.** The cerebellum looks normal in Friedreich ataxia. *AJNR Am J Neuroradiol* 2013; **34**: E22 [PMID: 23328073 DOI: 10.3174/ajnr.A3480]
- 133 **Selvadurai LP,** Harding IH, Corben LA, Stagnitti MR, Storey E, Egan GF, Delatycki MB, Georgiou-Karistianis N. Cerebral and cerebellar grey matter atrophy in Friedreich ataxia: the IMAGE-FRDA study. *J Neurol* 2016; **263**: 2215-2223 [PMID: 27522354 DOI: 10.1007/s00415-016-8252-7]
- 134 **Al-Maawali A,** Blaser S, Yoon G. Diagnostic approach to childhood-onset cerebellar atrophy: a 10-year retrospective study of 300 patients. *J Child Neurol* 2012; **27**: 1121-1132 [PMID: 22764178 DOI: 10.1177/0883073812448680]
- 135 **Lin DD,** Barker PB, Lederman HM, Crawford TO. Cerebral abnormalities in adults with ataxia-telangiectasia. *AJNR Am J Neuroradiol* 2014; **35**: 119-123 [PMID: 23886747 DOI: 10.3174/ajnr.A3646]
- 136 **Sardanelli F,** Parodi RC, Ottonello C, Renzetti P, Saitta S, Lignana E, Mancardi GL. Cranial MRI in ataxia-telangiectasia. *Neuroradiology* 1995; **37**: 77-82 [PMID: 7708196 DOI: 10.1007/BF00588526]
- 137 **Tavani F,** Zimmerman RA, Berry GT, Sullivan K, Gatti R, Bingham P. Ataxia-telangiectasia: the pattern of cerebellar atrophy on MRI. *Neuroradiology* 2003; **45**: 315-319 [PMID: 12740724 DOI: 10.1007/s00234-003-0945-9]
- 138 **Guimarães RP,** D'Abreu A, Yasuda CL, França MC Jr, Silva BH, Cappabianco FA, Bergo FP, Lopes-Cendes IT, Cendes F. A multimodal evaluation of microstructural white matter damage in spinocerebellar ataxia type 3. *Mov Disord* 2013; **28**: 1125-1132 [PMID: 23553599 DOI: 10.1002/mds.25451]
- 139 **Kang JS,** Klein JC, Baudrexel S, Deichmann R, Nolte D, Hilker R. White matter damage is related to ataxia severity in SCA3. *J Neurol* 2014; **261**: 291-299 [PMID: 24272589 DOI: 10.1007/s00415-013-7186-6]
- 140 **Hernandez-Castillo CR,** Vaca-Palomares I, Galvez V, Campos-Romo A, Diaz R, Fernandez-Ruiz J. Cognitive Deficits Correlate with White Matter Deterioration in Spinocerebellar Ataxia Type 2. *J Int Neuropsychol Soc* 2016; **22**: 486-491 [PMID: 26888086 DOI: 10.1017/S1355617716000084]
- 141 **Mascalchi M,** Toschi N, Giannelli M, Ginestroni A, Della Nave R, Nicolai E, Bianchi A, Tessa C, Salvatore E, Aiello M, Soricelli A, Diciotti S. Progression of microstructural damage in spinocerebellar ataxia type 2: a longitudinal DTI study. *AJNR Am J Neuroradiol* 2015; **36**: 1096-1101 [PMID: 25882284 DOI: 10.3174/ajnr.A4343]
- 142 **Clemm von Hohenberg C,** Schocke MF, Wigand MC, Nachbauer W, Guttmann CR, Kubicki M, Shenton ME, Boesch S, Egger K. Radial diffusivity in the cerebellar peduncles correlates with clinical severity in Friedreich ataxia. *Neurol Sci* 2013; **34**: 1459-1462 [PMID: 23640016 DOI: 10.1007/s10072-013-1402-0]
- 143 **Della Nave R,** Ginestroni A, Tessa C, Salvatore E, Bartolomei I, Salvi F, Dotti MT, De Michele G, Piacentini S, Mascalchi M. Brain white matter tracts degeneration in Friedreich ataxia. An in vivo MRI study using tract-based spatial statistics and voxel-based morphometry. *Neuroimage* 2008; **40**: 19-25 [PMID: 18226551 DOI: 10.1016/j.neuroimage.2007.11.050]
- 144 **Rizzo G,** Tonon C, Valentino ML, Manners D, Fortuna F, Gellera C, Pini A, Ghezzi A, Baruzzi A, Testa C, Malucelli E, Barbiroli B, Carelli V, Lodi R. Brain diffusion-weighted imaging in Friedreich's ataxia. *Mov Disord* 2011; **26**: 705-712 [PMID: 21370259 DOI: 10.1002/mds.23518]
- 145 **Vieira Karuta SC,** Raskin S, de Carvalho Neto A, Gasparetto EL, Doring T, Teive HA. Diffusion tensor imaging and tract-based spatial statistics analysis in Friedreich's ataxia patients. *Parkinsonism Relat Disord* 2015; **21**: 504-508 [PMID: 25801908 DOI: 10.1016/j.parkreldis.2015.02.021]
- 146 **Sahama I,** Sinclair K, Fiori S, Doecke J, Pannek K, Reid L, Lavin M, Rose S. Motor pathway degeneration in young ataxia telangiectasia patients: A diffusion tractography study. *Neuroimage Clin* 2015; **9**: 206-215 [PMID: 26413479 DOI: 10.1016/j.nicl.2015.08.007]
- 147 **Stefanescu MR,** Dohnalek M, Maderwald S, Thürling M, Minnerop M, Beck A, Schlamann M, Diedrichsen J, Ladd ME, Timmann D. Structural and functional MRI abnormalities of cerebellar cortex and nuclei in SCA3, SCA6 and Friedreich's ataxia. *Brain* 2015; **138**: 1182-1197 [PMID: 25818870 DOI: 10.1093/brain/aww064]
- 148 **Duarte JV,** Faustino R, Lobo M, Cunha G, Nunes C, Ferreira C, Januário C, Castelo-Branco M. Parametric fMRI of paced motor responses uncovers novel whole-brain imaging biomarkers in spinocerebellar ataxia type 3. *Hum Brain Mapp* 2016; **37**: 3656-3668 [PMID: 27273236 DOI: 10.1002/hbm.23266]
- 149 **Wu T,** Wang C, Wang J, Hallett M, Zang Y, Chan P. Preclinical and clinical neural network changes in SCA2 parkinsonism. *Parkinsonism Relat Disord* 2013; **19**: 158-164 [PMID: 23000299 DOI: 10.1016/j.parkreldis.2012.08.011]
- 150 **Cocozza S,** Saccà F, Cervo A, Marsili A, Russo CV, Giorgio SM, De Michele G, Filla A, Brunetti A, Quarantelli M. Modifications of resting state networks in spinocerebellar ataxia type 2. *Mov Disord* 2015; **30**: 1382-1390 [PMID: 26094751 DOI: 10.1002/mds.26284]
- 151 **Hernandez-Castillo CR,** Galvez V, Mercadillo RE, Díaz R, Yescas P, Martinez L, Ochoa A, Velazquez-Perez L, Fernandez-Ruiz J. Functional connectivity changes related to cognitive and motor performance in spinocerebellar ataxia type 2. *Mov Disord* 2015; **30**: 1391-1399 [PMID: 26256273 DOI: 10.1002/mds.26320]
- 152 **Harding IH,** Corben LA, Storey E, Egan GF, Stagnitti MR, Poudel GR, Delatycki MB, Georgiou-Karistianis N. Fronto-cerebellar dysfunction and dysconnectivity underlying cognition in friedreich ataxia: The IMAGE-FRDA study. *Hum Brain Mapp* 2016; **37**: 338-350 [PMID: 26502936 DOI: 10.1002/hbm.23034]
- 153 **Thomann PA,** Schäfer C, Seidl U, Santos VD, Essig M, Schröder J. The cerebellum in mild cognitive impairment and Alzheimer's disease - a structural MRI study. *J Psychiatr Res* 2008; **42**: 1198-1202 [PMID: 18215400 DOI: 10.1016/j.jpsychires.2007.12.002]
- 154 **Colloby SJ,** O'Brien JT, Taylor JP. Patterns of cerebellar volume loss in dementia with Lewy bodies and Alzheimer's disease: A VBM-DARTEL study. *Psychiatry Res* 2014; **223**: 187-191 [PMID: 25037902 DOI: 10.1016/j.psychres.2014.06.006]
- 155 **Łojkowska W,** Witkowski G, Bednarska-Makaruk M, Wehr H, Sienkiewicz-Jarosz H, Graban A, Bochyńska A, Wiśniewska A, Gugala M, Sławińska K, Sawicka B, Poniatowska R, Ryglewicz D. Correlations between cerebellar and brain volumes, cognitive impairments, ApoE levels, and APOE genotypes in patients with AD and MCI. *Curr Alzheimer Res* 2013; **10**: 964-972 [PMID: 24117117 DOI: 10.2174/15672050113106660161]
- 156 **Möller C,** Vrenken H, Jiskoot L, Versteeg A, Barkhof F, Scheltens P, van der Flier WM. Different patterns of gray matter atrophy in early- and late-onset Alzheimer's disease. *Neurobiol Aging* 2013; **34**: 2014-2022 [PMID: 23561509 DOI: 10.1016/j.neurobiolaging.2013.02.013]
- 157 **Raji CA,** Lopez OL, Kuller LH, Carmichael OT, Becker JT. Age, Alzheimer disease, and brain structure. *Neurology* 2009; **73**: 1899-1905 [PMID: 19846828 DOI: 10.1212/WNL.0b013e3181c3f293]

P- Reviewer: Quattrocchi CC **S- Editor:** Kong JX **L- Editor:** A
E- Editor: Lu YJ



Lymph node imaging in initial staging of prostate cancer: An overview and update

Jessica G Zarzour, Sam Galgano, Jonathan McConathy, John V Thomas, Soroush Rais-Bahrami

Jessica G Zarzour, Sam Galgano, Jonathan McConathy, John V Thomas, Soroush Rais-Bahrami, Department of Radiology, University of Alabama at Birmingham, Birmingham, AL 35249, United States

Soroush Rais-Bahrami, Department of Urology, University of Alabama at Birmingham, Birmingham, AL 35249, United States

Author contributions: Zarzour JG was responsible for the conception and design of the article, drafting and revision of the article, gives approval for the final version of the article, and serves as the corresponding author; Galgano S, McConathy J and Thomas JV contributed to the design of the project, participated in drafting and revising, and gives approval for the final version of the manuscript; and Rais-Bahrami S served as the supervision author, contributed to the design of the article, participated in drafting and revisions, and gives approval for the final version of the article.

Supported by Eli Lilly/Avid; AbbVie, consulting for GE Healthcare, Siemens Healthcare and Blue Earth Diagnostics.

Conflict-of-interest statement: The authors have no conflicts of interests to declare.

Open-Access: This article is an open-access article which was selected by an in-house editor and fully peer-reviewed by external reviewers. It is distributed in accordance with the Creative Commons Attribution Non Commercial (CC BY-NC 4.0) license, which permits others to distribute, remix, adapt, build upon this work non-commercially, and license their derivative works on different terms, provided the original work is properly cited and the use is non-commercial. See: <http://creativecommons.org/licenses/by-nc/4.0/>

Manuscript source: Invited manuscript

Correspondence to: Jessica G Zarzour, MD, Department of Radiology, University of Alabama at Birmingham, JTN 357, 619 19th Street South, Birmingham, AL 35294, United States. jjzarzour@uabmc.edu
Telephone: +1-205-9343166
Fax: +1-205-9753540

Received: February 10, 2017

Peer-review started: February 15, 2017

First decision: May 7, 2017

Revised: May 26, 2017

Accepted: July 14, 2017

Article in press: July 17, 2017

Published online: October 28, 2017

Abstract

Accurate nodal staging at the time of diagnosis of prostate cancer is crucial in determining a treatment plan for the patient. Pelvic lymph node dissection is the most reliable method, but is less than perfect and has increased morbidity. Cross sectional imaging with computed tomography (CT) and magnetic resonance imaging (MRI) are non-invasive tools that rely on morphologic characteristics such as shape and size of the lymph nodes. However, lymph nodes harboring metastatic disease may be normal sized and non-metastatic lymph nodes may be enlarged due to reactive hyperplasia. The optimal strategy for preoperative staging remains a topic of ongoing research. Advanced imaging techniques to assess lymph nodes in the setting of prostate cancer utilizing novel MRI contrast agents as well as positron emission tomography (PET) tracers have been developed and continue to be studied. Magnetic resonance lymphography utilizing ultra-small super paramagnetic iron oxide has shown promising results in detection of metastatic lymph nodes. Combining MRL with diffusion-weighted imaging may also improve accuracy. Considerable efforts are being made to develop effective PET radiotracers that are performed using hybrid-imaging systems that combine PET with CT or MRI. PET tracers that will be reviewed in this article include [¹⁸F]fluoro-D-glucose, sodium [¹⁸F]fluoride, [¹⁸F]choline, [¹¹C]choline, prostate specific membrane antigen binding ligands, [¹¹C]acetate, [¹⁸F]fluciclovine, gastrin releasing peptide receptor ligands, and androgen binding receptors. This article will review these advanced imaging modalities and ability to detect prostate cancer metastasis to lymph nodes. While more research is

needed, these novel techniques to image lymph nodes in the setting of prostate cancer show a promising future in improving initial lymph node staging.

Key words: Prostate cancer; Staging; Magnetic resonance imaging; Ultra-small super paramagnetic iron oxide; Molecular imaging; Positron emission tomography; Lymph nodes

© **The Author(s) 2017.** Published by Baishideng Publishing Group Inc. All rights reserved.

Core tip: Accurate nodal staging at time of prostate cancer diagnosis is crucial in determining a treatment plan for the patient. This review article highlights the newest imaging techniques that have been and are being developed for imaging of lymph nodes in the initial staging of prostate cancer. Magnetic resonance lymphography utilizing ultra-small super paramagnetic iron oxide has shown to detect metastatic disease in normal sized lymph nodes. Considerable efforts are being made in molecular imaging to develop effective positron emission tomography radiotracers that may be combined with computed tomography or magnetic resonance to detect prostate metastasis as well as potential therapeutic applications.

Zarzour JG, Galgano S, McConathy J, Thomas JV, Rais-Bahrami S. Lymph node imaging in initial staging of prostate cancer: An overview and update. *World J Radiol* 2017; 9(10): 389-399 Available from: URL: <http://www.wjgnet.com/1949-8470/full/v9/i10/389.htm> DOI: <http://dx.doi.org/10.4329/wjr.v9.i10.389>

INTRODUCTION

Prostate cancer is the most common cancer in American men and is associated with a significant likelihood of cure when patients have organ-confined disease through the use of local definitive therapy such as radical prostatectomy or radiation therapy^[1]. However, once prostate cancer spreads beyond the gland to the lymphatic tissues, the opportunity for cure with a local therapy is lost in most cases and significantly diminished in others^[1]. Due to the adverse prognostic implications associated with lymph node metastasis, detection of clinically occult lymph node metastasis is of extreme importance^[2]. Risk assessment tools are used to predict patients who are at risk for higher pathologic stage and use inputs such as PSA, biopsy Gleason sum, percent positive biopsies, and magnetic resonance imaging (MRI) findings^[3-5]. The prostate health index (PHI) test utilizes three forms of PSA (total PSA, free PSA and p2PSA) and the 4K panel (total PSA, free PSA, single chain intact PSA, and human kallikrein 2) have been shown to more accurately predict higher-grade prostate cancer^[6,7]. Patients who are deemed low risk, defined as a predicted < 5% (or in some more conservative guidelines ≤ 2%) for lymph node metastasis usually undergo definitive treatment with curative intent without

any further radiological imaging or lymph node dissection^[1]. Patients determined to be at higher risk for systemic disease need to undergo nodal staging. The most reliable method is pelvic lymph node dissection; however, this is invasive and may be associated with increased morbidity and risk of complications^[1]. Furthermore, pelvic lymph node dissection is less than perfect as several studies have reported positive lymph nodes outside the routine dissection template^[8-11]. Even extended pelvic lymph node dissections have been shown to miss up to 13% of metastatic lymph nodes^[12].

Cross sectional imaging is a non-invasive tool utilized for nodal staging and largely relies on morphologic characteristics such as size and shape. A meta-analysis found a pooled sensitivity of 42% and specificity of 82% for computed tomography (CT) imaging and similar 39% sensitivity and 82% specificity for MR imaging for detection of metastatic lymph nodes^[1]. Utilizing CT and MRI, determination of metastatic lymph nodes is determined largely by size. A threshold of 1.0 cm in short axis of oval nodes and 0.8 cm for round nodes are generally used as indicators of likely metastatic disease^[13]. However, more than half of lymph nodes involved with metastatic prostate cancer may be less than 1 cm^[14]. Moreover, non-metastatic nodes may be enlarged due to reactive hyperplasia. Given the lack of sensitivity of both CT and MRI based on size criteria alone, new techniques of MR lymphography (MRL) have been developed as well as molecular imaging techniques. Herein, we will discuss these modalities for improved prostate cancer lymph node staging.

LYMPH NODE IMAGING WITH MRI

MRL

High resolution MRI utilizing ultra-small super paramagnetic iron oxide (USPIO) has been utilized to improve sensitivity for detection of metastatic lymph nodes^[15,16]. Lymphotropic superparamagnetic nanoparticles are avidly taken up by lymph nodes where they are internalized by macrophages^[17]. Malignant nodes have a relatively paucity of macrophages compared to benign lymph nodes. The intracellular iron-containing particles cause benign lymph nodes to lose signal (appear dark) on T2* images (Figure 1) while lymph nodes affected by metastatic disease do not take up the USPIO as effectively due to the decreased macrophages and hence appear bright^[18]. This evaluation of macrophage function does not rely on nodal size to detect metastasis^[19]. Moreover, it does not depend on the functional activity of cancer in the lymph nodes as it labels normal macrophages in the lymph nodes^[20]. Given the high spatial resolution of MRI, more lymph nodes at smaller sizes can be detected and accurately characterized as benign or malignant with macrophage replacement by metastatic cancer cells^[20].

USPIO particles have been used extensively as a lymphotropic contrast agent for detection of metastatic prostate cancer in numerous clinical trials^[16,21-26]. In an initial study that utilized USPIO (ferumoxtran-10), nodes

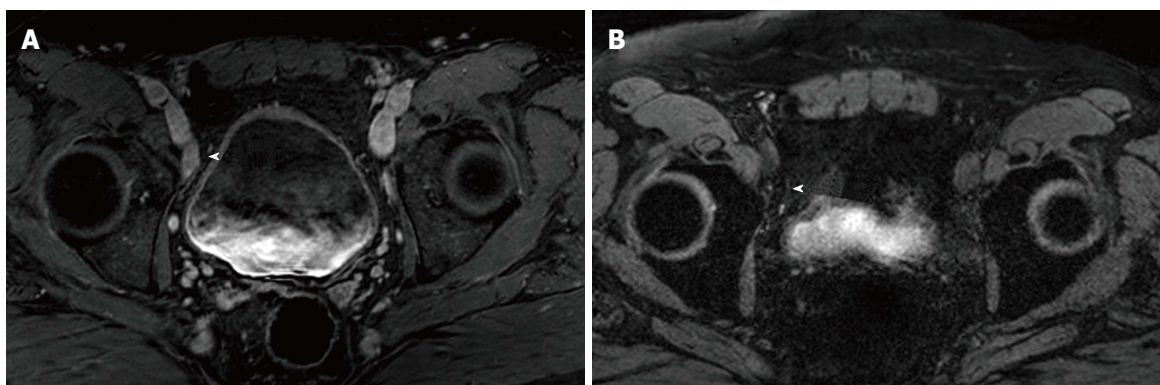


Figure 1 Selected images from a ferumoxytol enhanced magnetic resonance imaging in a 59-year-old man who underwent transrectal ultrasonography prostate biopsy for elevated PSA (10.8 ng/mL) which showed Gleason 3 + 4 disease of 4 cores. A: Initial prostate multiparametric T1 weighted post gadolinium magnetic resonance imaging (MRI) showed a 1.8 cm × 0.9 cm right external iliac chain lymph node that was suspicious based on size criteria (arrowhead); B: 24 h post injection of ferumoxytol (7.5 Fe/kg dose), T2* weighted MRI showed decreased signal intensity within the node (arrowhead), consistent with uptake of ferumoxytol. This was considered a benign lymph node based on these results. The patient underwent computed tomography guided biopsy for confirmation and the node was negative for malignancy.

were considered malignant when one of the following three criteria are present: (1) A decrease in signal intensity of less than 30 percent on T2-weighted fast spin-echo or gradient-echo sequences after the administration of USPIO; (2) a heterogeneous signal (giving the entire node a mottled appearance), discrete focal defects (isolated islands of high signal intensity), or both on gradient echo imaging; and (3) nodes with a central area of hyperintensity (excluding a fatty hilum) but a peripheral decrease in signal intensity^[15]. This initial study utilizing ferumoxtran-10 demonstrated a sensitivity for detection of malignant lymph nodes with short axis diameter of 5-10 mm was increased with use of USPIO compared to MRI alone (96.4% vs 28.5%, respectively)^[15]. Other studies have confirmed the ability of MR ferumoxtran-10-enhanced lymphography to detect metastatic disease in non-pathologically enlarged lymph nodes (< 7 mm) with high sensitivity and specificity^[20,23,24,27-30].

Meijer *et al.*^[31] showed a better prognosis in a subset of patients with MRL positive lymph nodes that were < 8 mm and better outcomes in patients in whom all MRL positive lymph nodes were resected. This highlights a window of opportunity for cure in these patients as those with MRL-detected positive nodes that were entirely removed had a five-year distant metastatic disease free survival of 80% compared to 35% in the patients who did not have all MRL-detected positive nodes removed^[31].

Additionally, the potential for MRL to detect metastatic lymph nodes outside of the routine dissection margin has potential for great clinical value including surgical and radiation therapy planning. In series of 269 men with moderate to high risk for nodal metastasis, 41% were found to have lymph node metastasis outside of the routine dissection area that were identified with MR ferumoxtran-10-enhanced lymphography^[24]. MRL has been utilized to guide radiation therapy as another study showed that 53% of prostate cancer patients had

MRL positive lymph nodes outside of the target volume for pelvic radiation^[32]. Salvage radiation therapy is associated with some toxicity^[33], and improved selection of patients and detection of nodal targets can decrease morbidity and improve cure rates^[25]. However, despite these promising results, ferumoxtran-10 failed to achieve Food and Drug Administration (FDA) approval and production was halted^[34].

Ferumoxytol is a newly released USPIO agent that has been more recently utilized in detection of malignant lymph nodes^[35]. Ferumoxytol is a compound closely related to ferumoxtran-10 that is FDA approved as iron replacement therapy in patients with chronic kidney failure with the recommended clinical dose of 1020 mg (two doses of 510 mg administered intravenously 3-8 d apart)^[35,36]. In phase I and II clinical trials, ferumoxytol was associated with low adverse event rate which the most common events including nausea, dizziness, and diarrhea^[37], although more serious reactions such as hypotension and anaphylaxis have been reported^[38,39]. This has led to the FDA releasing a safety communication recommending modifications to give ferumoxytol as a dilute infusion^[40].

Due to its large size, ferumoxytol remains in a relatively steady concentration within the intravascular space for several hours (circulating half-life is 14-15 h) and then is gradually cleared by macrophages from the blood pool over several days^[41]. Following macrophage breakdown, the iron oxide particles are taken up by the reticuloendothelial system^[41]. In a recent phase I dose escalation trial, it was shown that the signal intensity of normal lymph nodes drop in a dose dependent manner with the optimal dose determined to be 7.5 mg Fe/kg^[35]. A pilot study quantitatively compared the ability of ferumoxytol and ferumoxtran-10 to suppress signal intensity in normal lymph nodes (in patients with high risk prostate cancer) and showed that signal suppression was weaker for ferumoxytol MRL than for ferumoxtran-10 MRL^[42]. This study was limited in that

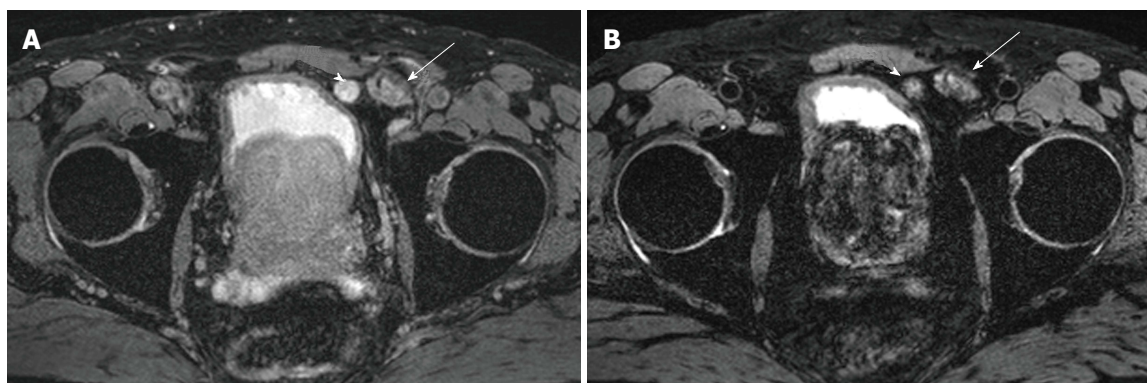


Figure 2 Selected images from a ferumoxytol enhanced magnetic resonance imaging in a 65 years old man status post magnetic resonance imaging/ultrasound fusion guided prostate biopsy revealing 3 + 3 prostate cancer and PSA 16.6 ng/mL. A: Baseline T2* weighted magnetic resonance imaging (MRI) showed a rounded lymph node anterior to the bladder (arrowhead) that measured 1.5 cm and was hyperintense. Lobular mass like lesion (arrow) lateral to the suspicious lymph node corresponds to hernia mesh; B: 24 h post injection of ferumoxytol (7.5 Fe/kg dose) enhanced MRI shows persistent heterogeneous hyperintensity within the node (arrowhead). The lack of ferumoxytol uptake within the node was suspicious for malignant involvement. Pathology revealed castleman's disease (false positive). Arrow again indicates hernia mesh.

only 4 patients received ferumoxytol and the dose was 6.0 mg Fe/kg, but further research is needed to validate the accuracy of ferumoxytol MRL^[42]. Ferumoxytol MRL has also been preliminarily evaluated in non-human primates for use as an intraprostatic injection to directly map lymph nodes draining the prostate gland, with a potential of guiding lymphatic drainage patterns for specific gland segments^[43].

MRL may have false positive results in the setting of reactive nodal hyperplasia or granulomatous diseases in which there are decreased number of macrophages in otherwise benign lymph nodes that may lead to mischaracterization of lymph nodes as malignant suspicion on imaging^[44] (Figure 2).

Diffusion-weighted imaging

In diffusion-weighted imaging (DWI), the Brownian motion of water molecules within a voxel of tissue is imaged and can be quantitatively expressed using the apparent diffusion coefficient (ADC) value. DWI can be performed quickly without the need of a contrast medium. Malignant tissue tends to have increased cellularity with enlarged nuclei and an abundance of macromolecular proteins, resulting in restricted diffusion^[45]. Typical malignant lesions appear hyperintense on images acquired at high b-values (800-1000 s/mm²) and hypointense on the corresponding ADC maps.

Malignant lymph nodes have been shown to have a lower ADC value when compared to benign lymph nodes^[46,47], but show less promising results in normal sized lymph nodes with a wide range of ADC values^[45,48]. In a study of 29 patients with prostate cancer and a total of 118 lymph nodes evaluated by DWI-MRI, a cut off value of 1.3×10^{-3} mm²/s yielded a sensitivity of 86% and specificity of 85%^[46]. ADC values can be elevated in necrotic nodes due to the free diffusion of water, which can lead to misclassification^[49]. While some authors have reporting the combination of nodal size and the relative ADC value nodes is more useful in

detecting pelvic lymph node metastasis^[50], others have found less promising results^[45]. Nevertheless, there can be an overlap of ADC values in benign and malignant lymph nodes^[51].

In a more recent prospective study utilizing a 3T MRI system and a non-quantitative approach to evaluation DWI and ADC maps, revealed 94% specificity and 41% sensitivity for anatomical region based analysis (mean positive lymph node size was 1.2 cm)^[52]. In a prospective evaluation of detection of normal sized metastatic lymph nodes in initial staging of prostate and bladder carcinoma, there was increased detection utilizing DWI when compared to conventional cross-section imaging techniques with detection of metastasis in 64%-79% of patients^[51]. Evaluating additional morphologic features at MR imaging such as round shape, irregular border, low T2 signal may improve specificity than relying only on diffusion weighted imaging^[51]. Further advances in DWI-MRI technique will require standardization of the technique, image acquisition and sequence parameters of different scanner platforms^[53].

Combining DWI-MRI with other techniques such as USPIO or choline show perhaps the most promising results^[30,54]. In a study evaluating 2,993 normal sized lymph nodes in patients with prostate or bladder cancer, combining DWI-MRI with USPIO improved sensitivity and specificity (65%-75% and 93%-96%; compared to 55%-65% and 71%-91%, respectively) and decreased imaging interpretation time compared to USPIO alone^[30].

PET TRACERS FOR INITIAL NODAL STAGING OF PROSTATE CANCER

PET

Considerable efforts are currently being made to develop effective radiotracers to image prostate cancer in both the setting of primary staging as well as biochemical recurrence. Although not the focus of this paper, there is substantial evidence supporting the use of PET tracers for

Table 1 Selected positron emission tomography tracers used for prostate cancer imaging

PET tracers	Mechanism of action
[¹⁸ F]FDG	Glucose metabolism
Sodium [¹⁸ F]fluoride	Chemisorption to bone matrix
[¹⁸ F]choline, [¹¹ C]choline	Cell membrane metabolism
[¹⁸ F]DCFBC, [⁶⁸ Ga]HBED-CC	PSMA binding
[¹¹ C]acetate	Fatty acid metabolism
[¹⁸ F]fluciclovine	Amino acid transport
[⁶⁸ Ga]DOTA-bombesin	GRPR receptor binding
[¹⁸ F]FDHT	Androgen receptor binding

PET: Positron emission tomography; [¹⁸F]FDG: (¹⁸F)fluoro-D-glucose; [¹⁸F]DCFBC: (¹⁸F)fluorobenzyl-L-cysteine; GRPR: Gastrin-releasing peptide receptor.

biochemical recurrence, and two PET tracers [(¹¹C)choline and (¹⁸F)fluciclovine] have been approved by the FDA for the detection and staging of biochemical recurrence. However, there has been less investigation regarding the use of PET in the initial nodal staging of prostate cancer. A wide range of PET tracers have been developed and investigated for prostate cancer imaging, and this section summarizes PET tracers that have demonstrated utility for detecting lymph node metastases from prostate cancer. These tracers and their key properties are summarized in Table 1.

Positron emission tomography (PET) is currently performed using hybrid imaging systems that combine PET with CT or MRI for attenuation correction and anatomic localization of the PET findings. In PET imaging, a positron emitting radiotracer is administered to the patient, which then emits 511 keV gamma rays through annihilation of the positron with an electron in the tissue which can be localized through coincidence detection^[55]. Compared to conventional planar scintigraphy and single photon computed tomography (SPECT), PET provides higher spatial and temporal resolution. One of the limitations of PET is resolution, with decreased sensitivity of the detection and characterization of PET tracer uptake in lesions less than 8 mm. However, the use of hybrid imaging PET/CT or PET/MRI allows the combination of anatomical imaging from the CT or MRI with molecular information from PET.

PET tracers for prostate cancer imaging have been labeled with several different radionuclides that vary in terms of their physical half-life ($t_{1/2}$) and their chemistries. PET radionuclides include carbon-11 ($t_{1/2}$ = 20 min), fluorine-18 ($t_{1/2}$ = 110 min), and gallium-68 ($t_{1/2}$ = 68 min). Carbon-11 and fluorine-18 are produced using cyclotrons while gallium-68 is produced using a generator system. Fluorine-18 is widely available, and its long half-life facilitates production of large batches of PET tracers and distribution to sites that do not have onsite production capabilities.

The most commonly used radiotracer for clinical oncologic imaging is 2-deoxy-2-(¹⁸F)fluoro-D-glucose (FDG), but this tracer is of limited utility for the initial staging of prostate cancer due to the low metabolic activity in the early phase of the disease which results

in poor sensitivity^[56]. Another disadvantage of FDG is urinary excretion, potentially decreasing sensitivity for pelvic lymph nodes^[57]. For the evaluation of bony metastases, sodium(¹⁸F) fluoride (NaF) has been used for skeletal scintigraphy which takes advantage of higher spatial resolution when compared with conventional planar (^{99m}Tc)methyldiphosphinate (MDP). Several studies have demonstrated that cross-sectional skeletal scintigraphy with fluoride-PET/CT or MDP-SPECT/CT have superior sensitivity and specificity for detection of osseous metastases when compared to conventional planar bone scans (96% and 98%, respectively)^[58]. The uptake of (¹⁸F)fluoride is based on bone turnover with increased binding to newly deposited mineralize bone matrix that occurs in bone metastases, particularly osteoblastic metastases. While (¹⁸F)fluoride-PET/CT may be useful in preoperative skeletal staging in prostate cancer, this tracer is not useful for the detection of lymph node metastases.

Choline is a naturally-occurring small molecule that is incorporated into tumor cells after phosphorylation by choline kinase, which is up regulated in prostate cancer^[59]. (¹¹C)choline uptake in metastatic lymph nodes occurs in the presence of viable malignant tissue, and (¹¹C)choline has been approved by the FDA for use in the detection and localization of suspected biochemically recurrent prostate cancer. This PET tracer has been used for prostate cancer with a pooled sensitivity of 49.2% and specificity of 95% for detection lymph node metastasis^[60]. Results are better for larger nodes, but sensitivity is limited in lymph nodes smaller than 7 mm^[20]. Several studies combining (¹¹C)choline PET/CT and diffusion weighted MRI showed that sensitivity remained too low to be clinically useful for initial staging^[54,61].

Fluorinated analogues of choline have been developed to take advantage of the longer half-life of fluorine-18 [e.g., (¹⁸F)fluorocholine and 2-(¹⁸F)fluoroethyl choline]. However, these fluorinated choline analogues have similar limited capability in detecting lymph node metastasis (sensitivity 40% and specificity 96%)^[62,63]. Combining ¹⁸F-choline PET and MRI may help improve the results of choline PET imaging, but further research is needed^[64,65]. The value of choline for the detection of recurrent prostate cancer in patients with low PSA levels (< 2.5 ng/mL) is limited^[66,67]. Additionally, ¹⁸F-labeled analogues of choline are eliminated *via* the kidney and urinary tract activity, which is undesirable for pelvic imaging.

Acetate is a naturally occurring metabolic substrate that can enter the fatty acid metabolic pathway which is overexpressed in prostate cancer cells^[68]. Most research has been done with (¹¹C)acetate and has shown sensitivity of 68% and specificity of 78% in one study of intermediate and high risk prostate cancer^[69], but has the disadvantage of requiring an onsite cyclotron due to the short half-life of 20 min.

Prostate specific membrane antigen (PSMA) is a protein expressed by the prostate and overexpressed in prostate cancer^[70]. The initial molecular imaging

agent targeting PSMA that gained widespread use was (^{111}In)indium capromab pendetide, a radiolabeled monoclonal antibody that targets the intracellular portion of PSMA and is imaged utilizing SPECT/CT. While initial results showed improvement over conventional techniques, there was limited sensitivity and specificity^[71,72]. However with the additional of MRI, sensitivity and specificity were increased^[73]. The main disadvantage of (^{111}In)indium capromab pendetide is that it targets an intracellular protein making imaging only a possibility upon apoptosis or necrosis and not in viable tissue^[55,70,74]. Additionally, the slow kinetics of (^{111}In)indium capromab pendetide requires imaging 5-7 d after injection. More recently, a great deal of research has been focused on small molecule ligands that bind to the extracellular portion of PSMA^[75,76].

Novel small molecule imaging PSMA ligands have been developed such as *N*-{*N*-[(*S*)-1,3-dicarboxypropyl] carbamoyl}-4-(^{18}F)fluorobenzyl-L-cysteine [(^{18}F)DFBC], which binds irreversibly to the extracellular component of PSMA and has been shown to improve detection of metastatic prostate cancer^[77,78]. The most commonly used PSMA ligand in Europe is ^{68}Ga -*N,N'*-bis [2-hydroxy-5-(carboxyethyl)benzyl] ethylenediamine-*N,N'*-diacetic acid (HBED-CC) (Figure 3). In a study utilizing ^{68}Ga -labeled PSMA ligand (HBED-CC), there was improved accuracy of lymph node staging over conventional imaging with 65.9% sensitivity and 98.9% specificity^[79]. A retrospective study examining ^{68}Ga -PSMA PET/CT in initial staging of patients with high risk of lymph node metastasis found 33.3% sensitivity and 100% specificity (mean size of true positive nodes was 13.6 cm and of false positive node was 4.3 mm)^[80].

Amino acid radiotracers can accumulate in prostate cancer cells through the upregulation of transmembrane amino acid transport in prostate cancer^[81]. The most work with a synthetic amino acid PET radiotracer for prostate cancer has been with (^{18}F)fluciclovine for detection of recurrent disease, and this PET tracer was approved by the FDA for use in biochemically recurrent prostate cancer in 2016 (Figure 4). Preliminary studies have reported results for initial staging^[81,82]. In a multicenter phase IIb clinical trial for staging of initial prostate cancer, diagnostic accuracy of (^{18}F)fluciclovine PET/CT was compared to conventional imaging with CT and bone scan^[83]. Overall accuracies were similar (85.5% for (^{18}F)fluciclovine PET/CT and 87.3% for conventional imaging); however, (^{18}F)fluciclovine PET/CT was positive in 5-9 mm nodes and skeletal lesions that were not detected by conventional imaging.

An additional molecular target that is currently under investigation is the gastrin-releasing peptide receptor (GRPR) which is overexpressed in prostate but has lower levels in benign prostate tissue including benign prostatic hyperplasia^[84]. Initial studies demonstrate GRPR overexpression in 63%-100% of primary prostate carcinomas and 50%-85% of nodal and osseous metastases^[85]. A number of peptide based ligands for GRPR have been developed including the 14 amino acid peptide bombesin, as well as analogues of the 27-amino

acid gastrin releasing peptide (GRP)^[86]. A single human trial utilizing a ^{68}Ga -labeled GRPR antagonist for pre-operative staging has been completed^[87]. This trial enrolled 11 patients with primary prostate carcinoma and three patients with evidence of biochemical recurrence, demonstrating a sensitivity of 88% and specificity of 81% for detection of the primary lesion (within a sextant level) and found evidence of biochemical recurrence in lymph nodes and the prostate bed in two out of three patients^[88].

Androgen sensitivity and receptor expression remain a mainstay in the diagnosis and treatment of prostate carcinoma. Importantly, androgen receptor expression plays a role in both initial treatment strategies and in the setting for treatment for biochemical recurrence/metastatic disease. Preliminary human imaging studies have been performed using the androgen receptor ligand 16β -(^{18}F)fluoro-5 α -dihydrotestosterone (FDHT). The initial human study compared FDHT and FDG, which demonstrated FDHT uptake in 46/59 lesions in seven patients with progressive metastatic prostate cancer (compared to FDG uptake in 57/59)^[89]. The role, if any, of (^{18}F)FDHT in the pre-operative evaluation of prostate cancer is not yet defined.

An interesting future in targeted molecular imaging of metastatic prostate carcinoma is the use of PSMA and bombesin agents for targeted therapy with alpha-emitters or beta-emitters (including ^{90}Y and ^{177}Lu). These agents are currently being utilized in clinical trials for patients with biochemical recurrence, but are not currently approved for use in the United States^[90,91]. These compounds may play a future role in adjuvant therapy post prostatectomy as the previously described molecular targeted PET agents become established for initial staging.

An exciting development that may increase the impact of molecular imaging for prostate carcinoma is the recent FDA approval of hybrid PET/MRI scanners. These scanners can acquire PET and MRI data simultaneously and combine targeted molecular imaging with PET with the soft tissue contrast and anatomic detail provided by pelvic MRI. The MRI component of PET/MRI can significantly increase detection of lesions compared to the non-contrast CT typically performed with conventional PET/CT. Evaluation of the prostate bed can also be significantly improved utilizing PET/MRI vs PET/CT. Given the established role of MRI for prostate cancer staging and lesion detection, PET/MRI may become the preferred platform for prostate cancer imaging in certain clinical scenarios. However, more data are needed to define the role of PET/MRI in the initial staging of prostate cancer.

CONCLUSION

Conventional imaging (CT and MRI) cannot depict small metastases in normal sized and normal appearing lymph nodes. The optimal strategy for the preoperative staging of prostate cancer remains a topic of ongoing

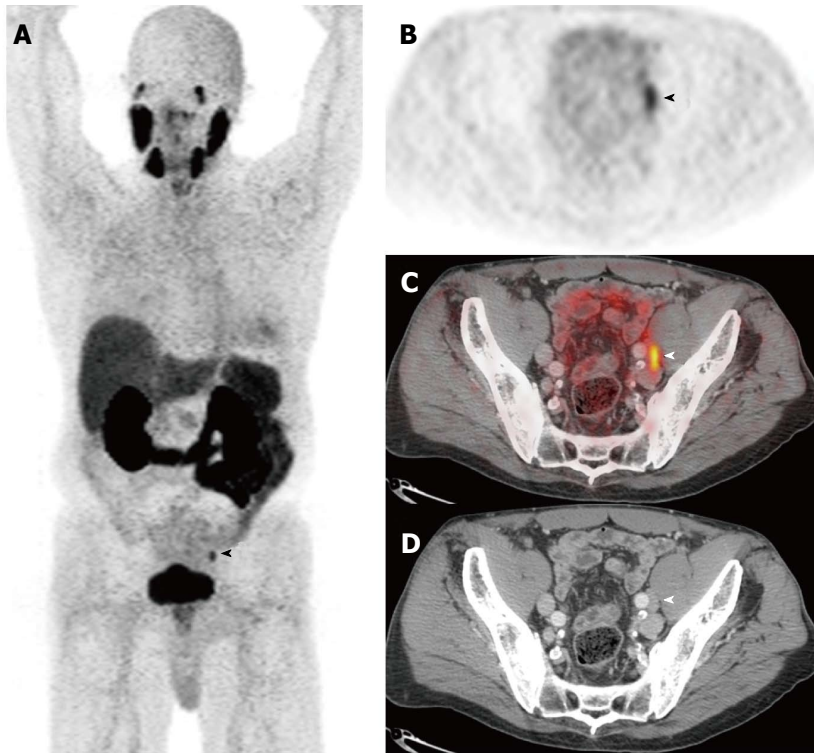


Figure 3 Prostate specific membrane antigen. Selected images from a [⁶⁸Ga]PSMA-11-PET/CT study performed prior to therapy in a man with biopsy-proven Gleason 9 prostate adenocarcinoma, a serum PSA of 11.6 ng/mL, and a clinical tumor stage of cT2b. The anterior maximum intensity projection (MIP) image (A) and the axial PET (B), fusion (C), and CT (D) images through the pelvis demonstrate focal activity in a left external iliac lymph node. This appearance is highly suspicious for a lymph node metastasis. Images courtesy of Tom Hope, MD, University of California San Francisco, Department of Radiology. PSMA: Prostate specific membrane antigen; PET/CT: Positron emission tomography/computed tomography.

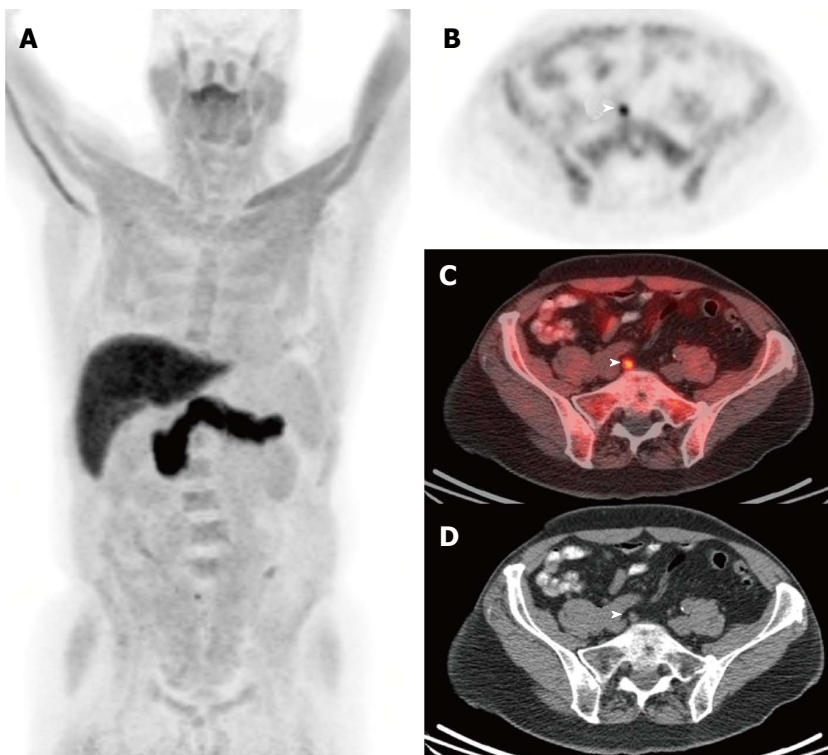


Figure 4 Fluciclovine. Selected images from a (¹⁸F)fluciclovine-positron emission tomography/computed tomography study performed in a man who underwent prostatectomy for Gleason 8 prostate adenocarcinoma 11 years ago. He developed biochemical recurrence with a serum PSA of 0.8 ng/mL and a PSA doubling time of 14 mo at the time of the (¹⁸F)fluciclovine-PET/CT study. The anterior maximum intensity projection (MIP) image (A) and the axial PET (B), fusion (C), and CT (D) images near the level of the pelvic inlet demonstrate focal activity in a subcentimeter right common iliac lymph node. This appearance is highly suspicious for a lymph node metastasis. Images courtesy of Ephraim Parent MD, PhD, and David Schuster, MD, Emory University, Department of Radiology. PET/CT: Positron emission tomography/computed tomography.

research. Advanced imaging techniques to assess lymph nodes in the setting of prostate cancer utilizing novel MRI contrast agents as well as PET tracers have been developed and continue to be studied. MRL utilizing USPIO has shown high sensitivity and specificity in detection of normal sized lymph nodes containing metastatic disease and thus a positive finding may alter the treatment course for the patient. Ongoing research is occurring in molecular imaging and continues to show a promising future for detection of prostate metastasis as well as potential therapeutic applications.

REFERENCES

- Hövels AM, Heesakkers RA, Adang EM, Jager GJ, Strum S, Hoogeveen YL, Severens JL, Barentsz JO. The diagnostic accuracy of CT and MRI in the staging of pelvic lymph nodes in patients with prostate cancer: a meta-analysis. *Clin Radiol* 2008; **63**: 387-395 [PMID: 18325358 DOI: 10.1016/j.crad.2007.05.022]
- Kothari PS, Scardino PT, Ohori M, Kattan MW, Wheeler TM. Incidence, location, and significance of periprostatic and periseminal vesicle lymph nodes in prostate cancer. *Am J Surg Pathol* 2001; **25**: 1429-1432 [PMID: 11684961]
- Makarov DV, Trock BJ, Humphreys EB, Mangold LA, Walsh PC, Epstein JI, Partin AW. Updated nomogram to predict pathologic stage of prostate cancer given prostate-specific antigen level, clinical stage, and biopsy Gleason score (Partin tables) based on cases from 2000 to 2005. *Urology* 2007; **69**: 1095-1101 [PMID: 17572194 DOI: 10.1016/j.urol.2007.03.042]
- D'Amico AV, Whittington R, Malkowicz SB, Schultz D, Schnall M, Tomaszewski JE, Wein A. Combined modality staging of prostate carcinoma and its utility in predicting pathologic stage and postoperative prostate specific antigen failure. *Urology* 1997; **49**: 23-30 [PMID: 9123732]
- D'Amico AV. Combined-modality staging for localized adenocarcinoma of the prostate. *Oncology* (Williston Park) 2001; **15**: 1049-1059; discussion 1060-106, 1064-1065, 1069-1070, 1073-1075 [PMID: 11548976]
- Loeb S, Catalona WJ. The Prostate Health Index: a new test for the detection of prostate cancer. *Ther Adv Urol* 2014; **6**: 74-77 [PMID: 24688603 DOI: 10.1177/1756287213513488]
- McDonald ML, Parsons JK. 4-Kallikrein Test and Kallikrein Markers in Prostate Cancer Screening. *Urol Clin North Am* 2016; **43**: 39-46 [PMID: 26614027 DOI: 10.1016/j.ucl.2015.08.004]
- Allaf ME, Palapattu GS, Trock BJ, Carter HB, Walsh PC. Anatomical extent of lymph node dissection: impact on men with clinically localized prostate cancer. *J Urol* 2004; **172**: 1840-1844 [PMID: 15540734]
- Burkhard FC, Studer UE. The role of lymphadenectomy in prostate cancer. *Urol Oncol* 2004; **22**: 198-202; discussion 202-204 [PMID: 15271316 DOI: 10.1016/j.urolonc.2004.04.032]
- McDowell GC 2nd, Johnson JW, Tenney DM, Johnson DE. Pelvic lymphadenectomy for staging clinically localized prostate cancer. Indications, complications, and results in 217 cases. *Urology* 1990; **35**: 476-482 [PMID: 2353374]
- Schuessler WW, Pharand D, Vancaillie TG. Laparoscopic standard pelvic node dissection for carcinoma of the prostate: is it accurate? *J Urol* 1993; **150**: 898-901 [PMID: 8345606]
- Joniau S, Van den Bergh L, Lerut E, Deroose CM, Haustermans K, Oyen R, Budiharto T, Ameye F, Bogaerts K, Van Poppel H. Mapping of pelvic lymph node metastases in prostate cancer. *Eur Urol* 2013; **63**: 450-458 [PMID: 22795517 DOI: 10.1016/j.eururo.2012.06.057]
- Jager GJ, Barentsz JO, Oosterhof GO, Witjes JA, Ruijs SJ. Pelvic adenopathy in prostatic and urinary bladder carcinoma: MR imaging with a three-dimensional TI-weighted magnetization-prepared-rapid gradient-echo sequence. *AJR Am J Roentgenol* 1996; **167**: 1503-1507 [PMID: 8956585 DOI: 10.2214/ajr.167.6.8956585]
- Davis GL. Sensitivity of frozen section examination of pelvic lymph nodes for metastatic prostate carcinoma. *Cancer* 1995; **76**: 661-668 [PMID: 8625162]
- Harisinghani MG, Barentsz J, Hahn PF, Deserno WM, Tabatabaei S, van de Kaa CH, de la Rosette J, Weissleder R. Noninvasive detection of clinically occult lymph-node metastases in prostate cancer. *N Engl J Med* 2003; **348**: 2491-2499 [PMID: 12815134 DOI: 10.1056/NEJMoa022749]
- Bellin MF, Roy C, Kinkel K, Thoumas D, Zaim S, Vanel D, Tuchmann C, Richard F, Jacqmin D, Delcourt A, Challier E, Lebre T, Cluzel P. Lymph node metastases: safety and effectiveness of MR imaging with ultrasmall superparamagnetic iron oxide particles—initial clinical experience. *Radiology* 1998; **207**: 799-808 [PMID: 9609907 DOI: 10.1148/radiology.207.3.9609907]
- Weissleder R, Elizondo G, Wittenberg J, Lee AS, Josephson L, Brady TJ. Ultrasmall superparamagnetic iron oxide: an intravenous contrast agent for assessing lymph nodes with MR imaging. *Radiology* 1990; **175**: 494-498 [PMID: 2326475 DOI: 10.1148/radiology.175.2.2326475]
- Wunderbaldinger P, Josephson L, Bremer C, Moore A, Weissleder R. Detection of lymph node metastases by contrast-enhanced MRI in an experimental model. *Magn Reson Med* 2002; **47**: 292-297 [PMID: 11810672]
- Hricak H, Choyke PL, Eberhardt SC, Leibel SA, Scardino PT. Imaging prostate cancer: a multidisciplinary perspective. *Radiology* 2007; **243**: 28-53 [PMID: 17392247 DOI: 10.1148/radiol.2431030580]
- Fortuin AS, Deserno WM, Meijer HJ, Jager GJ, Takahashi S, Debats OA, Reske SN, Schick C, Krause BJ, van Oort I, Witjes AJ, Hoogeveen YL, van Lin EN, Barentsz JO. Value of PET/CT and MR lymphography in treatment of prostate cancer patients with lymph node metastases. *Int J Radiat Oncol Biol Phys* 2012; **84**: 712-718 [PMID: 22417806 DOI: 10.1016/j.ijrobp.2011.12.093]
- Harisinghani MG, Saini S, Slater GJ, Schnall MD, Rifkin MD. MR imaging of pelvic lymph nodes in primary pelvic carcinoma with ultrasmall superparamagnetic iron oxide (Combixen): preliminary observations. *J Magn Reson Imaging* 1997; **7**: 161-163 [PMID: 9039609]
- Harisinghani MG, Saksena MA, Hahn PF, King B, Kim J, Torabi MT, Weissleder R. Ferumoxtran-10-enhanced MR lymphangiography: does contrast-enhanced imaging alone suffice for accurate lymph node characterization? *AJR Am J Roentgenol* 2006; **186**: 144-148 [PMID: 16357394 DOI: 10.2214/AJR.04.1287]
- Heesakkers RA, Hövels AM, Jager GJ, van den Bosch HC, Witjes JA, Raat HP, Severens JL, Adang EM, van der Kaa CH, Fütterer JJ, Barentsz J. MRI with a lymph-node-specific contrast agent as an alternative to CT scan and lymph-node dissection in patients with prostate cancer: a prospective multicohort study. *Lancet Oncol* 2008; **9**: 850-856 [PMID: 18708295 DOI: 10.1016/S1470-2045[08]70203-1]
- Heesakkers RA, Jager GJ, Hövels AM, de Hoop B, van den Bosch HC, Raat F, Witjes JA, Mulders PF, van der Kaa CH, Barentsz JO. Prostate cancer: detection of lymph node metastases outside the routine surgical area with ferumoxtran-10-enhanced MR imaging. *Radiology* 2009; **251**: 408-414 [PMID: 19401573 DOI: 10.1148/radiol.2512071018]
- Ross RW, Zietman AL, Xie W, Coen JJ, Dahl DM, Shipley WU, Kaufman DS, Islam T, Guimaraes AR, Weissleder R, Harisinghani M. Lymphotropic nanoparticle-enhanced magnetic resonance imaging (LNMRI) identifies occult lymph node metastases in prostate cancer patients prior to salvage radiation therapy. *Clin Imaging* 2009; **33**: 301-305 [PMID: 19559353 DOI: 10.1016/j.clinimag.2009.01.013]
- Froehlich JM, Triantafyllou M, Fleischmann A, Vermathen P, Thalmann GN, Thoeny HC. Does quantification of USPIO uptake-related signal loss allow differentiation of benign and malignant normal-sized pelvic lymph nodes? *Contrast Media Mol Imaging* 2012; **7**: 346-355 [PMID: 22539405 DOI: 10.1002/cmim.503]
- Thoeny HC, Triantafyllou M, Birkhaeuser FD, Froehlich JM, Tshering DW, Binsler T, Fleischmann A, Vermathen P, Studer UE. Combined ultrasmall superparamagnetic particles of iron oxide-enhanced and diffusion-weighted magnetic resonance imaging reliably detect pelvic lymph node metastases in normal-sized nodes of bladder

- and prostate cancer patients. *Eur Urol* 2009; **55**: 761-769 [PMID: 19144456 DOI: 10.1016/j.eururo.2008.12.034]
- 28 **Triantafyllou M**, Studer UE, Birkhäuser FD, Fleischmann A, Bains LJ, Petralia G, Christe A, Froehlich JM, Thoeny HC. Ultrasmall superparamagnetic particles of iron oxide allow for the detection of metastases in normal sized pelvic lymph nodes of patients with bladder and/or prostate cancer. *Eur J Cancer* 2013; **49**: 616-624 [PMID: 23084842 DOI: 10.1016/j.ejca.2012.09.034]
- 29 **Heesakkers RA**, Fütterer JJ, Hövels AM, van den Bosch HC, Scheenen TW, Hoogeveen YL, Barentsz JO. Prostate cancer evaluated with ferumoxtran-10-enhanced T2*-weighted MR Imaging at 1.5 and 3.0 T: early experience. *Radiology* 2006; **239**: 481-487 [PMID: 16641354 DOI: 10.1148/radiol.2392050411]
- 30 **Birkhäuser FD**, Studer UE, Froehlich JM, Triantafyllou M, Bains LJ, Petralia G, Vermathen P, Fleischmann A, Thoeny HC. Combined ultrasmall superparamagnetic particles of iron oxide-enhanced and diffusion-weighted magnetic resonance imaging facilitates detection of metastases in normal-sized pelvic lymph nodes of patients with bladder and prostate cancer. *Eur Urol* 2013; **64**: 953-960 [PMID: 23916692 DOI: 10.1016/j.eururo.2013.07.032]
- 31 **Meijer HJ**, Debats OA, van Lin EN, Witjes JA, Kaanders JH, Barentsz JO. A retrospective analysis of the prognosis of prostate cancer patients with lymph node involvement on MR lymphography: who might be cured. *Radiat Oncol* 2013; **8**: 190 [PMID: 23898991 DOI: 10.1186/1748-717X-8-190]
- 32 **Meijer HJ**, Debats OA, Kunze-Busch M, van Kollenburg P, Leer JW, Witjes JA, Kaanders JH, Barentsz JO, van Lin EN. Magnetic resonance lymphography-guided selective high-dose lymph node irradiation in prostate cancer. *Int J Radiat Oncol Biol Phys* 2012; **82**: 175-183 [PMID: 21075555 DOI: 10.1016/j.ijrobp.2010.09.023]
- 33 **Pisansky TM**, Kozelsky TF, Myers RP, Hillman DW, Blute ML, Buskirk SJ, Chevillet JC, Ferrigni RG, Schild SE. Radiotherapy for isolated serum prostate specific antigen elevation after prostatectomy for prostate cancer. *J Urol* 2000; **163**: 845-850 [PMID: 10687990]
- 34 **George AK**, Turkbey B, Valayil SG, Muthigi A, Mertan F, Kongnyuy M, Pinto PA. A urologist's perspective on prostate cancer imaging: past, present, and future. *Abdom Radiol (NY)* 2016; **41**: 805-816 [PMID: 27138438 DOI: 10.1007/s00261-016-0751-6]
- 35 **Turkbey B**, Agarwal HK, Shih J, Bernardo M, McKinney YL, Daar D, Griffiths GL, Sankineni S, Johnson L, Grant KB, Weaver J, Rais-Bahrami S, Harisinghani M, Jacobs P, Dahut W, Merino MJ, Pinto PA, Choyke PL. A Phase I Dosing Study of Ferumoxytol for MR Lymphography at 3 T in Patients With Prostate Cancer. *AJR Am J Roentgenol* 2015; **205**: 64-69 [PMID: 26102381 DOI: 10.2214/AJR.14.13009]
- 36 **Vasanawala SS**, Nguyen KL, Hope MD, Bridges MD, Hope TA, Reeder SB, Bashir MR. Safety and technique of ferumoxytol administration for MRI. *Magn Reson Med* 2016; **75**: 2107-2111 [PMID: 26890830 DOI: 10.1002/mrm.26151]
- 37 **Pai AB**, Garba AO. Ferumoxytol: a silver lining in the treatment of anemia of chronic kidney disease or another dark cloud? *J Blood Med* 2012; **3**: 77-85 [PMID: 22973119 DOI: 10.2147/JBM.S29204]
- 38 **Bailie GR**. Comparison of rates of reported adverse events associated with i.v. iron products in the United States. *Am J Health Syst Pharm* 2012; **69**: 310-320 [PMID: 22302256 DOI: 10.2146/ajhp110262]
- 39 **Santosh S**, Podaralla P, Miller B. Anaphylaxis with elevated serum tryptase after administration of intravenous ferumoxytol. *NDT Plus* 2010; **3**: 341-342 [PMID: 25949425 DOI: 10.1093/ndtplus/sfq084]
- 40 FDA Drug Safety Communication: FDA strengthens warnings and changes prescribing instructions to decrease the risk of serious allergic reactions with anemia drug Feraheme. 2015, accessed December 5 2016. Available from: URL: <https://www.fda.gov/Drugs/DrugSafety/ucm440138.htm>
- 41 **Bashir MR**, Bhatti L, Marin D, Nelson RC. Emerging applications for ferumoxytol as a contrast agent in MRI. *J Magn Reson Imaging* 2015; **41**: 884-898 [PMID: 24974785 DOI: 10.1002/jmri.24691]
- 42 **Debats OA**, Fortuin AS, Meijer HJ, Hambroek T, Litjens GJ, Barentsz JO, Huisman HJ. Intranodal signal suppression in pelvic MR lymphography of prostate cancer patients: a quantitative comparison of ferumoxtran-10 and ferumoxytol. *PeerJ* 2016; **4**: e2471 [PMID: 27781154 DOI: 10.7717/peerj.2471]
- 43 **Sankineni S**, Smedley J, Bernardo M, Brown AM, Johnson L, Muller B, Griffiths GL, Kobayashi H, Rais-Bahrami S, Pinto PA, Wood BJ, Keele B, Choyke PL, Turkbey B. Ferumoxytol as an intraprostatic MR contrast agent for lymph node mapping of the prostate: a feasibility study in non-human primates. *Acta Radiol* 2016; **57**: 1396-1401 [PMID: 26013022 DOI: 10.1177/0284185115586023]
- 44 **Saokar A**, Braschi M, Harisinghani M. Lymphotropic nanoparticle enhanced MR imaging (LNMRI) for lymph node imaging. *Abdom Imaging* 2006; **31**: 660-667 [PMID: 16680506 DOI: 10.1007/s00261-006-9006-2]
- 45 **Roy C**, Bierry G, Matau A, Bazille G, Pasquali R. Value of diffusion-weighted imaging to detect small malignant pelvic lymph nodes at 3 T. *Eur Radiol* 2010; **20**: 1803-1811 [PMID: 20182732 DOI: 10.1007/s00330-010-1736-4]
- 46 **Eiber M**, Beer AJ, Holzapfel K, Tauber R, Ganter C, Weirich G, Krause BJ, Rummeny EJ, Gaa J. Preliminary results for characterization of pelvic lymph nodes in patients with prostate cancer by diffusion-weighted MR-imaging. *Invest Radiol* 2010; **45**: 15-23 [PMID: 19996762 DOI: 10.1097/RLI.0b013e3181bbdc2f]
- 47 **Akduman EI**, Momtahan AJ, Balci NC, Mahajann N, Havlioglu N, Wolverson MK. Comparison between malignant and benign abdominal lymph nodes on diffusion-weighted imaging. *Acad Radiol* 2008; **15**: 641-646 [PMID: 18423322 DOI: 10.1016/j.acra.2007.12.023]
- 48 **Budiharto T**, Joniau S, Lerut E, Van den Bergh L, Mottaghy F, Deroose CM, Oyen R, Ameye F, Bogaerts K, Haustermans K, Van Poppel H. Prospective evaluation of 11C-choline positron emission tomography/computed tomography and diffusion-weighted magnetic resonance imaging for the nodal staging of prostate cancer with a high risk of lymph node metastases. *Eur Urol* 2011; **60**: 125-130 [PMID: 21292388 DOI: 10.1016/j.eururo.2011.01.015]
- 49 **Sumi M**, Van Cauteren M, Nakamura T. MR microimaging of benign and malignant nodes in the neck. *AJR Am J Roentgenol* 2006; **186**: 749-757 [PMID: 16498102 DOI: 10.2214/AJR.04.1832]
- 50 **Choi EK**, Kim JK, Choi HJ, Park SH, Park BW, Kim N, Kim JS, Im KC, Cho G, Cho KS. Node-by-node correlation between MR and PET/CT in patients with uterine cervical cancer: diffusion-weighted imaging vs size-based criteria on T2WI. *Eur Radiol* 2009; **19**: 2024-2032 [PMID: 19277675 DOI: 10.1007/s00330-009-1350-5]
- 51 **Thoeny HC**, Froehlich JM, Triantafyllou M, Huesler J, Bains LJ, Vermathen P, Fleischmann A, Studer UE. Metastases in normal-sized pelvic lymph nodes: detection with diffusion-weighted MR imaging. *Radiology* 2014; **273**: 125-135 [PMID: 24893049 DOI: 10.1148/radiol.14132921]
- 52 **von Below C**, Daouacher G, Wassberg C, Grzegorek R, Gestblom C, Sörensen J, Ahlström H, Waldén M. Validation of 3 T MRI including diffusion-weighted imaging for nodal staging of newly diagnosed intermediate- and high-risk prostate cancer. *Clin Radiol* 2016; **71**: 328-334 [PMID: 26774372 DOI: 10.1016/j.crad.2015.12.001]
- 53 **Giannarini G**, Petralia G, Thoeny HC. Potential and limitations of diffusion-weighted magnetic resonance imaging in kidney, prostate, and bladder cancer including pelvic lymph node staging: a critical analysis of the literature. *Eur Urol* 2012; **61**: 326-340 [PMID: 22000497 DOI: 10.1016/j.eururo.2011.09.019]
- 54 **Heck MM**, Souvatzoglou M, Retz M, Nawroth R, Kübler H, Maurer T, Thalgott M, Gramer BM, Weirich G, Rondak IC, Rummeny EJ, Schwaiger M, Gschwend JE, Krause B, Eiber M. Prospective comparison of computed tomography, diffusion-weighted magnetic resonance imaging and [11C]choline positron emission tomography/computed tomography for preoperative lymph node staging in prostate cancer patients. *Eur J Nucl Med Mol Imaging* 2014; **41**: 694-701 [PMID: 24297503 DOI: 10.1007/s00259-013-2634-1]
- 55 **Fortuin A**, Rooij Md, Zamecnik P, Haberkorn U, Barentsz J. Molecular and functional imaging for detection of lymph node metastases in prostate cancer. *Int J Mol Sci* 2013; **14**: 13842-13875 [PMID: 23823804 DOI: 10.3390/ijms140713842]
- 56 **Ghanem N**, Uhl M, Brink I, Schäfer O, Kelly T, Moser E, Langer M. Diagnostic value of MRI in comparison to scintigraphy, PET, MS-CT and PET/CT for the detection of metastases of bone. *Eur J Radiol*

- 2005; **55**: 41-55 [PMID: 15950100 DOI: 10.1016/j.ejrad.2005.01.016]
- 57 **Shreve PD**, Grossman HB, Gross MD, Wahl RL. Metastatic prostate cancer: initial findings of PET with 2-deoxy-2-[F-18]fluoro-D-glucose. *Radiology* 1996; **199**: 751-756 [PMID: 8638000 DOI: 10.1148/radiology.199.3.8638000]
- 58 **Tateishi U**, Morita S, Taguri M, Shizukuishi K, Minamimoto R, Kawaguchi M, Murano T, Terauchi T, Inoue T, Kim EE. A meta-analysis of (18)F-Fluoride positron emission tomography for assessment of metastatic bone tumor. *Ann Nucl Med* 2010; **24**: 523-531 [PMID: 20559896 DOI: 10.1007/s12149-010-0393-7]
- 59 **Ackerstaff E**, Glunde K, Bhujwala ZM. Choline phospholipid metabolism: a target in cancer cells? *J Cell Biochem* 2003; **90**: 525-533 [PMID: 14523987 DOI: 10.1002/jcb.10659]
- 60 **Evangelista L**, Guttilla A, Zattoni F, Muzzio PC, Zattoni F. Utility of choline positron emission tomography/computed tomography for lymph node involvement identification in intermediate- to high-risk prostate cancer: a systematic literature review and meta-analysis. *Eur Urol* 2013; **63**: 1040-1048 [PMID: 23036576 DOI: 10.1016/j.euro.2012.09.039]
- 61 **Van den Bergh L**, Lerut E, Haustermans K, Deroose CM, Oyen R, Isebaert S, Budiharto T, Ameye F, Mottaghy FM, Bogaerts K, Van Poppel H, Joniau S. Final analysis of a prospective trial on functional imaging for nodal staging in patients with prostate cancer at high risk for lymph node involvement. *Urol Oncol* 2015; **33**: 109.e23-109.e31 [PMID: 25655681 DOI: 10.1016/j.urolonc.2014.11.008]
- 62 **Tilki D**, Reich O, Graser A, Hacker M, Silchinger J, Becker AJ, Khoder W, Bartenstein P, Stief CG, Loidl W, Seitz M. 18F-Fluoroethylcholine PET/CT identifies lymph node metastasis in patients with prostate-specific antigen failure after radical prostatectomy but underestimates its extent. *Eur Urol* 2013; **63**: 792-796 [PMID: 22902037 DOI: 10.1016/j.euro.2012.08.003]
- 63 **Vali R**, Loidl W, Pirich C, Langesteger W, Beheshti M. Imaging of prostate cancer with PET/CT using (18)F-Fluorocholine. *Am J Nucl Med Mol Imaging* 2015; **5**: 96-108 [PMID: 25973332]
- 64 **Wetter A**, Lipponer C, Nensa F, Beiderwellen K, Olbricht T, Rübber H, Bockisch A, Schlosser T, Heusner TA, Lauenstein TC. Simultaneous 18F choline positron emission tomography/magnetic resonance imaging of the prostate: initial results. *Invest Radiol* 2013; **48**: 256-262 [PMID: 23462678 DOI: 10.1097/RLI.0b013e318282c654]
- 65 **Pinaquy JB**, De Clermont-Galleran H, Pasticier G, Rigou G, Alberti N, Hindie E, Mokrane Y, Fernandez P. Comparative effectiveness of [(18)F]-fluorocholine PET-CT and pelvic MRI with diffusion-weighted imaging for staging in patients with high-risk prostate cancer. *Prostate* 2015; **75**: 323-331 [PMID: 25393215 DOI: 10.1002/pros.22921]
- 66 **Rinnab L**, Simon J, Hautmann RE, Cronauer MV, Hohl K, Buck AK, Reske SN, Mottaghy FM. [(11)C]choline PET/CT in prostate cancer patients with biochemical recurrence after radical prostatectomy. *World J Urol* 2009; **27**: 619-625 [PMID: 19234708 DOI: 10.1007/s00345-009-0371-7]
- 67 **Giovacchini G**, Picchio M, Coradeschi E, Bettinardi V, Gianolli L, Scattoni V, Cozzarini C, Di Muzio N, Rigatti P, Fazio F, Messa C. Predictive factors of [(11)C]choline PET/CT in patients with biochemical failure after radical prostatectomy. *Eur J Nucl Med Mol Imaging* 2010; **37**: 301-309 [PMID: 19756592 DOI: 10.1007/s00259-009-1253-3]
- 68 **Våvere AL**, Kridel SJ, Wheeler FB, Lewis JS. 1-11C-acetate as a PET radiopharmaceutical for imaging fatty acid synthase expression in prostate cancer. *J Nucl Med* 2008; **49**: 327-334 [PMID: 18199615 DOI: 10.2967/jnumed.107.046672]
- 69 **Haseebuddin M**, Dehdashti F, Siegel BA, Liu J, Roth EB, Nepple KG, Siegel CL, Fischer KC, Kibel AS, Andriole GL, Miller TR. 11C-acetate PET/CT before radical prostatectomy: nodal staging and treatment failure prediction. *J Nucl Med* 2013; **54**: 699-706 [PMID: 23471311 DOI: 10.2967/jnumed.112.111153]
- 70 **Ghosh A**, Heston WD. Tumor target prostate specific membrane antigen (PSMA) and its regulation in prostate cancer. *J Cell Biochem* 2004; **91**: 528-539 [PMID: 14755683 DOI: 10.1002/jcb.10661]
- 71 **Rosenthal SA**, Haseman MK, Polascik TJ. Utility of capromab pentetide (ProstaScint) imaging in the management of prostate cancer. *Tech Urol* 2001; **7**: 27-37 [PMID: 11272670]
- 72 **Ponsky LE**, Cherullo EE, Starkey R, Nelson D, Neumann D, Zippe CD. Evaluation of preoperative ProstaScint scans in the prediction of nodal disease. *Prostate Cancer Prostatic Dis* 2002; **5**: 132-135 [PMID: 12497003 DOI: 10.1038/sj.pcan.4500570]
- 73 **Hardie AD**, Rieter WJ, Bradshaw ML, Gordon LL, Young MA, Keane TE. Improved performance of SPECT-CT In-111 capromab pentetide by correlation with diffusion-weighted magnetic resonance imaging for identifying metastatic pelvic lymphadenopathy in prostate cancer. *World J Urol* 2013; **31**: 1327-1332 [PMID: 23595605 DOI: 10.1007/s00345-013-1079-2]
- 74 **Troyer JK**, Beckett ML, Wright GL Jr. Location of prostate-specific membrane antigen in the LNCaP prostate carcinoma cell line. *Prostate* 1997; **30**: 232-242 [PMID: 9111600]
- 75 **Osborne JR**, Akhtar NH, Vallabhajosula S, Anand A, Deh K, Tagawa ST. Prostate-specific membrane antigen-based imaging. *Urol Oncol* 2013; **31**: 144-154 [PMID: 22658884 DOI: 10.1016/j.urolonc.2012.04.016]
- 76 **Rowe SP**, Gorin MA, Allaf ME, Pienta KJ, Tran PT, Pomper MG, Ross AE, Cho SY. PET imaging of prostate-specific membrane antigen in prostate cancer: current state of the art and future challenges. *Prostate Cancer Prostatic Dis* 2016; **19**: 223-230 [PMID: 27136743 DOI: 10.1038/pcan.2016.13]
- 77 **Rowe SP**, Macura KJ, Ciarallo A, Mena E, Blackford A, Nadal R, Antonarakis ES, Eisenberger MA, Carducci MA, Ross AE, Kantoff PW, Holt DP, Dannals RF, Mease RC, Pomper MG, Cho SY. Comparison of Prostate-Specific Membrane Antigen-Based 18F-DCFB PET/CT to Conventional Imaging Modalities for Detection of Hormone-Naïve and Castration-Resistant Metastatic Prostate Cancer. *J Nucl Med* 2016; **57**: 46-53 [PMID: 26493203 DOI: 10.2967/jnumed.115.163782]
- 78 **Eder M**, Eisenhut M, Babich J, Haberkorn U. PSMA as a target for radiolabelled small molecules. *Eur J Nucl Med Mol Imaging* 2013; **40**: 819-823 [PMID: 23463331 DOI: 10.1007/s00259-013-2374-2]
- 79 **Maurer T**, Gschwend JE, Rauscher I, Souvatzoglou M, Haller B, Weirich G, Wester HJ, Heck M, Kübler H, Beer AJ, Schwaiger M, Eiber M. Diagnostic Efficacy of (68)Gallium-PSMA Positron Emission Tomography Compared to Conventional Imaging for Lymph Node Staging of 130 Consecutive Patients with Intermediate to High Risk Prostate Cancer. *J Urol* 2016; **195**: 1436-1443 [PMID: 26682756 DOI: 10.1016/j.juro.2015.12.025]
- 80 **Budäus L**, Leyh-Bannurah SR, Salomon G, Michl U, Heinzer H, Huland H, Graefen M, Steuber T, Rosenbaum C. Initial Experience of (68)Ga-PSMA PET/CT Imaging in High-risk Prostate Cancer Patients Prior to Radical Prostatectomy. *Eur Urol* 2016; **69**: 393-396 [PMID: 26116958 DOI: 10.1016/j.euro.2015.06.010]
- 81 **Schuster DM**, Nanni C, Fanti S. Evaluation of Prostate Cancer with Radiolabeled Amino Acid Analogs. *J Nucl Med* 2016; **57**: 61S-66S [PMID: 27694174 DOI: 10.2967/jnumed.115.170209]
- 82 **Odewole OA**, Tade FI, Nieh PT, Savir-Baruch B, Jani AB, Master VA, Rossi PJ, Halkar RK, Osunkoya AO, Akin-Akintayo O, Zhang C, Chen Z, Goodman MM, Schuster DM. Recurrent prostate cancer detection with anti-3-[(18)F]FACBC PET/CT: comparison with CT. *Eur J Nucl Med Mol Imaging* 2016; **43**: 1773-1783 [PMID: 27091135 DOI: 10.1007/s00259-016-3383-8]
- 83 **Suzuki H**, Inoue Y, Fujimoto H, Yonese J, Tanabe K, Fukasawa S, Inoue T, Saito S, Ueno M, Otaka A. Diagnostic performance and safety of NMK36 (trans-1-amino-3-[18F] fluorocyclobutanecarboxylic acid)-PET/CT in primary prostate cancer: multicenter Phase IIb clinical trial. *Jpn J Clin Oncol* 2017; **47**: 283 [PMID: 27920097 DOI: 10.1093/jco/hyw177]
- 84 **Wibmer AG**, Burger IA, Sala E, Hricak H, Weber WA, Vargas HA. Molecular Imaging of Prostate Cancer. *Radiographics* 2016; **36**: 142-159 [PMID: 26587888 DOI: 10.1148/rg.2016150059]
- 85 **Mansi R**, Fleischmann A, Mäcke HR, Reubi JC. Targeting GRPR in urological cancers--from basic research to clinical application. *Nat Rev Urol* 2013; **10**: 235-244 [PMID: 23507930 DOI: 10.1038/nrurol.2013.42]
- 86 **Dijkgraaf I**, Franssen GM, McBride WJ, D'Souza CA, Laverman P, Smith CJ, Goldenberg DM, Oyen WJ, Boerman OC. PET of tumors expressing gastrin-releasing peptide receptor with an 18F-labeled bombesin analog. *J Nucl Med* 2012; **53**: 947-952 [PMID: 22570329]

DOI: 10.2967/jnumed.111.100891]

- 87 **Zhang H**, Abiraj K, Thorek DL, Waser B, Smith-Jones PM, Honer M, Reubi JC, Maecke HR. Evolution of bombesin conjugates for targeted PET imaging of tumors. *PLoS One* 2012; **7**: e44046 [PMID: 23024746 DOI: 10.1371/journal.pone.0044046]
- 88 **Kähkönen E**, Jambor I, Kemppainen J, Lehtiö K, Grönroos TJ, Kuisma A, Luoto P, Sipilä HJ, Tolvanen T, Alanen K, Silén J, Kallajoki M, Roivainen A, Schäfer N, Schibli R, Dragic M, Johayem A, Valencia R, Borkowski S, Minn H. In vivo imaging of prostate cancer using [68Ga]-labeled bombesin analog BAY86-7548. *Clin Cancer Res* 2013; **19**: 5434-5443 [PMID: 23935037 DOI: 10.1158/1078-0432.CCR-12-3490]
- 89 **Larson SM**, Morris M, Gunther I, Beattie B, Humm JL, Akhurst TA, Finn RD, Erdi Y, Pentlow K, Dyke J, Squire O, Bornmann W, McCarthy T, Welch M, Scher H. Tumor localization of 16beta-18F-fluoro-5alpha-dihydrotestosterone vs 18F-FDG in patients with progressive, metastatic prostate cancer. *J Nucl Med* 2004; **45**: 366-373 [PMID: 15001675]
- 90 **Rahbar K**, Ahmadzadehfar H, Kratochwil C, Haberkorn U, Schäfers M, Essler M, Baum RP, Kulkarni HR, Schmidt M, Drzezga A, Bartenstein P, Pfestroff A, Luster M, Lützen U, Marx M, Prasad V, Brenner W, Heinzel A, Mottaghy FM, Ruf J, Meyer PT, Heuschkel M, Eveslage M, Bögemann M, Fendler WP, Krause BJ. German Multicenter Study Investigating 177Lu-PSMA-617 Radioligand Therapy in Advanced Prostate Cancer Patients. *J Nucl Med* 2017; **58**: 85-90 [PMID: 27765862 DOI: 10.2967/jnumed.116.183194]
- 91 **Chatalic KL**, Konijnenberg M, Nonnekens J, de Blois E, Hoeben S, de Ridder C, Brunel L, Fehrentz JA, Martinez J, van Gent DC, Nock BA, Maina T, van Weerden WM, de Jong M. In Vivo Stabilization of a Gastrin-Releasing Peptide Receptor Antagonist Enhances PET Imaging and Radionuclide Therapy of Prostate Cancer in Preclinical Studies. *Theranostics* 2016; **6**: 104-117 [PMID: 26722377 DOI: 10.7150/thno.13580]

P- Reviewer: Arcangeli S, Huang SP S- Editor: Kong JX

L- Editor: A E- Editor: Lu YJ



MR neurography in intraosseous median nerve entrapment

Ankita Aggarwal, Manisha Jana, Vijay Kumar, Deep Narayan Srivastava, Kanwaljeet Garg

Ankita Aggarwal, Manisha Jana, Deep Narayan Srivastava, Department of Radiodiagnosis, All India Institute of Medical Sciences, New Delhi 110029, India

Vijay Kumar, Department of Orthopedics, All India Institute of Medical Sciences, New Delhi 110029, India

Kanwaljeet Garg, Department of Neurosurgery, All India Institute of Medical Sciences, New Delhi 110029, India

Author contributions: Aggarwal A and Srivastava DN designed the research; Aggarwal A, Jana M and Srivastava DN performed the research; Kumar V and Srivastava DN provided administrative support; Aggarwal A and Garg K prepared the manuscript.

Institutional review board statement: Ethics clearance for this study was taken from the Ethics Committee of All India Institute of Medical Sciences, New Delhi, India.

Informed consent statement: All study participants, or their legal guardian, provided informed written consent prior to study enrollment.

Conflict-of-interest statement: The authors do not have any conflict of interest.

Open-Access: This article is an open-access article which was selected by an in-house editor and fully peer-reviewed by external reviewers. It is distributed in accordance with the Creative Commons Attribution Non Commercial (CC BY-NC 4.0) license, which permits others to distribute, remix, adapt, build upon this work non-commercially, and license their derivative works on different terms, provided the original work is properly cited and the use is non-commercial. See: <http://creativecommons.org/licenses/by-nc/4.0/>

Manuscript source: Unsolicited manuscript

Correspondence to: Deep Narayan Srivastava, Professor, Department of Radiodiagnosis, All India Institute of Medical Sciences, Room No 69, Ground Floor, Near South Extension, New Delhi 110029, India. drdeepsrivastava@rediffmail.com
Telephone: +91-98-99245764

Received: February 13, 2017

Peer-review started: February 14, 2017

First decision: April 19, 2017

Revised: June 24, 2017

Accepted: July 7, 2017

Article in press: July 10, 2017

Published online: October 28, 2017

Abstract

Intraosseous entrapment of the median nerve is an uncommon complication of elbow dislocation and fractures. The condition is seen to occur in adolescent age group with a remote history of trauma. We report two rare cases of type 2 intraosseous median nerve entrapment. Though the diagnosis of median neuropathy is made with clinical tests and neurophysiological studies, however exact site of entrapment and presurgical mapping of nerve is done accurately with MR neurography. Imaging thus plays a pivotal role in management of this condition.

Key words: Intraosseous; MR neurography; Median nerve

© **The Author(s) 2017.** Published by Baishideng Publishing Group Inc. All rights reserved.

Core tip: Intraosseous entrapment of median nerve at the level of elbow joint is rare but serious complication of closed reduction of posterior elbow dislocation. We report two cases of type 2 intraosseous median nerve entrapment (wherein the median nerve gets entrapped in fractured medial epicondyle) and discuss the role of MR neurography. MR delineates the posterior course of median nerve with altered signal intensity, thickening and loss of fascicular pattern. In addition, secondary denervation changes in muscles supplied by median nerve is indirect evidence of nerve pathology. Management of such cases would differ depending on the time of diagnosis.

Aggarwal A, Jana M, Kumar V, Srivastava DN, Garg K. MR neurography in intraosseous median nerve entrapment. *World J Radiol* 2017; 9(10): 400-404 Available from: URL: <http://www.wjnet.com/1949-8470/full/v9/i10/400.htm> DOI: <http://dx.doi.org/10.4329/wjr.v9.i10.400>

INTRODUCTION

Intraosseous entrapment of the median nerve at the level of elbow joint is a rare but serious complication of closed reduction of posterior elbow dislocation^[1]. The diagnosis often gets delayed due to subtle symptoms which leads to grave damage to nerve. Imaging plays a major role preoperatively determining the site of entrapment. We report two cases of type 2 intraosseous median nerve entrapment and discuss their MR neurography findings.

CASE REPORT

Case 1

An 18-year-old male suffered fracture of medial epicondyle of left humerus along with elbow dislocation after he fell from rooftop about two years back. He was managed with closed reduction of elbow, followed by cast immobilization and physiotherapy. After removal of cast, he progressively started having symptoms of median neuropathy in the form of numbness and paresthesia along the median nerve distribution in forearm and hand with inability to form a fist and weak hand movements (Figure 1A). Gradually there was thinning of the forearm muscles. On clinical examination, there was atrophy of forearm muscles (of the anterior compartment) and of thenar muscles (Figure 1B). He had weakness of small hand muscles as well in the median nerve distribution. Clinical impression was median nerve palsy. Ulnar and radial nerve function was normal on clinical examination. Nerve conduction studies revealed median nerve neuropathy at the level of elbow.

High resolution USG was done, which revealed grossly thickened and hypoechoic median nerve in the region of distal arm with an abrupt cut off at the level of elbow (Figure 1C). The nerve fibers were seen coursing posteriorly and distal median nerve could not be traced. Limited MR neurography of the elbow was done for further confirmation of diagnosis. It revealed the median nerve to be swollen and having abnormal signal intensity (hyperintense on T2) in the distal arm (Figures 1D and 2). It was seen to have an altered course as the median nerve was seen to course posteriorly through the fractured medial epicondyle and subsequently was entrapped between the olecranon of ulna and olecranon fossa of humerus. Thereafter, the nerve was not visualized for some distance after which it reappeared with decreased calibre in its normal course in forearm with normal signal intensity. The muscles of the anterior compartment, supplied by median nerve, showed hyperintense signal on T1w and T2w sequence suggesting chronic denervation with fatty infiltration. These features were suggestive of type 2 median nerve entrapment.

Case 2

A 20-year-old patient suffered supracondylar fracture

of humerus 1 year back. The patient was managed conservatively by immobilization. Patient noticed weakness of hand grip and hand movements and decreased sensations of lateral half of forearm and lateral half of hand after immobilization was removed.

On examination, there was atrophy of anterior compartment muscles of right forearm and thenar eminence of hand. There was weakness of lateral half of hand fingers. All tests for median nerve were also positive in this case. NCV confirmed median neuropathy with likely site to be at elbow.

MR neurography revealed markedly thickened median nerve and was T2 hyperintense in the region of arm proximal to fracture site and traversed through the fractured fragment of humerus and coursed posteriorly (Figure 3). The nerve was entrapped between the olecranon and olecranon fossa and was seen coursing anteriorly back to its normal course with normal intensity and mildly decreased thickness. There was secondary atrophy of flexor digitorum profundus (lateral belly), flexor digitorum superficialis, flexor pollicis longus, pronator teres and of thenar muscles with fatty change s/o chronic insult.

DISCUSSION

Intraosseous median nerve entrapment is relatively rare complication of elbow dislocation and fractures of lower end humeral, frequency of which varies from 1%-12.5%^[2]. It was first described by Gurdjian and Smathers^[3] in 1945. The condition is seen to occur in a relative younger age group (adolescents) with a slight male predominance^[4].

Four types of intraosseous median nerve entrapment are described^[5]. The first three types have been described by Hallett while type IV was described by al-Danielsson *et al*^[6], Hallett *et al*^[7], Steiger *et al*^[8], Ozkoç *et al*^[9], Noonan *et al*^[10]. In type 1 intraosseous median nerve entrapment, the medial collateral ligament is torn and the median nerve slips posteriorly adhering to the posterior surface of humerus and gets entrapped between trochlea and olecranon process. In type 2, median nerve is entrapped in the fractured medial epicondyle. Type 3 is when nerve gets entrapped between the distal end of humerus and ulna in the ulno-humeral joint without any fracture. Type 4 is combination of type 1 and 2^[11]. Both our cases were of type 2 variety; the median nerve was entrapped in the fractured medial epicondyle. Both the patients were young adolescent males having a remote history of trauma and were managed non-operatively.

Intraosseous entrapment of the median nerve should be suspected when there is failure of concentric reduction, presence of joint widening post reduction or the clinical symptoms persist or if there occurs cortical depression with surrounding sclerotic changes in the distal metaphysis of humerus (matev sign)^[1,12,13].

Imaging played a pivotal role in preoperative diagnosis of this condition. Altered signal intensity and thickening of the median nerve with loss of fascicular

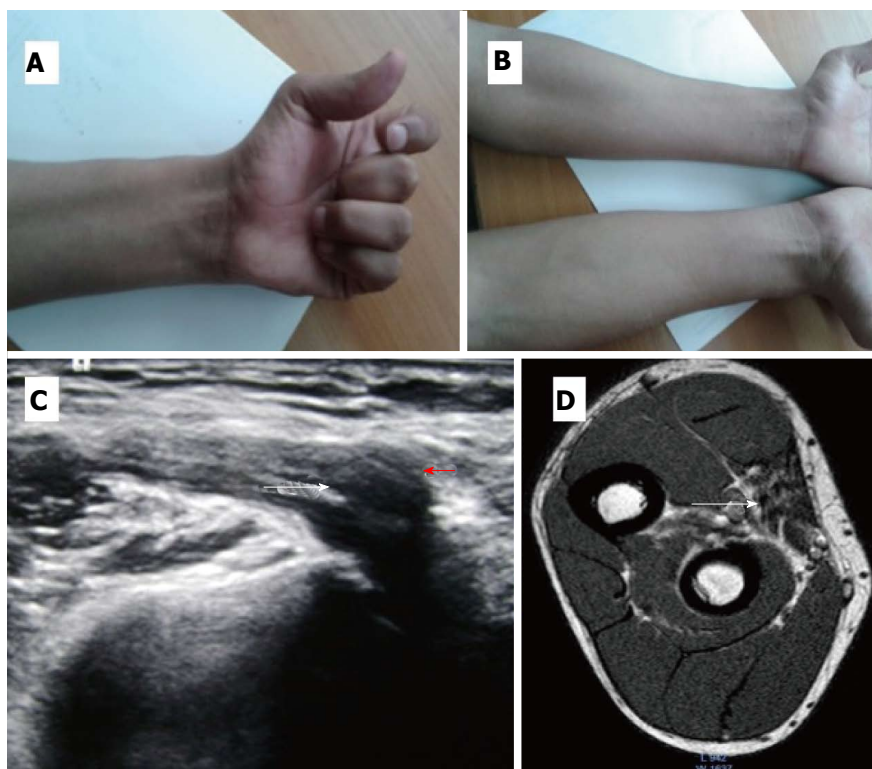


Figure 1 Images of first patient with intraosseous median nerve entrapment. A: Clinical Photograph showing inability to close fist completely with partial flexion of the index finger; B: Atrophy of anterior compartment muscles of left forearm; C: Sonogram shows thickened and hypoechoic median nerve (arrow), coursing posteriorly through the fractured bone; D: SE T1 W MR axial image shows atrophy of anterior compartment muscles of forearm with fatty infiltration s/o chronic denervation changes (arrow).

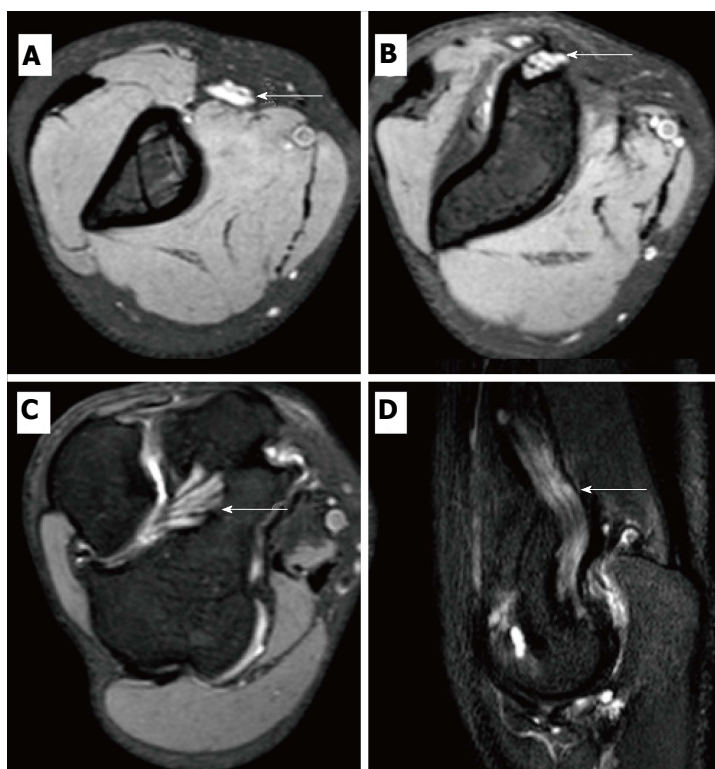


Figure 2 Images of second patient with intraosseous median nerve entrapment. A-C: 3D GRE T2W images showing markedly thickened and hyperintense entrapped median nerve (arrow), coursing posteriorly through the fractured medial epicondyle; D: STIR Coronal image showing markedly thickened and hyperintense median nerve (arrow).

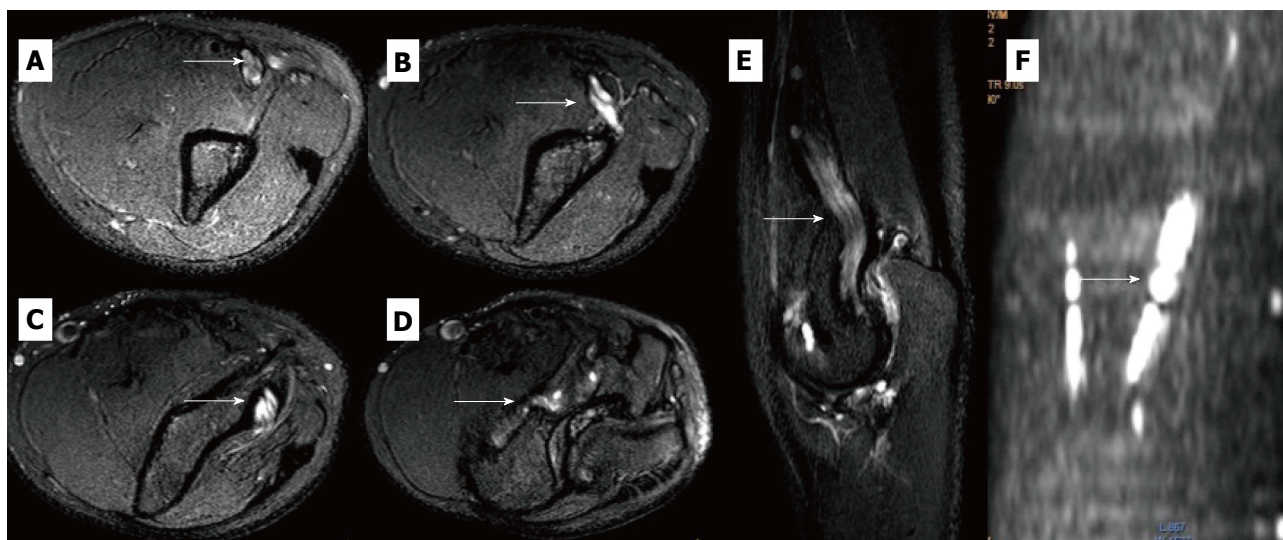


Figure 3 Images of third patient with intraosseous median nerve entrapment. A-D: SE T2W FS axial MR image shows markedly thickened and hyperintense nerve coursing through the fractured medial epicondyle; E: STIR coronal MR image shows entrapped median nerve coursing posteriorly; F: DWIBS coronal reformat highlights the abnormal median nerve.

pattern pointed towards the abnormality of the nerve. MRI clearly delineated the posterior course of the median nerve. In addition, secondary denervation changes in muscles supplied by median nerve were also seen.

Management of such cases would differ depending on the time of diagnosis. Usually the symptoms of median nerve entrapment are mild hence detection of this neuropathy is delayed. If detected early, relocation of the nerve from posterior to anterior compartment is done. If detected later then excision of the diseased segment with either nerve repair (end to end) or nerve grafting is done (with sural nerve graft). Early diagnosis and treatment ensures better prognosis. Both the cases we encountered were of chronic insult due to delayed diagnosis. The first case was lost to follow up and the second underwent nerve grafting.

MR neurography plays a vital role in the diagnosis of intraosseous entrapment of median nerve following medial epicondyle fracture by clearly demonstrating its altered course in the posterior compartment leading to its entrapment. In addition, presurgical mapping of the nerve can be accurately done with MRI and it also helps in deciding the correct management of the patient.

COMMENTS

Case characteristics

Numbness and paresthesia along the median nerve distribution in forearm and hand with inability to form a fist, and weak hand movements with gradual thinning of the forearm muscles.

Clinical diagnosis

Weakness and atrophy of muscles of median nerve distribution.

Differential diagnosis

Traumatic/entrapment/infectious/inflammatory neuropathy.

Laboratory diagnosis

Nerve conduction study will reveal reduced velocity across the median nerve.

Imaging diagnosis

MR delineates the posterior course of median nerve with altered signal intensity, thickening and loss of fascicular pattern.

Pathological diagnosis

Neuropathy at the fracture level.

Treatment

If detected early, relocation of the nerve from posterior to anterior compartment is done and if detected later then excision of the diseased segment with either nerve repair (end to end) or nerve grafting is done (with sural nerve graft).

Related reports

Four types of intraosseous median nerve entrapment are described. Intraosseous entrapment of the median nerve should be suspected when there is failure of concentric reduction, presence of joint widening post reduction or the clinical symptoms persist or if there occurs cortical depression with surrounding sclerotic changes in the distal metaphysis of humerus (matev sign). MRI clearly delineated the posterior course of the median nerve. In addition, secondary denervation changes in muscles supplied by median nerve were also seen.

Term explanation

Intraosseous entrapment of the median nerve is a rare complication of closed reduction of posterior elbow dislocation.

Experiences and lessons

MR neurography plays a vital role in the diagnosis of intraosseous entrapment of median nerve following medial epicondyle fracture by clearly demonstrating its altered course in the posterior compartment leading to its entrapment.

Peer-review

The case studies are described clearly and it is easy for the reader to follow.

REFERENCES

- Gurdjian ES, Smathers HM. Peripheral nerve injury in fractures

- and dislocations of long bones. *J Neurosurg* 1945; **2**: 202-219 [DOI: 10.3171/jns.1945.2.3.0202]
- 2 **Landin LA**, Danielsson LG. Elbow fractures in children. An epidemiological analysis of 589 cases. *Acta Orthop Scand* 1986; **57**: 309-312 [PMID: 3788491 DOI: 10.3109/17453678608994398]
 - 3 **Fourrier P**, Levai JP, Collin JP. [Median nerve entrapment in elbow dislocation]. *Rev Chir Orthop Reparatrice Appar Mot* 1977; **63**: 13-16 [PMID: 141697]
 - 4 **al-Qattan MM**, Zuker RM, Weinberg MJ. Type 4 median nerve entrapment after elbow dislocation. *J Hand Surg Br* 1994; **19**: 613-615 [PMID: 7822921 DOI: 10.1016/0266-7681(94)90127-9]
 - 5 **Ayala H**, De Pablos J, Gonzalez J, Martinez A. Entrapment of the median nerve after posterior dislocation of the elbow. *Microsurgery* 1983; **4**: 215-220 [DOI: 10.1002/micr.1920040403]
 - 6 **Danielsson LG**. Median nerve entrapment in elbow dislocation. A case report. *Acta Orthop Scand* 1986; **57**: 450-452 [PMID: 3811894 DOI: 10.3109/17453678609014770]
 - 7 **Hallett J**. Entrapment of the median nerve after dislocation of the elbow. A case report. *J Bone Joint Surg Br* 1981; **63-B**: 408-412 [PMID: 7263756]
 - 8 **Steiger RN**, Larrick RB, Meyer TL. Median-nerve entrapment following elbow dislocation in children. A report of two cases. *J Bone Joint Surg Am* 1969; **51**: 381-385 [PMID: 5767328 DOI: 10.2106/0004623-196951020-00017]
 - 9 **Ozkoç G**, Akpınar S, Hersekli MA, Ozalay M, Uysal M, Tandoğan NR. Type 4 median nerve entrapment in a child after elbow dislocation. *Arch Orthop Trauma Surg* 2003; **123**: 555-557 [PMID: 12920535 DOI: 10.1007/s00402-003-0565-1]
 - 10 **Noonan KJ**, Blair WF. Chronic median-nerve entrapment after posterior fracture-dislocation of the elbow. A case report. *J Bone Joint Surg Am* 1995; **77**: 1572-1575 [PMID: 7593068 DOI: 10.2106/00004623-199510000-00014]
 - 11 **Webb S**, Lourie J. Median nerve entrapment in an unreduced fracture-dislocation of the elbow: case report. *P N G Med J* 1986; **29**: 185-187 [PMID: 3465102]
 - 12 **Matev I**. A radiological sign of entrapment of the median nerve in the elbow joint after posterior dislocation. A report of two cases. *J Bone Joint Surg Br* 1976; **58**: 353-355 [PMID: 956256]
 - 13 **Simon D**, Masquijo JJ, Duncan MJ, Kontio K. Intra-articular median nerve incarceration after spontaneous reduction of a pediatric elbow dislocation: case report and review of the literature. *J Pediatr Orthop* 2010; **30**: 125-129 [PMID: 20179558 DOI: 10.1097/BPO.0b013e3181cf3bfd]

P- Reviewer: Demonacos C **S- Editor:** Ji FF **L- Editor:** A
E- Editor: Lu YJ





Published by **Baishideng Publishing Group Inc**
7901 Stoneridge Drive, Suite 501, Pleasanton, CA 94588, USA
Telephone: +1-925-223-8242
Fax: +1-925-223-8243
E-mail: bpgoffice@wjgnet.com
Help Desk: <http://www.f6publishing.com/helpdesk>
<http://www.wjgnet.com>

